Cluster and Short-Range Order Influence on the Electrical Resistivity of Binary Alloys

Dissertation
von
Lucian Dorel Dulca

vorgelegt dem
Fachbereich 1 (Physik und Elektrotechnik)
der Universität Bremen
zur Erlangung des Grades
eines Doktors der Naturwissenschaften
(Dr. rer. nat.)

Bremen, November 2000

1. Gutachter: Prof. Dr. G. Czycholl
2. Gutachter: Dr. Hab. J. Banhart

Contents

List of Figures

List of Tables

Chapter 1

Introduction

The electrical resistivity of multi-component metallic systems is extremely sensitive to the microscopic arrangement of the various atom species on the crystal lattice. For example, alloys where an ordered and a disordered state exists show a strong dependence of the electrical resistivity on the state of order. Such an alloy, e.g. Cu_3Au, shows a comparatively high resistivity in the disordered phase, whereas after the transition to the ordered state the resistivity drops to a very low value although the transition from one to the other state merely involves some exchanges of atoms of the two types.

The theoretical treatment of the transport properties of completely disordered alloys has seen major advances since the advent of certain first-principles methods for the calculation of the electronic structure of such systems and sophisticated formulae for the determination of observables. In particular, an approach which starts from a *local density functional* description of the many-particle problem, treats disorder in the framework of the *coherent potential approximation* (CPA) in conjunction with the *Korringa-Kohn-Rostoker (KKR)* method and uses the *Kubo-Greenwood-formula* of linear response theory for the transport calculation has lead to excellent results (see e.g. [4, 5])

Besides ordered systems, which in the limit of zero temperature and perfect long-range order do not show any electrical resistivity at all and random alloys, however, there is a wide range of states of order, namely states of short-range order. This type of order also influences the electrical resistivity but the changes imposed by this short-range order are mostly less than 5% of the absolute resistivity. The interesting fact is that, in contrast to long-range order, short-range order can increase and decrease resistivity. The theoretical treatment of short-range ordered systems is difficult, because neither Bloch's theorem holds, nor an effective medium can be introduced in a simple way as it is done for random alloys.

Systems without translational invariance could be treated within the framework of multiple scattering theory and expressions for "simple" electronic quantities such as the density of states were obtained [3]. The more complicated transport quantities, however, have not been investigated very thoroughly up to now.

In the present work we applied the multiple scattering methods, which have been

shown to be extremely successful for disordered alloys, to alloys with short-range order. We used the following procedure: we started from a fully self-consistent KKR–CPA calculation for the electronic structure of a disordered alloy A_xB_{1-x}. The result of such a calculation was used to calculate the electronic structure and the resistivity of a large but finite cluster of atoms. By considering a large variety of different cluster configurations we were able to model short-range order by introducing statistical weights according to the desired short-range order parameter.

The present work is organized as follows: In Chapter 2 problem of ordering in alloys is discussed. Chapter 3 presents the theoretical framework. The derivation of the calculation of the electronic structure of a finite cluster is presented in some detail. Chapter 4 containes the results of the application of CPA and cluster methods to the calculations of densities of states and resistivities of binary alloys. Conclusions and an outlook are finally outlined in Chapter 5.

In the following part of this chapter some general definitions of the notions involved within the work are given.

1.1 Metals and Alloys

1.1.1 The Structure of Metals and Alloys

Interest in the crystal structures of metals, alloys, and other substances has been steadily increasing as the phase diagrams have become better known, as the relationship of properties to crystal structure has been studied in greater detail, and as attempts have continued to understand the basic principles governing the stability of structures.

Crystals may be classified according to types of binding forces as follows: (i) *Metallic crystals* consist of positive ions immersed in a "gas" of negative electrons. The attraction of the positive ions for the negative electrons holds the structure together and balances the repulsive forces of the ions for one another and of electrons for other electrons. The electrons move freely trough the lattice and provide good electrical and thermal conductivity. (ii) *Ionic crystals* are bound together by the electrostatic attraction between positive and negative ions. They are combinations of strongly electronegative and electropositive elements. (iii) *Covalent crystals* ("homopolar" or "valence" crystals) are held together by the sharing of electrons between neighboring atoms. The crystals are characterized by poor conductivity and great hardness. (iv) *Molecular crystals* are composed of inactive atoms of neutral molecules bound by weak van der Waals forces. They have low melting points.

Many crystals are intermediate between these "ideal" types. For example, some alloy phases have metallic conductivity and other properties associated with metallic binding and yet at the same time resemble covalent crystals. It is possible for some interatomic bonds in a crystal to be of one type, say ionic, and others to be of another type, say covalent; or each bond may be somewhat intermediate in type

between some of those listed above. For details on the crystal structure of metals and alloys the reader is referred to standard textbooks (see, for example, [44, 43]).

1.1.2 Solid Solutions

When atoms of two or more elements are able to share, with changing proportions, various sites of a given crystal structure, a *solid solution* is formed. The replacement of nickel atoms by copper atoms on the lattice of nickel is an example of a *substitutional* solid solution. Nickel can dissolve copper at all proportions, providing an example of *complete solid solubility*. This is usually only possible if the sizes of the atoms differ by no more than about 15 percent. There are many examples of *restricted mutual solid solubilities* even between elements with similar crystal structures and atom sizes ([40]).

If the mutual solid solubility is restricted, as it is in the Cu-Ag system, to only those proportions of the diagram that are linked to the pure elements, the resulting phases are known as *primary or terminal solid solutions*. Such solutions have, of course, the same structure as the elements on which they are based. If other phases are present in the system, they are usually known as *intermediate phases* or *intermetallic phases* and they frequently possess structures that are quite different from the structure of either of the component elements.

Interstitial solid solutions are formed when atoms with small radii are accommodated in the interstices of the lattice of a solvent. The solid solution of carbon in γ-Fe (austenite) is an example of this type; the iron atoms are on FCC lattice points, and the carbon atoms occupy interstitial positions. In general, because of the restricted size of the interstices, only rather small atoms dissolve interstitially. The radii of atoms known (or likely) to form interstitial solutions are less than 1.0 Å. When a solvent accepts one of these interstitially, there is always an expansion of the unit cell.

In multicomponent systems some atoms may be dissolved interstitially and others substitutionally, as in manganese steel, where manganese atoms replace iron atoms on lattice points and carbon atoms enter the interstices. Both interstitial and substitutional solid solutions can be *random*, with a statistical distribution of atom sites, or they may be partially or completely ordered, forming a superlattice, in which case the atoms of different kinds show preference for being neighbors of one another. The tendency of unlike atoms to become neighbors is called *ordering*. Alternatively, the like atoms may tend to associate together to form clusters within the solid solution. This tendency is called *clustering*. Again, the cluster may be dispersed randomly or they may be ordered or oriented in various ways, producing a variety of complex arrangements within the solid solution.

While it is possible to consider a completely random solid solution as an idealized example, the mounting experimental evidence, based mainly upon diffuse X-ray scattering, suggests that complete randomness (like perfect crystallinity) is probably never found in nature. Hence, solid solutions that are in a thermodynamical equilib-

rium may be considered to be truly *homogeneous* on a macroscopic scale, but they need not be homogeneous on a submicroscopic scale where atoms are considered individually.

Within the subject of this work only substitutional solid solutions are treated.

1.1.3 Substitutional Solid Solutions – An Overview

As mentioned earlier, substitutional disorder results when atoms of a given kind, say A, in a material are replaced with atoms of a second kind, say B. When there are only a few such replacements or when one wishes to focus attention on a single replacement, it is convenient to refer to the given material as the *host* and to the foreign atoms as *impurities*.

In the crudest model of substitutional disorder the replacement of an atom of a given kind by an atom of a different kind results in a perturbation confined to the site of the replacement. In this model, such a replacement does not affect the positions or potentials of the other atoms in the material, which are assumed to be distributed over the sites of a rigid lattice. The actual physical situation is, however, very different and much richer in content. Some of the most important effects caused by the substitution of one kind of atom by another in a material are summarized bellow.

The most evident effect of atom substitution is the change in the potential energy at the replacement site. This change commonly referred to as *diagonal disorder*. It is quite likely that not only the potential at the replacement site but also that at neighboring sites may be affected by atom replacement. Charge flow away from or toward an impurity may bring about such change in potential. A change in potential and hence in the wavefunction associated with an impurity site may affect electron propagation, or charge flow, in the neighborhood of that site. Charge flow and changes in potential are intertwined and must be treated in a self-consistent manner. The assumption that atom replacements can take place on the sites of an undisturbed rigid lattice is in general rather unrealistic. Different atoms are often of different sizes and will often have different ionic sizes in a solid. Electrostatic forces may cause atoms (or ions) to move toward or away from one another in a disordered material. Atom (or ion) size and electrostatic effects are so important that are often the sole factors that determine the solubility of two materials ([39]). In addition they may determine particular phases of the solutions and may bring about phase transitions between different crystal structure. Thus, it is to be expected that the positions of the atoms in substitutional alloys deviate from the sites determined by a regular lattice. In most treatments of substitutional disorder, it is assumed that the atoms of various kinds involved are distributed randomly over the sites of a regular lattice. In such alloys, the probability of finding an atom of a given species on a site is independent of the nature of the atoms occupying neighboring sites. However, various effects such as size and electrostatic effects may tend to cause atoms of a given kind to aggregate together (clustering), or to be preferentially surrounded by atoms

of a different kind (ordering). Clustering and ordering are referred to collectively as *short-range order* (SRO).

1.1.4 Dilute and Concentrated Alloys

We define a dilute alloys as one in which the impurity atoms are in sufficiently small concentration that they have no effect on the electronic structure of the bulk alloy, although localized perturbations may result. In this regime the impurity atoms will act as independent scattering centers for the conduction electrons so that the effect of N impurity atoms is just N times that of a single impurity. This will only be possible if the impurity atoms are widely separated (and hence randomly distributed), implying no direct or indirect interaction between them.

At higher impurity concentrations the electronic structure of the bulk alloy will start to suffer perturbations, and the impurity atoms may no longer be randomly distributed. Such alloys will be described as concentrated alloys and are the main concern of this work.

The problem of ordering in concentrated alloys is treated extensively in chapter 2 of the present work, being important in the study of the effects of short-range order on the resistivity of alloys.

1.2 Resistivity – Fundamentals

Understanding the physical processes that determine the electrical resistivity of a concentrated metallic alloy is a discouraging task because of the large number of possible contributions that could be involved. In addition to conduction electron scattering from thermally induced atomic displacements, there will be other direct contributions from atomic disorder, strain and band structure effects. The magnitude of such effects will be influenced by the homogeneity of the microstructure and will depend specifically upon whether the spatial extent or "scale" of the inhomogeneity is greater or less than the conduction electron mean free path. The purpose of the remaining part of this first chapter is to introduce in a general way the relation between the electrical resistivity and conduction electron scattering.

1.2.1 Resistivity and Electron Scattering in Solids

The electrical resistivity of a solid can be determined by passing a current i through the specimen of cross-section area a and measuring the resultant voltage drop v over a distance l. The electrical resistivity ρ is then given by

$$\begin{aligned} \rho &= \frac{va}{il} \\ &= \frac{ra}{l} \end{aligned} \tag{1.1}$$

where $r = v/i$ is the resistance of the specimen between the potential contacts. The resistivities of metals and alloy are usually given in units $\mu\Omega$·cm. Under the influence of an applied field the conduction electrons drift through an ionic array, the resistance being determined by the rate at which they are scattered from some initial state $\Phi_{\mathbf{k}}$ into a final state $\Psi_{\mathbf{k}'}$. As evident from the Fermi-Dirac distribution of electron energies, only electrons within an energy range $\sim k_B T$ around the Fermi surface can increase their energy by some small amount under the influence of the external field. However, since the Fermi energy $E_F \gg k_B T$ over the normal range of temperatures of interest, the vectors $\mathbf{k}$ and $\mathbf{k}'$ must terminate on the sharply defined Fermi surface. In the case of a spherical Fermi surface the maximum amplitude of the scattering wave vector is equal to $2k_F$. The scattering rate will be determined by the strength of the scattering potential $V(\mathbf{r})$ and, in non-simple metals, the availability of states into which the electrons can be scattered. The scattering probability can be written as [61]

$$P_{\mathbf{k}\mathbf{k}'} = \frac{2\pi}{\hbar}|\langle\Psi_{\mathbf{k}'}|V(\mathbf{r})|\Phi_{\mathbf{k}}\rangle|^2 N(E_F), \tag{1.2}$$

where $\langle\Psi_{\mathbf{k}'}|V(\mathbf{r})|\Phi_{\mathbf{k}}\rangle$ is the scattering amplitude for transitions between an initial state $\Phi_{\mathbf{k}}$ and a final state $\Psi_{\mathbf{k}'}$ (i.e., the matrix element of the scattering potential $V(\mathbf{r})$ between the states $\Phi_{\mathbf{k}}$ and $\Psi_{\mathbf{k}'}$) and $N(E_F)$ is the density of states at the Fermi energy E_F into which the electrons can be scattered. This latter term arises because of the necessity to have vacant states ready to accept the scattered electrons.

This scattering rate may be approximately described in terms of a relaxation time τ averaged over the Fermi surface. In the simple case of a spherical Fermi surface (i.e., free conduction electrons) $|\mathbf{k}'| = |\mathbf{k}| = k_F$, the scattering probability $P_{\mathbf{k}\mathbf{k}'}$ will depend only upon the angle θ between $\mathbf{k}$ and $\mathbf{k}'$. The relaxation time averaged over the Fermi surface can then be written as

$$\frac{1}{\tau} \propto \int P(\theta)(1 - \cos\theta) d\mathbf{S} \tag{1.3}$$

or

$$\frac{1}{\tau} \propto \int P(\theta)(1 - \cos\theta)\sin\theta d\theta \tag{1.4}$$

where $P(\theta)$ is now simply the probability of scattering through an angle θ into the element of area $d\mathbf{S}$ on the Fermi surface. The term $(1 - \cos\theta)$ essentially arises because we are only interested in the total change in momentum resolved in the direction of the electric field.

The final step in determining the resistivity is given by the Drude formula

$$\rho = \frac{m_e}{ne^2\tau} \tag{1.5}$$

where n is the number of electrons of mass m_e and charge e per unit volume. It should be emphasized that this simple derivation has been given mainly to illustrate

the link between the scattering process and the electrical resistivity. The assumption of free electrons and a uniform scattering rate over a spherical Fermi surface are clearly severe restrictions on its applicability. One might expect them to be reasonable within the first Brillouin zone, but generally the distortion of the Fermi surface and its intersection with the Brillouin zone boundaries might be expected to produce deviations from such simple behavior in most metals or alloys. Nevertheless, in many concentrated alloys of interest (particularly those that do not contain transition metals) it appears that the Fermi surface is still roughly spherical, at least as far as the majority charge carriers are concerned, so that a "nearly" free electron calculation can proceed. In other cases one clearly must take into account the effects of stronger scattering on the band structure of the alloy.

The degree of periodicity of the ionic array determines the amount of electron scattering and hence the electrical resistivity. For example, in a perfectly periodic array (implying an infinite array of identical ions each at rest on a lattice site) the electrons will suffer only Bragg scattering. While the probability of scattering is very large at the Bragg wavevectors, the scattering probability averaged over the Fermi surface is zero. This is because the Bragg scattering is very sharp and localized to a vanishingly small fraction of the Fermi surface, the width of the Bragg peaks being inversely proportional to the number of ions in the array.

The first Brillouin zone is also shown to emphasize the fact that Bragg diffraction occurs where the Fermi surface intersects the Brillouin zone boundary. In real solids the lack of perfect periodicity will give rise to additional diffuse scattering contributions, in direct analogy to the additional scattering (e.g., size or strain induced X-ray line broadening, short-range order diffuse scattering and thermal diffuse scattering) observed in a diffraction experiment. This additional scattering will lead to a non-zero scattering probability when averaged over the Fermi surface and hence result in a finite value of the electrical resistivity.

1.2.2 Isotropic and Anisotropic Scattering

A purely random, free electron alloy would produce isotropic scattering with the scattering probability (and hence the relaxation time τ) having the same value at all points on the Fermi surface. However, as the deviation from randomness increases, the diffuse scattering will become unevenly distributed over the Fermi surface, leading to an anisotropic relaxation time $\tau(\mathbf{k})$ that varies over the Fermi surface. Similar behavior will result if the electron wavefunctions are not spherically symmetric since the electrons at different places on the non-spherical Fermi surface will have wavefunctions of different s-, p- and d-like character. Applying equation (1.4) would then lead to errors since it gives only an average reciprocal relaxation time $\langle 1/\tau \rangle$ rather than properly taking into account the parallel contribution of all electrons to the total current flow. In the meantime it is important to note that an anisotropic relaxation time does not imply a direction dependence of the resistivity in real space. This is because the resistivity is determined from the average over all

scattering directions and will thus be isotropic in a cubic system in real space. In fact it is this averaging process that makes interpretation of resistivity data so difficult. Unlike conventional diffraction techniques, which can map out scattered intensities in two- or three-dimensional reciprocal space, an electrical resistivity measurement gives only a single value at any particular temperature and state of disorder. As there is no means of performing the back-transform from this single point, analysis of resistivity data must rely on calculation of electron scattering based on some model of the structure or microstructure concerned.

1.2.3 Atomic Correlations

It is also important to consider the spatial extent or "scale" of the atomic correlations. This is because there is a characteristic conduction electron mean free path Λ defined by

$$\Lambda = v_F \tau, \tag{1.6}$$

where v_F is the velocity of the electron at the Fermi level. This quantity is based on an average scattering probability and should not be simply interpreted as the real distance between scattering centers. However, it may be taken as a measure of the coherence length of the electron wave. Within this context, the conduction electrons will only be scattered coherently by deviations from perfect periodicity which occur within a volume $\sim \Lambda^3$. This is because scattering centers separated by a distance greater than Λ do not produce coherent scattering, the electron having effectively 'forgotten' its phase once it has traveled a distance $\sim \Lambda$. This increases the complexity of the problem considerably: we need to consider deviations from perfect periodicity on a scale Λ, but Λ is in turn determined by electron scattering effects, and hence the degree of imperfection. Such considerations do allow for the definition of "short" and "long" range atomic correlations, depending upon whether their spatial extent (or correlation length) is less than or greater than Λ respectively.

1.2.4 Lattice Scattering

So far we have assumed that the initial and final states $\mathbf{k}$ and $\mathbf{k}'$ lie on the Fermi surface, i.e. the scattering is elastic since there is no change in energy. We now want to consider this point in more detail. There are two constraints that must be applied to the scattering process: one relates to the fact that the vibrational energy levels of the lattice are restricted by the discrete nature of the lattice and the other is that the momentum of the system is conserved.

If there where no loss of energy from the electrons to the lattice, the electrons would steadily gain energy by being accelerated in the applied field and their effective temperature would rise indefinitely above that of the lattice. Since this does not occur, the scattering cannot be purely elastic. However, if the collision between an electron and an ion is treated classically the fraction of the kinetic energy lost by the

electron to the ion would be proportional to the ratio of their masses. For a typical metal this ratio is $\sim 10^{-5} - 10^{-6}$ and is small enough in relation to the Fermi energy to be neglected in the scattering process. It is large enough, however, to ensure that the electrons remain in thermal equilibrium with the lattice.

This problem can also be considered in terms of the elementary excitations of the lattice. In the Debye model of a solid the upper limit of phonon energy is by definition $k_B\Theta_D$, where Θ_D is the Debye temperature which typically lies in the range $100 - 500$ K. Thus, at any temperature the maximum energy that can be transferred in a single phonon process (the most likely event) is $\sim 200k_B - 400k_B$. As this is much less than typical Fermi energies ($\sim 10^5 k_B$) the scattering can again be considered as essentially elastic, although there is still the small but necessary energy transfer to the lattice. Note that this assumption is only true as far as resistivity is concerned. Other properties such as the thermopower and thermal conductivity by electrons are sensitive to the magnitude of energy transfer in relation to k_B rather than E_F and so one cannot neglect the inelastic scattering in such cases.

1.2.5 Conservation of Momentum

In a simple metal the conduction electrons are described by a wavefunction of the form

$$\Psi_{\mathbf{k}} = \frac{1}{\sqrt{\Omega}} e^{-i\mathbf{k}\cdot\mathbf{r}} \tag{1.7}$$

and carry a crystal momentum $\hbar\mathbf{k}$. In a non-simple metal the momentum is no longer constant but varies from place to place throughout the lattice, in which case $\hbar\mathbf{k}$ can be taken as a measure of the average momentum. When scattered from a state $\mathbf{k}$ to a state $\mathbf{k}'$ the momentum change $\hbar(\mathbf{k} - \mathbf{k}')$ is transmitted ultimately to the center of mass of the solid. The condition of conservation of momentum requires that

$$\mathbf{k}' - \mathbf{k} = \pm\mathbf{q} + \mathbf{g} \tag{1.8}$$

where $\mathbf{g}$ is a reciprocal lattice vector (or zero) and $\pm\mathbf{q}$ corresponds to the creation ($-$) a destruction ($+$) of a phonon of wavevector $\mathbf{q}$ with a consequential change in electron state. If $\mathbf{g} = 0$, $\mathbf{k}' - \mathbf{k} = \pm\mathbf{q}$ corresponds to the simple absorption or emission of a phonon. However, in the Debye model there is an upper limit to $|\mathbf{q}|$, this being the Debye wave number $|\mathbf{q}_D|$, and so the scattering angle in such "normal" processes is limited. The condition $\mathbf{k}' - \mathbf{k} = \mathbf{g}$ (i.e. $\mathbf{q} = 0$) corresponds to Bragg diffraction of the electrons from the set of lattice planes described by $\mathbf{g}$. Equation (1.8) with non-zero $\mathbf{g}$ thus corresponds to Bragg diffraction and simultaneous creation or anihilation of a phonon. This is called an Umklapp-process. These two scattering processes ($g = 0$ and $g \neq 0$ are often referred to simply as N-processes (normal processes) or U-processes.

The general importance of both of these scattering processes has been discussed in many texts (see e.g. [77]). The transfer of momentum to the phonons can cause them to drift in real space along with (N-processes) or against (U-processes) the electrons. This is called phonon drag and has significant effect on the thermoelectric properties of dilute alloys. However, in concentrated alloys there will usually be sufficient impurity scattering of the phonons to prevent such a phenomenon.

1.2.6 Residual Resistivity

The characteristic property of a metal is its electrical resistivity. In a pure metal this is governed mainly by the scattering of electrons by the lattice vibrations. At high temperatures, where the quantization of lattice waves is irrelevant, we may expect the scattering to be proportional to the square of the amplitude of the fluctuations of the ions about their equilibrium sites, hence

$$\rho \propto T, \quad T > \Theta_D \tag{1.9}$$

But, when we go below the Debye temperature, the lattice motion must be analyzed into phonons, and the proper description of the scattering of electrons is through the electron-phonon interaction, which gives rise to elementary processes (N- and/or U-processes). The potentialities for the scattering of electrons are much reduced. Because of the conservation of crystal momentum, and the smallness of q for the average phonon at low temperatures, the electron can only be scattered through a small angle. This reduces the electrical resistivity greatly, both because the actual effect of a single scattering through a small angle is not large and because the number of lattice modes which can take part in the scattering is greatly reduced. The resistivity varies approximately according to the low

$$\rho \propto T^5, \quad T < \Theta_D \tag{1.10}$$

In any actual metal specimen, we seldom see precisely this behavior, because of the effects of impurities and imperfections. These scatter the electrons with a more or less constant cross-section. The electrical resistivity due to impurities is independent of temperature

$$\rho_r = \text{constant}. \tag{1.11}$$

If we take our specimen to sufficiently low temperatures, this type of resistivity will finally remain, when the phonon scattering has become negligible. This is called *residual resistivity*.

In the remaining part of this introduction we shall give some general rules disclosed by experiments and their theoretical interpretation.

Matthiessen's Rule

In dilute alloys the scattering from impurity atoms is nearly independent of temperature and so the total resistivity $\rho_{tot}(T)$ at any measuring temperature T can be written as the sum of two components

$$\rho_{tot}(T) = \rho_r + \rho_h(T), \tag{1.12}$$

where ρ_r is the temperature independent residual (i.e. impurity) resistivity and $\rho_h(T)$ is the resistivity of the pure host material at that temperature. This is known as Matthiessen's rule and will only be valid if the impurity and phonon scattering are independent and if the relaxation time is isotropic. These assumptions are only partly true in most systems and there is a large body of work devoted to studying "deviations from Matthiessen's rule", DMR.

Matthiessen's rule is often applied to the case of concentrated alloys. This extrapolation of Matthiessen's original work is then written as

$$\rho_{tot}(T) = \rho_r + \rho_p(T), \tag{1.13}$$

and collects all contributions from scattering due to atomic disorder (excluding that due to thermally induced lattice displacements) into a residual resistivity ρ_r, leaving separate the phonon scattering of the alloy lattice $\rho_p(T)$. The first of these is usually described as being "temperature independent". This means that, while ρ_r may of course depend on temperature through the degree of atomic disorder which changes with temperature, it does not have the intrinsic temperature dependence of $\rho_p(T)$.

Nordheim's Rule

The residual resistivity of a binary alloy containing a mole fraction x of element A and $(1-x)$ of element B varies as

$$\rho_r(x) \propto x(1-x) \tag{1.14}$$

This means that ρ_r describe an inverted parabola as we go from pure A to pure B. In many cases the rule is quite well obeyed, especially when one allows the gradual change of the basic electronic properties of the solid as one goes from A to B. Sometimes, however, there are significant deviations from the rule, as when transition metals are alloyed with noble metals.

Order-Disorder Effects

The residual resistivity of an ordered alloy phase is zero. This can be seen very clearly in studies of the Cu–Au system (see e.g. [42]). The fall in resistivity as the alloy passes through each of the critical compositions Cu_3Au, CuAu and $CuAu_3$ clearly proves this principle. The argument is, of course, that in the ordered alloy, as

in the pure metal, the regular lattice structure only alters the dynamical properties of the electrons and does not cause them to be scattered incoherently.

As the main concern in this work is the influence of order on the residual resistivity, the next chapter is entirely dedicated to the subject of order in crystal lattices. A detailed treatment of the calculation of resistivity adopted in this work is postponed to chapter 3.

Chapter 2

Order in Crystal Lattices

A large number of solid solutions become ordered at low temperatures. The process of ordering involves a change from a statistically nearly random distribution of atoms among the lattice sites into a more regular arrangement, whereby designated sites are occupied predominantly by one kind of atoms. In a *disordered* alloy of composition AB, for example, any given atom site is occupied randomly by either A or B atoms, but on ordering, A and B atoms segregate more or less completely to designated atomic sites, so that the resulting arrangement can be described as a lattice of A atoms inter-penetrating a lattice of B atoms. The segregation of atoms to particular sites may take place with little or no deformation of the lattice, creating an *ordered solid solution*, or *superlattice*, or *superstructure*, out of a random solid solution.

In a disordered solid solution, crystallographically equivalent planes of atoms are identical (statistically) with one another, but in an ordered superlattice this need not be true. For example, alternate planes of a set may become A-rich and B-rich planes, respectively, and the distance between identical planes may become twice the distance between identical planes of the disordered alloy (or some other multiple of this distance). Hence, the structures of ordered alloys usually produce diffraction patterns that have additional Bragg reflection, the *superlattice lines* associated with the new and larger unit cells which are not present in the patterns of the disordered alloys.

The formation of superlattices, frequently described as *long-range order*, takes place at relatively low temperatures and usually at compositions expressed by a simple formula such as AB or AB_3 or at compositions near these. At all temperatures above a certain critical temperature the usual randomness persists; when the temperature is lowered through the critical point, order sets in and increases as the temperature drops, approaching perfection only at low temperatures. Nevertheless, over certain ranges of composition and at temperatures above the critical temperature, the structures may at times be neither perfectly random nor perfectly ordered; even in the disordered state certain correlations may be described as *short-range order*. Such correlations frequently exist in alloys which do not show a state with long-range order at any temperature.

2.1 Theoretical Considerations of the State of Order

All solid phases are solutions since impurities will always be present in the form of either substitutional or interstitial impurity. Even in "pure" crystals whose impurity content is immeasurably small, vacancies, considered as solute impurities, must be present at all finite temperatures even at 0 K.

The distribution of atoms on lattice sites is generally not random, i.e., some correlation is usually present. In this section, we examine how correlations are defined, and how various averaging techniques lead to the concepts of short-range and long-range order.

2.1.1 Site Occupation

Let there be p kinds of atoms in a solid solution. An average lattice is defined in such a way that each kind of atom may be associated uniquely with a lattice point. A lattice vector will be denoted by

$$\mathbf{R}_m = \sum_i i\mathbf{a}_i \qquad (i = 1, 2, 3) \tag{2.1}$$

where $\mathbf{a}_i$ are lattice translation vectors and i are integers.

Site occupation operators are defined by [30]

$$\sigma^\alpha(\mathbf{R}_m) = \sigma_m^\alpha = \begin{cases} 1 & \text{if an atom of type } \alpha \text{ is at site } m, \\ 0 & \text{if an atom of type } \beta \neq \alpha \text{ is at site } m, \end{cases} \tag{2.2}$$

with

$$\alpha = \underbrace{A, B, C, \ldots}_{p \text{ kinds}} \tag{2.3}$$

The crystal average of σ_m^α, or concentration of atom of type α is defined as

$$\bar{c}_\alpha = \frac{1}{N} \sum_m \sigma_m^\alpha, \tag{2.4}$$

where the sum extends over all lattice points m of the crystal or portion of the crystal considered. Deviations from the mean occupation are given by

$$\gamma_m^\alpha = \sigma_m^\alpha - \bar{c}_\alpha = \begin{cases} 1 - \bar{c}_\alpha \\ -\bar{c}_\alpha \end{cases} \tag{2.5}$$

We have the following conservation relations, or sum rules:

$$\sum_{\alpha} \sigma_m^{\alpha} = \sum_{\alpha} \bar{c}_{\alpha} = 1 \tag{2.6}$$

$$\sum_{\alpha} \gamma_m^{\alpha} = \sum_{m} \gamma_m^{\alpha} = 0 \tag{2.7}$$

In an $(p+1)$-component solution, there are thus p independent concentrations.

Consider an N-point cluster. The *state of order* of a solution can be characterized by specifying sets of configuration variables $\langle \ldots \rangle$ which denote the probability of finding, in an ensemble of $\mathcal{M}$ systems, a cluster with α-type atom at m, β-type at n, ..., γ-type at l. We have, for the expectation value of that particular cluster (or cluster frequency or probability)

$$\langle \sigma_m^{\alpha} \sigma_n^{\beta} \ldots \sigma_l^{\gamma} \rangle = \sum_{states} \sigma_m^{\alpha} \sigma_n^{\beta} \ldots \sigma_l^{\gamma} \mathcal{P}(state) \tag{2.8}$$

where $\mathcal{P}$ is the probability of finding the system in the state considered. For example, if a canonical ensemble is used

$$\mathcal{P}(state) = \frac{1}{\mathcal{Z}} e^{-\frac{E(state)}{k_B T}} \tag{2.9}$$

where $\mathcal{Z}$ is the partition function, E denoting the internal energy of a system, T, the absolute temperature, and k_B, Boltzmann's constant. Canonical ensemble averaging implies that each system must have the same atom concentration $\bar{c}_{\alpha}$ ($\alpha = A, B, \ldots$), as given by Eq. (2.4).

2.1.2 Long-Range Order Parameter

At high temperatures, or when the compositions deviate from ideal values, very imperfect states of order must exist in which the crystal is only partially ordered. Recognition of this fact has created a further need for suitable general description of imperfectly ordered crystals. In such crystals both the unit cell and the translation group lose their strict significance since the lattice translation vectors may sometimes join atoms of different kinds rather than identical atoms only, as in the perfectly ordered structures. The state of order may then be more conveniently described by a set of parameters related to *pair-density functions*, which describe the state of occupation not of single sites but in terms of pairs of sites. The point of view of the earlier theories of Bragg-Williams [9] and Bethe [7] (quasi-chemical theories) will now be considered in some detail and will be followed by an outline of pair-density theories.

Nontrivial single-site averages are often required. These can be obtained by sublattice averaging as follows: Consider an ensemble of systems, each containing $N_1 \times N_2 \times N_3$ unit cells. Assume that initially all systems had identical distributions σ_m^{α}. Then allow some defect exchanges to take place within each system, while

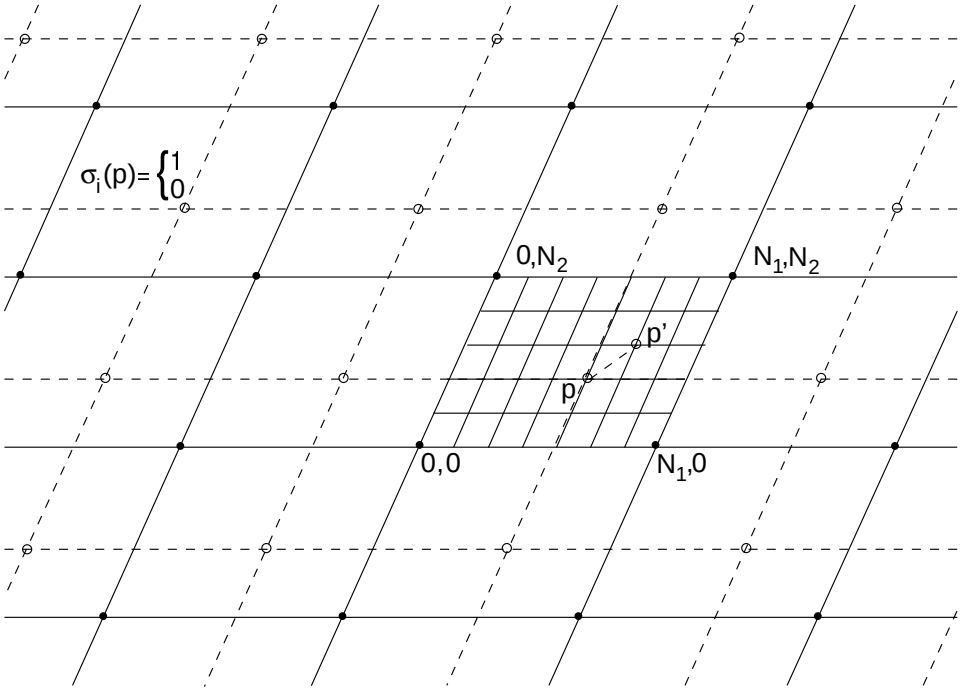

Figure 2.1: Ensemble of supercells each containing $N_1 \times N_2 \times N_3$ unit cells. Superlattice through p shown dashed. [29]

conserving the value of the integral energy E_0. This procedure automatically insures long-range correlations between systems so that the micro-canonical ensemble average gives

$$c_m^\alpha = \langle \sigma_m^\alpha \rangle_0 = \frac{1}{\mathcal{M}} \sum_{syst.} \sigma_m^\alpha. \tag{2.10}$$

A fictitious average crystal can now be defined, such as the one outlined in Fig. 2.1, each lattice point of which is a microsystem characterized by continuously varying concentrations

$$0 \leq c_m^\alpha \leq 1. \tag{2.11}$$

The resulting sample average crystal or supercell necessarily has periodic boundary conditions. The grids through the lattice points of the ensemble may be interpreted as sublattices in the Bragg-Williams sense. For example, β-brass ordering can be described by an average system consisting of a single BCC unit cell, with one "average atom" at (000), and the other at $\left(\frac{1}{2}\frac{1}{2}\frac{1}{2}\right)$.

In general, *long-range order* (LRO) *parameters* are defined as linear combinations of the micro-canonical average concentrations $c_m^\alpha(p)$. There may be N such LRO parameters, $N = N_1 \times N_2 \times N_3$ being chosen large enough to display the essential features of the single-site distributions one wishes to describe.

In a fully ordered alloy there are great distances within a crystal through which there is a perfect arrangement of A atoms on one set of lattice points and B atoms on another set. The ordering is consistent, in step, through long distances. The degree of this long-range order may be defined by a fraction S, which varies from zero at complete disorder up to unity at complete order; S, for an AB superlattice, is the fraction of the atoms that are in their right positions on a given sublattice minus the fraction that are in wrong positions. As an example, consider an alloy AB in which 100 A atoms and 100 B atoms are randomly arranged; just half of the A atoms are in the places they would occupy in the ordered structure, and the other half are in wrong positions; and the same would be true for the B atoms, giving $S = 0$. If 75 A atoms were right and 25 wrong, the degree of order would be $0.75 - 0.25 = 0.50$.

This definition may be generalized to cover the condition in which n atomic positions of a total number of N can be occupied by either kind of atom. In a A_3B structure the fraction $n/N = \frac{1}{2}$, since even in the completely disordered state, half the atomic positions are still occupied exclusively by A kind of atoms. Suppose a fraction r of the n sites is occupied by A atoms in the state of perfect order; these nr sites are right positions for A atoms. In a partially ordered alloy, some of these positions are filled by A and some by B atoms. If p is the probability that a right position for an A atom is filled by an A atom, the long-distance order may be defined by the relation

$$S = \frac{p - r}{1 - r} \tag{2.12}$$

which varies from 0 to 1 as order increases.

2.1.3 Short-Range Order Parameter

For the point cluster, in a canonical ensemble, the trivial single-site average is obtained

$$\langle \sigma_m^\alpha \rangle = \bar{c}_\alpha \tag{2.13}$$

all points of the system's Bravais lattice being assumed equivalent.

Of more interest is the pair probability $\langle \sigma_m^\alpha \sigma_n^\beta \rangle$, or rather, the pair correlation function

$$q_{mn} = \langle \gamma_m^\alpha \gamma_n^\beta \rangle = \langle \sigma_m^\alpha \sigma_n^\beta \rangle - \bar{c}_\alpha \bar{c}_\beta. \tag{2.14}$$

We also have, by application of the mean value theorem,

$$q_{mn} = \bar{c}_\alpha [P_{mn}^{\alpha\beta} - \bar{c}_\beta] = \bar{c}_\beta [P_{mn}^{\alpha\beta} - \bar{c}_\alpha] \tag{2.15}$$

where

$$P_{mn}^{\alpha\beta} = \frac{\langle \sigma_m^\alpha \sigma_n^\beta \rangle}{\langle \sigma_m^\alpha \rangle} \tag{2.16}$$

is the probability of finding a β-type defect at n, given one of α-type at m. By Eqs. (2.14) and (2.15), the pair correlation function at the origin, or autocorrelation, is

$$q^0_{mn} \equiv q_{mn}(0) = \bar{c}_\alpha(\delta_{\alpha\beta} - \bar{c}_\beta) = \bar{c}_\beta(\delta_{\beta\alpha} - \bar{c}_\alpha), \tag{2.17}$$

where $\delta_{\alpha\beta}$ vanishes unless α and β are equal. The normalized pair correlation function gives the Warren-Cowley *short-range order* (SRO) *parameters*

$$\alpha_{mn}(r) = \frac{q_{mn}(r)}{q^0_{mn}} \tag{2.18}$$

whose value at the origin ($r = 0$) must be unity. In an $(n + 1)$-component solution there are $n(n + 1)/2$ linearly independent pair correlation functions.

The presence of both long-range order and short-range order can be measured experimentally by their effect on the scattering of X-rays, electrons, and neutrons, and by their influence upon certain mechanical, physical, and thermal properties.

2.2 Detection of Order with X-Rays

2.2.1 General Remarks

The degree of long-distance order in a superlattice may be determined from the intensity of the superlattice lines. For example, if the equation for the intensity of reflection is evaluated for $AuCu_3$, where atoms with scattering power f_{Au} are at positions with coordinates (000) and atoms with scattering power f_{Cu} are at $(\frac{1}{2}\frac{1}{2}0)$, $(\frac{1}{2}0\frac{1}{2})$, and $(0\frac{1}{2}\frac{1}{2})$, it will be seen that there are two classes of reflections. The main reflections occur when indices are all odd or all even, and have intensities proportional to $|F|^2 = (f_{Au} + 3f_{Cu})^2$. The superlattice lines occur when indices are mixed odd and even, and have intensities proportional to $|F|^2 = (f_{Au} - f_{Cu})^2$ in a completely ordered alloy and proportional to $S^2(f_{Au} - f_{Cu})^2$ in a partially ordered alloy having S as the degree of long-range order. Thus, in a fully disordered alloy $S = 0$ and the superlattice lines vanish, since each lattice point then has, on the average, the same scattering power. Measurements of long-range order by reflected intensities require consideration of the geometry used, absorption, extinction, the multiplicity of the reflection, and the temperature factor, and have been made using both powder and single-crystal methods. If the atomic scattering factors posses nearly equal values as, for example, in the Cu-Zn system, the intensity of the superlattice reflections may be insufficient to be recorded unless special techniques are used. With powder techniques one can sometimes employ X-rays of special wavelength which enhance the difference as a result of divergence in the anomalous scattering factors. Even more helpful are single-crystal methods where the diffractometer counter can be positioned directly at the expected superlattice reflections.

Single-crystal methods have the advantage of giving greater intensities. The use of diffractometers permits a detailed study of the changes of intensity with time and

the determination of the shape of the superlattice reflections.

The nature of the short-range order in alloys has been studied by investigating the intensity of the diffuse background between the main lattice reflections in the region where superlattice peaks would appear with long-range order. The X-ray techniques for measuring short-range order have been developed to a large degree by Warren [72] and his colleagues [17, 74]. Wilchinsky [74] showed that short-range order parameters could be determined from powder photographs, but because of difficulty in accurately correcting for the diffuse scattering arising from thermal motion of the atoms, powder methods are inferior to single-crystal methods. The classical single-crystal, X-ray diffuse scattering study of short-range order in Cu_3Au was made by Cowley [17] using single-crystal diffracted intensities with monochromatized radiation. A number of corrections have been introduced into this method in later studies but the general nature of the short-range order seems to be about the same as was indicated by the original measurements: there is an excess of Cu atoms in the first shell around an atom of Au compared with a random distribution, a deficiency in the second shell, and a very small deviation from randomness in the third shell; non-randomness extends out much farther than had previously been thought.

Following the original work of Cowley the diffraction theory describing the diffuse X-ray scattering has been modified and extended to include a number of other effects which can produce diffuse scattering contributions to the diffraction pattern of an alloy. The measured intensity is the sum of at least five major contributions:

$$I = I_{CM} + I_T + I_{LO} + I_{SE} + I_A \tag{2.19}$$

where I_{CM} is the Compton modified scattering, I_T is the temperature-diffuse scattering, I_{LO} is the diffuse scattering due to local order, I_{SE} is a diffuse modulation in scattering due to atom-size effects in solid solutions, and I_A is air scattering. In addition, if measurements are made in the very low-angle region of 2θ, the double Bragg scattering can interfere. The I_{CM} and I_A contributions are readily determined, I_A by direct measurement and I_{CM} by use of tabulated values. However, the remaining contributions present several problems. The particular effects of scattering due to static displacements resulting from disparity of atomic sizes and dynamic displacements produced by thermal vibrations of the lattice have been given much attention.

The existence of short-range order in an alloy produces diffuse peaks at the positions of sharp peaks that occur with an ordered alloy, which are superimposed on a diffuse background that is modulated by the existence of differing interatomic distances between nearest neighbors – the so-called size-effect modulation I_{SE}. By measuring diffraction intensities from powders, it is possible to make corrections and compute some approximate short-range order coefficients; but a more reliable procedure is to use intensities from a single crystal, with measurements throughout the volume of an unsymmetrical portion of a unit cell in the reciprocal lattice, determining the short-range order coefficients in a series representing the size effect, combining the data from peaks and from diffuse scattering.

Many investigations of local order and size effect were based only on measurements of the diffuse scattering between fundamental peaks, but in some investigations the diffuse scattering data were supplemented by integrated intensities of peaks, treating the displacements due to atom-size disparity as a quasi temperature reduction in the intensities of the fundamental reflections. A further improvement is possible if the different kinds of atoms are treated individually, and if the corrections for I_T and I_{SE} are minimized by measuring the intensities in a unit cell of reciprocal space that is near the origin, where these corrections are smaller than they are at larger distances from the origin.

An experimental determination of short-range order coefficients involves the measurements of weak intensities at many orientations, preferably at temperatures above the critical temperature for long-range ordering; it also involves standardizing the intensities with respect to the intensity of the incident beam, and it requires corrections that frequently amount to a considerable fraction of the entire measured intensity. An experimental determination of size-effect modulation and the determination of size-effect coefficients encounter similar difficulties.

2.2.2 Diffuse X-Ray Scattering Modulated by Local Order

It was pointed out by von Laue [49] that when two kinds of atoms are randomly distributed on a lattice X-ray diffraction will produce a monotonic diffuse intensity expressed in electron units per atom as

$$\frac{I_{eu}}{N} = c_A c_B (f_A - f_B)^2 \tag{2.20}$$

where the alloy consists of atomic fractions c_A and c_B of A and B atoms, with atomic scattering factors f_A and f_B, respectively, and N is the total number of atoms irradiated by the beam. Not only did von Laue assume that the A and B atoms were randomly distributed, but he also assumed that the atoms are precisely at their lattice sites.

With the observation of long-range order in certain alloys, it became clear that, in at least some cases, an atom may have preference for certain kinds of near neighbors. Also, because atoms are of different sizes, they may be displaced slightly from their normal lattice sites due to a non-centrosymmetric arrangement of their neighbors. These two effects cause the Laue monotonic diffuse intensity to be modulated. Thus a study of how this diffuse scattering is modulated could lead to an understanding of the long- and short-range interactions between atoms in an alloy.

We assume the atoms are precisely on their lattice sites and treat only the fact that they are not randomly distributed. The total coherent intensity in electron units is given by the well-known formula

$$I_{eu} = \sum_m \sum_n f_m f_n e^{i\mathbf{k}\cdot(\mathbf{R}_m - \mathbf{R}_n)} \tag{2.21}$$

where f_m and f_n are the atomic scattering factors for the atoms occupying the sites m and n separated by the interatomic lattice vector $\mathbf{R}_m - \mathbf{R}_n$ and the vector $\mathbf{k} = 2\pi(\mathbf{S}-\mathbf{S_0})/\lambda$ with $\mathbf{S}$ and $\mathbf{S_0}$ being unit vectors in the directions of the scattered and incident beams, respectively, of wavelength λ. The sums are to be taken over all possible pairs of atoms that can be formed in the crystal with a separation of $\mathbf{R}_m-\mathbf{R}_n$, i.e., all pairs formed by each of N atoms irradiated in the incident beamsIn performing the double sum, we shall always view this as a summation over pairs of atoms such that the indices m and n differ by a constant. Since the X-ray beam averages many pairs, we are able to recover only this average. Thus we should keep in mind that $f_m f_n$ and $\mathbf{R}_m - \mathbf{R}_n$ are averages to be taken over all pairs of atoms that can be formed in the crystal for a constant value of $m - n$. If we remove from the double sum of Eq. (2.21) all those pairs for which $m = n$, we obtain the sum over all A atoms plus all B atoms with themselves plus the term for $m \neq n$. If there are N atoms in the crystal, the number of AA pairs is Nc_A and the number of BB pairs is Nc_B when $\mathbf{R}_m - \mathbf{R}_n = 0$. Therefore,

$$I_{eu} = N(c_A f_A^2 + c_B f_B^2) + \sum_m \sum_{n \neq m} f_m f_n e^{i\mathbf{k}\cdot(\mathbf{R}_m - \mathbf{R}_n)} \tag{2.22}$$

The first term of Eq. (2.22) represents the average over all values $\mathbf{k}$ of the total coherent intensity from our alloy $\langle I \rangle_{Total}$, and the second term is just the phase factor which distributes this intensity in reciprocal or $\mathbf{k}$ space. We are interested in the modulation of the diffuse intensity caused by the order among the atoms which only extends over some unit cell dimensions and not in the fundamental crystalline Bragg reflections. Hence we want to subtract from Eq. (2.22) that intensity associated with the fundamental Bragg reflections. These reflections are independent of the state of order in the crystal. They depend only on the average composition and are given by

$$I_{Fund} = \sum_m \sum_n (c_A f_A + c_B f_B)^2 e^{i\mathbf{k}\cdot(\mathbf{R}_m - \mathbf{R}_n)} \tag{2.23}$$

If we subtract the average value $\langle I \rangle_{Fund} = N(c_A f_A + c_B f_B)^2$ from the average total intensity $\langle I \rangle_{Total} = N(c_A f_A^2 + c_B f_B^2)$ we have

$$\langle I \rangle_{Diffuse} = N c_A c_B (f_A - f_B)^2 \tag{2.24}$$

This is just the Laue monotonic diffuse scattering for a random distribution of A and B atoms. This intensity arises from the fact that there are two kinds of atoms present and depends on the difference in their scattering factors.

We will now introduce the concept of order into Eq. (2.22) using the conditional probability P_{mn}^{AB} which is defined as the probability of finding an A atom at the lattice site m after having found a B atom at n. After rearranging a few terms, we shall subtract the intensity due to the fundamental Bragg reflections, leaving the Laue monotonic diffuse intensity modulated due to the ordered arrangement of the

atoms. The term $c_B P_{mn}^{AB}$ is the probability of reaching into the crystal at random a B atom at site n then finding an A atom at the site m. Since the number of BA pairs must equal the AB pairs, $c_B P_{mn}^{AB} = c_A P_{mn}^{BA}$. Also

$$\begin{aligned} P_{mn}^{BB} &= 1 - P_{mn}^{AB} \\ P_{mn}^{AA} &= 1 - P_{mn}^{BA} \end{aligned}$$

We want to evaluate the second term of Eq. (2.22) using these conditional probabilities. We assume N large enough to neglect edge effects. To include all possible pairs, $f_m f_n$ is evaluated for AA, AB, BA, and BB pairs separated a distance $\mathbf{R}_m - \mathbf{R}_n$ such that

$$\langle f_m f_n \rangle = c_A P_{mn}^{AA} f_A^2 + c_A P_{mn}^{BA} f_A f_B + c_B P_{mn}^{AB} f_B f_A + c_B P_{mn}^{BB} f_B^2 \tag{2.25}$$

Using this relation for $f_m f_n$ in the double sum of Eq. (2.22) and substituting

$$\begin{aligned} P_{mn}^{AB} &= \frac{P_{mn}^{BA} c_A}{c_B} \\ P_{mn}^{AA} &= 1 - P_{mn}^{BA} \\ P_{mn}^{BB} &= 1 - \frac{P_{mn}^{BA} c_A}{c_B} \end{aligned}$$

we have

$$\begin{aligned} I_{eu} &= N\left(c_A f_A^2 + c_B f_B^2\right) \\ &\quad + \sum_m \sum_{n \neq m} \left[c_A \left(1 - P_{mn}^{BA}\right) f_A^2 + 2 c_A P_{mn}^{BA} f_A f_B + c_B \left(1 - P_{mn}^{BA} \frac{c_A}{c_B}\right) f_B^2 \right] \\ &\quad \times e^{i\mathbf{k}\cdot(\mathbf{R}_m - \mathbf{R}_n)} \end{aligned} \tag{2.26}$$

At this point we wish to separate from Eq. (2.26) the term representing the sharp fundamental Bragg reflections that are unaffected by order. We subtract Eq. (2.23) from Eq. (2.26) to arrive at the intensity I_{order} due to order in the alloy,

$$I_{eu} - I_{fund} = I_{order} \tag{2.27}$$

$$\begin{aligned} &= N c_A c_B (f_A - f_B)^2 \\ &\quad + \sum_m \sum_{n \neq m} \Big[c_A (1 - P_{mn}^{BA}) f_A^2 + 2 c_A P_{mn}^{BA} f_A f_B \\ &\quad + c_B \left(1 - P_{mn}^{BA} \frac{c_A}{c_B}\right) f_B^2 - (c_A f_A + c_B f_B)^2 \Big] e^{i\mathbf{k}\cdot(\mathbf{R}_m - \mathbf{R}_n)} \end{aligned} \tag{2.28}$$

By rearranging terms and with the substitutions

$$\begin{aligned} c_A - c_A^2 &= c_A c_B \\ c_B - c_B^2 &= c_A c_B \end{aligned}$$

Eq. (2.28) can be written as

$$\begin{aligned} I_{order} &= N c_A c_B (f_A - f_B)^2 \\ &\quad + \sum_m \sum_{n \neq m} c_A c_B (f_A - f_B)^2 \left(1 - \frac{P_{mn}^{BA}}{c_B}\right) e^{i\mathbf{k}\cdot(\mathbf{R}_m - \mathbf{R}_n)} \end{aligned} \tag{2.29}$$

Finally, the order coefficient is defined as

$$\alpha_{mn} = \frac{1 - P_{mn}^{BA}}{c_B} \tag{2.30}$$

and the first term of Eq. (2.29) is placed under double summation giving

$$I_{order} = \sum_m \sum_n c_A c_B (f_A - f_B)^2 \alpha_{mn} e^{i\mathbf{k}\cdot(\mathbf{R}_m - \mathbf{R}_n)} \tag{2.31}$$

This result was first given by Cowley [17]. It is completely general and may be specialized for a binary alloy of any crystal structure. The only assumption is that the atoms are precisely on their lattice sites. From Eq. (2.30), we have on the average, for a random distribution of atoms, $\alpha_{mn} = 0$ if $m \neq n$, but $\alpha_{mn} = 1$ if $m = n$ in all cases because $P_{m=n}^{BA} = 0$ as it is impossible to find a B atom on the same site as an A atom.

Walker and Keating [70, 71], however, have pointed out that the thermal vibrations of the atoms also affect the order parameters. The α_{mn}'s are reduced by an $e^{-2M\phi}$ factor, where $2M$ is the usual Debye-Waller factor and ϕ is a function of $\mathbf{R}_m - \mathbf{R}_n$ being slightly different for each coordination shell. The lower-order α_{mn}'s are less affected than those of higher order, and if the intensity measurements are made in the region of the first reciprocal unit cell at low temperatures the effect is small. For the case of Cu_3Au with intensity measurements made at 405°C near the (100) superstructure reflection, Moss [56] found that this temperature factor affected the α_{mn}'s by approximately one percent.

A preference for the atoms to choose unlike nearest neighbors is referred to as short-range order. In this case the diffuse intensity is distributed away from the fundamental Bragg reflections. A preference for like nearest neighbors is termed clustering and the diffuse intensity is found nearer to the fundamental Bragg peaks because the first nearest-neighbor α will be positive. For alloys having a strong tendency to cluster, low-angle scattering techniques are useful or necessary to measure the intensity distribution.

The order coefficients can also be used to describe long-range order as shown by Cowley [17, 18]. In this case their absolute values would be a maximum. They are

related to the Bragg-Williams [9] order parameter S, which is proportional to the square root of the intensity of the superstructure reflections. The long-range order parameter S is unity for the fully ordered case and zero if the atoms are distributed at random.

For complete long-range order, all the Laue monotonic diffuse intensity is gathered up into sharp superstructure reflections. When there is only partial long-range order, that part of the Laue monotonic diffuse scattering associated with the superstructure reflections is equal to S^2. Thus S is related to the number of wrongly occupied sites. Chipman [13] separated the superstructure reflections from the diffuse background for partially ordered Cu_3Au crystal and was able to determine how the wrongly occupied sites were distributed.

2.3 Detection of Order Using Electrical Resistivity Measurements

A particular feature of alloy systems is that frequently the atoms concerned are difficult to distinguish by X-ray diffraction. This arises when, as is often the case, the elements lie close together in the periodic table and therefore have similar numbers of electrons and similar scattering factors for X-rays. In the classic case of β-brass it is not possible to show up the ordering unless the frequency of the X-rays is very carefully chosen. Only by selecting a frequency which is close to that of an absorption line is the ratio of the scattering factors of the Cu and Zn atoms made sufficiently different from unity for the superlattice to be observed.

Another useful method of investigation of order in alloys, which is almost entirely restricted to metallic systems, is that using electrical resistivity measurements. For alloys this is a simple and sensitive method of detecting order-disorder transitions. The quantitative relationship between resistivity and order was given in the work of Rossiter [61]. For the resistivity of a short-range ordered state, ρ_{SRO}, relative to that of a completely disordered state, ρ_D, he gives

$$\frac{\rho_{SRO}}{\rho_D} = \sum_i z_i \alpha_i Y_i \tag{2.32}$$

where α_i are the Warren-Cowley SRO parameters, z_i represent different coordination spheres and Y_i is an oscillating function which depends on Fermi wave number, coordination radius and atomic potential. In the case of long-range order, Rossiter gives

$$\frac{\rho_{LRO}}{\rho_D} = \frac{1 - S^2}{1 - CS^2} \tag{2.33}$$

where S is the LRO parameter and the constant C depends on the specific band structure.

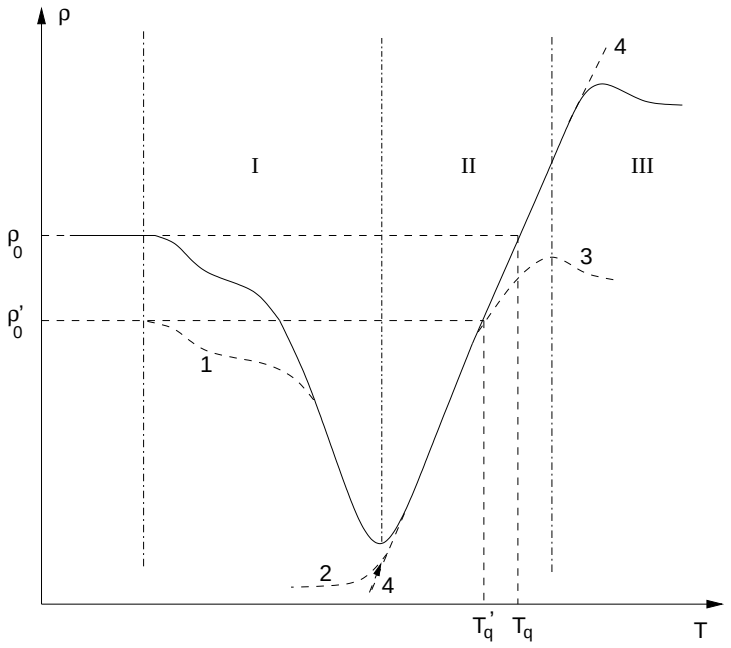

Figure 2.2: Schematic plot of residual resistivity as a function of temperature during isochronal annealing for the case of a decrease of resistivity with increasing degree of order.

Eq. (2.33) allows a direct determination of LRO parameter from resistivity measurements by using the constant C as a fit parameter. Eq. (2.32) is of more complicated character, where besides the SRO parameters in different coordinations spheres there enter details of the band structure (Y_i) which influence sign and magnitude of resistivity variation with degree of SRO. However, restricting to nearest neighbors and using an adequate model for the dependence of α on temperature and concentration, reliable SRO parameters have been deduced from resistivity measurements for several solid solutions (see e.g. [59]).

By applying isochronal and isothermal heat treatment to samples, temperature treatments for resistivity measurements, which allow observations of ordering or disordering with temperature and time, are done. A typical plot of resistivity against temperature as measured during isochronal annealing where temperature is increased in steps, each level being held constant for the same time interval, is given in Fig. 2.2. Several features of the alloy system as sign and magnitude of resistivity variation with degree of order, or influence of thermal or mechanical treatment can be determined from such investigations [60].

Range I of Fig. 2.2 corresponds to an increase of order due to a growing atomic mobility of surplus and thermal vacancies that allow rearrangements of atoms and the formation of ordered states. Range II encloses the "equilibrium curve" (curve 4), where every measured resistivity is an equilibrium value due to the fact that the annealing time at these temperatures is long enough for the system to become

ordered during this time. Range III extends over high temperatures at which the reordering rate during the quench is so fast that deviations of measured resistivity from equilibrium curve are encountered. Curve 1 corresponds to a sample that suffered a different thermal and mechanical pre-treatment. Curve 2 corresponds is obtained when the atomic mobility is frozen. Curve 3 shows the influence of quenching rate. T_q and $T_q^{'}$ are the temperatures at which the same resistivity as that at the beginning of the experiment, ρ_0 and $\rho_0^{'}$ for the two different pre-treated samples, respectively, is measured.

Figure 2.2 is that of a sample by which the resistivity decreases with order. The opposite case of increasing resistivity with order can also be encountered. The plot in such a case is simply the mirror image of Fig. 2.2 relative to the temperature axis.

Two kinds of complication arise. Firstly, if the ordered form has a domain structure the scattering of the electrons at the domain walls may cause the resistivity to be unduly large. Secondly, what has been said about the effect of order on resistivity is valid for long-range order (section 1.2.6: Order-Disorder Effects), but the situation for short-range order is more obscure. Indeed, an increase of short-range order may lead either to an increase or a decrease in resistivity [20, 31]. The quantity discussed in these papers is the residual resistivity, i.e., the value obtained by quenching the alloy from the temperature of interest and then measuring its resistivity at liquid helium temperature. In this way effects due to atomic vibrations are avoided. Damask [20] examined Cu_3Au above the order-disorder transition temperature and also α-brass ($Cu_{0.7}Zn_{0.3}$). He found that as the temperature from which the alloy was quenched was increased, thereby decreasing the short-range order, Cu_3Au showed a decrease in resistivity, whilst α-brass showed an increase.

Several solid solutions have been investigated with respect to SRO kinetics using residual resistivity measurements and thermal treatments [8, 62]. In addition to the measurements on recrystallized materials (thermal treatment), measurements on samples which were cold-worked to about 80% reduction of area were performed [53]. Plastic deformation influences the instantaneous degree of SRO by moving dislocations [14]. The usual picture is that moving dislocations destroy the atomic correlations and that is the way deformation reduces the instantaneous degree of SRO. Such a behavior has been observed for several alloys as for example AgZn. In this case the degree of order was the lower the higher was the degree of deformation [54].

2.4 Generation of Configurations with SRO

Experimental determination of the state of order was discussed above. In order to study the influence of SRO on physical properties theoretically, one has to generate configurations with certain degrees of order. This nontrivial task is discussed in this section.

Consider a binary alloy with components A and B having concentrations c_A and

c_B, respectively. We adopt the following definition of the SRO parameter [78]

$$\Gamma_{mn} = \frac{1}{2}\mathcal{P}_{AB} - c_A c_B \tag{2.34}$$

that accounts for the deviation of the probability of finding an AB-pair at lattice sites m and n in an ordered cluster, $\mathcal{P}_{AB}$, from the probability of finding such a pair in a random distribution of the atoms, $c_A c_B$. $\mathcal{P}_{AB}$ is defined as

$$\mathcal{P}_{AB} = \lim_{N\to\infty} \frac{N_{AB}}{\frac{1}{2}zN} \tag{2.35}$$

where N is the number of atoms in the cluster, z is the coordination number of atoms, and N_{AB} is the number of AB pairs in the cluster.

For a random arrangement of atoms

$$\frac{1}{2}\mathcal{P}_{AB} = c_A c_B \tag{2.36}$$

and the SRO parameter is zero. It is positive when the probability of finding an AB-pair is greater in the ordered state than in a random arrangement of atoms (ordering) and negative for clustering (AA- or BB-pairs are more probably found). Γ_{mn} can in principle take any value between the limits

$$-c_A c_B \leq \Gamma_{mn} \leq [min(c_A, c_B)]^2 \tag{2.37}$$

The above defined Γ_{mn} is related to the Warren-Cowley SRO parameter, α_{mn},

$$\Gamma_{mn} = -c_A c_B \alpha_{mn} \tag{2.38}$$

In order to generate configurations, we will consider only the correlation between the first nearest neighbors and use the simplified notation Γ_1 to denote the corresponding SRO parameter.

We started the generation of configurations with the building up of a cluster of atomic sites with a certain lattice structure (FCC and BCC were considered here). We generated spherical clusters, in which all lattice sites around a given central site up to a given cluster radius were included. Tables 2.1 and 2.2 list the size of spherical clusters and the number of sites in such clusters for FCC and BCC lattices, respectively. For such clusters, two ways of building up SRO configurations were considered and discussed in the remaining part of the chapter.

2.4.1 Procedure *i*

We start with determining the type of the atom at the central site of the cluster. The central atom is of type A with the probability c_A or of type B with the probability $c_B = 1 - c_A$. We determine then the type of each neighbor of the central atom as follows: if at the central site there is an A atom then each of its nearest neighbors is of type A according to the probability

Table 2.1: Shells and clusters in a FCC lattice.

shell	no. of sites in shell	generating vector	shell radius	no. of sites in cluster
0	1	(0.0, 0.0, 0.0)	0.0	1
1	12	(0.5, 0.5, 0.0)	0.5	13
2	6	(1.0, 0.0, 0.0)	1.0	19
3	24	(1.0, 0.5, 0.5)	1.5	43
4	12	(1.0, 1.0, 0.0)	2.0	55
5	24	(1.5, 0.5, 0.0)	2.5	79
6	8	(1.0, 1.0, 1.0)	3.0	87
7	48	(1.5, 1.0, 0.5)	3.5	135
8	6	(2.0, 0.0, 0.0)	4.0	141
9	24	(2.0, 0.5, 0.5)	4.5	165
10	12	(1.5, 1.5, 0.0)	4.5	177
11	24	(2.0, 1.0, 0.0)	5.0	201
⋮	⋮	⋮	⋮	⋮
16	24	(2.0, 1.5, 1.5)	8.5	405

Table 2.2: Shells and clusters in a BCC lattice.

shell	no. of sites in shell	generating vector	shell radius	no. of sites in cluster
0	1	(0.0, 0.0, 0.0)	0.00	1
1	8	(0.5, 0.5, 0.5)	0.75	9
2	6	(1.0, 0.0, 0.0)	1.00	15
3	12	(1.0, 1.0, 0.0)	2.00	27
4	24	(1.5, 0.5, 0.5)	2.75	51
5	8	(1.0, 1.0, 1.0)	3.00	59
6	6	(2.0, 0.0, 0.0)	4.00	65
7	24	(1.5, 1.5, 0.5)	4.75	89
8	24	(2.0, 1.0, 0.0)	5.00	113
9	24	(2.0, 1.0, 1.0)	6.00	137
10	32	(2.5, 0.5, 0.5)	6.75	169
⋮	⋮	⋮	⋮	⋮
18	48	(3.5, 0.5, 0.5)	12.75	387

$$p_A^A = c_A - \frac{\Gamma_1}{c_A} \tag{2.39}$$

and/or of type B with the probability

$$p_B^A = c_B + \frac{\Gamma_1}{c_A} = 1 - p_A^A \tag{2.40}$$

As one can see in Eqs. (2.39) and (2.40), ordering (i.e. $\Gamma_1 > 0$) increases the probability of AB-pairs to be generated, decreasing at the same time and with the same amount (Γ_1/c_A) the probability of generating AA-pairs.

If the central atom is of type B then each of its neighbors is of type B with the probability

$$p_B^B = c_B - \frac{\Gamma_1}{c_B} \tag{2.41}$$

and/or of type A according to

$$p_A^B = c_A + \frac{\Gamma_1}{c_B} = 1 - p_B^B \tag{2.42}$$

As before, ordering implies increased probability for generation of AB-pairs.

In the above equations, Γ_1 is the desired order parameter given as input. The next step consists in taking each of the nearest neighbors of the central atom and generate its own nearest neighbors, that were not yet been generated, using the probabilities given in Eqs. (2.39) to (2.42). The procedure is continued for each new generated atom until all lattice sites have an associated atom type.

We calculate next the SRO parameter for the resulting configuration by counting the total number of generated AB pairs and making use of Eqs. (2.34) and (2.35). For resistivity calculations we need configurational averages. To get such averages we generate 10 configurations, calculate the resulting SRO parameter of each configuration and then take the algebraic average of them. The resulting value, denoted Γ_{out}, is plotted as a function of the SRO parameter given as input at the construction of the configurations, Γ_1.

One expects a linear relation between Γ_{out} and Γ_1 that lie on the first bisector of the (Γ_1, Γ_{out}) plane. The obtained dependence is plotted in Figs. 2.3 and 2.4 for underlying BCC and FCC lattices, respectively. Clusters of various sizes were used.

For the BCC structure (Fig. 2.3) one sees a deviation from the expected linear relation which becomes more pronounced as the cluster size is increased. The deviation is explainable if one notes that the type of an atom is determined through the correlation to only one of its neighbors, while the correlations to its other neighbors are not taken into account. This means that some of the correlations between the atoms in the cluster are not fulfilled so that one encounters deviations of the resulting SRO (correlation) parameter from that given as input at the construction of the configuration. A bigger cluster means more atoms, that is, more correlations

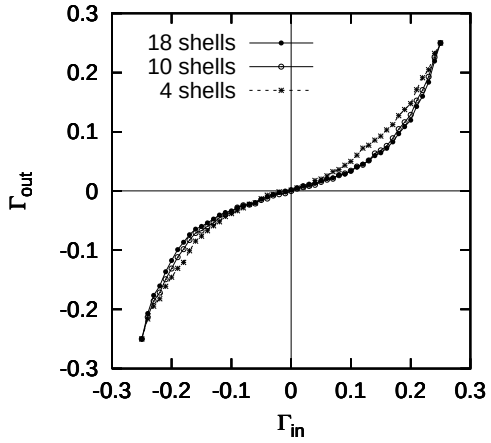

Figure 2.3: Relation between input and output SRO parameters for a BCC structure. The procedure i was used. $c_A = c_B = 0.5$. Different cluster sizes were used.

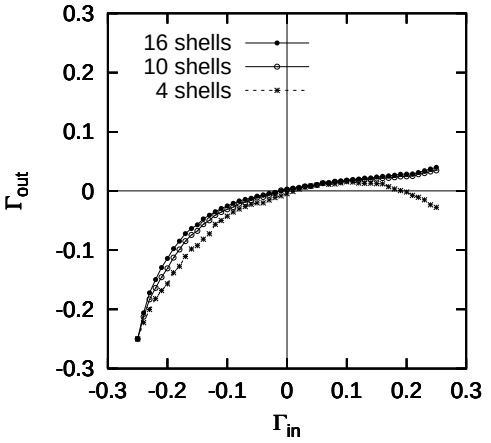

Figure 2.4: Same as Fig. 2.3 for a FCC structure.

that need to be fulfilled simultaneously and thus, more correlations that remain unfulfilled.

The relation between Γ_1 and Γ_{out} displays some particularities in the case of FCC structure (Fig. 2.4). Within the negative regime of Γ_1 (clustering) the behavior is very similar to that encountered at the BCC structure, except that the deviation from a linear relation seems to be more pronounced. An interesting aspect, however, is the behavior in the regime of positive Γ_1 (ordering). The curve not only deviates from the bisector, but it also does not reach the bisector even at the extreme value of $\Gamma_1 = 0.25$ as was the case for the BCC structure. It seems to become "saturated" at quite small Γ_{out}. This is due to the character of the FCC structure that is a so-called *frustrated* structure. In such a structure, encountered, for example, at magnetic ordering of spins [], there are concurrent correlations that cannot be all simultaneously satisfied and that hinder the building up of highly ordered configurations.

Another reason for the unexpected relation between Γ_1 and Γ_{out} is that each of the generated configurations has, in general, calculated SRO parameters and concentrations of components that are more or less different from the input values. These drawbacks could, in principle, be overridden in the process of averaging over several configuration. However, it does not happen. This means that, in order to get a number of, say, M configurations that give on the average the desired values for concentrations and SRO parameter, one has to generate more than M configurations and take averages over all possible arrangements of M of them. This leads to a drastical increase of the time for getting the appropriate M configurations. The computation time can be reduced in that, in the averaging process, only those configurations are taken which have computed values for Γ_1 and c_A and c_B that are the same with the input ones within some limit. In this way, conditions are

imposed for both output order parameters and output concentrations.

The aim of using a second procedure of generating configurations is, thus, two-fold. Firstly, we try to improve the procedure *i*, so that the type of the atom at a site to be determined by the correlations to all of its neighbors. Secondly, we make a comparison between the results obtained in the case of configurations restricted as described above, and the case where non-restricted configurations where used in the averaging process in order to see whether restricted (faster generated) configurations could be used.

2.4.2 Procedure *ii*

Within the new procedure we do not "grow" the cluster from the central site any more. We choose a lattice site m at random. The atom type at m is determined from the correlations to its already generated nearest neighbors. As long as no nearest neighbors of site m are generated, the type of the atom at m is A with the probability c_A and/or B with the probability c_B. Each A-type neighbor of site m decreases the probability of having an A atom at m with an amount $-\Gamma_1/c_A$ and each B-type neighbor of site m increases the probability of having an A atom at site m with an amount Γ_1/c_B (see Eqs. (2.39) and (2.42)). When n_A of the already generated nearest neighbors of site m are of type A and n_B of the already generated nearest neighbors of site m are of type B the type of the atom at m is of type A with a probability

$$p_A = c_A + \frac{\Gamma_1}{c_B}\left[(n_B - n_A) + n_A\frac{c_A - c_B}{c_A}\right] \tag{2.43}$$

The probability to have a B atom at m is easily calculated as

$$p_B = 1 - p_A \tag{2.44}$$

Let us discuss Eq. (2.43). Consider the simpler case of an alloy containing atoms A and B in equal proportions ($c_A = c_B$). Then

$$p_A = c_A + \frac{\Gamma_1}{c_B}\left[(n_B - n_A)\right] \tag{2.45}$$

Thus, the probability of having an A atom at m varies as a function of the difference between the A-type and B-type nearest neighbors. In case of ordering ($\Gamma_1 > 0$), for example, the probability to have an A atom at m is greater when around m are more B atoms than A atoms, leading to an increased probability to find AB pairs in the cluster. Returning to Eq. (2.43) and considering the example presented above (ordering) one can see that a concentration of A-type atoms less than that of the B-type atoms reduces the probability of having an A atom at m and contribute this way to a better control of the concentrations of components.

On comparing procedures *i* and *ii* one can see (Figs. 2.5 and 2.6) that procedure *ii* gives results in complete agreement with the expectations. The fact that no output

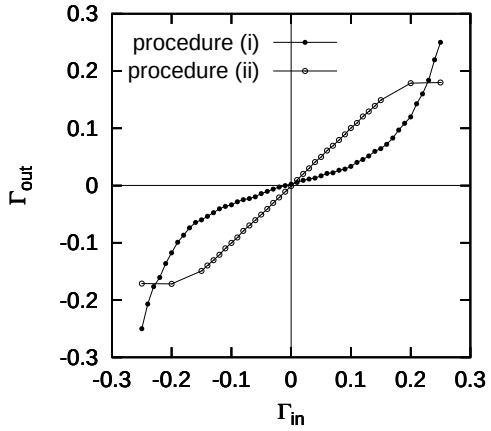

Figure 2.5: Comparison between procedures *i* and *ii* for generating configurations. BCC cluster of 18 shells. $c_A = 0.5$, $c_B = 0.5$

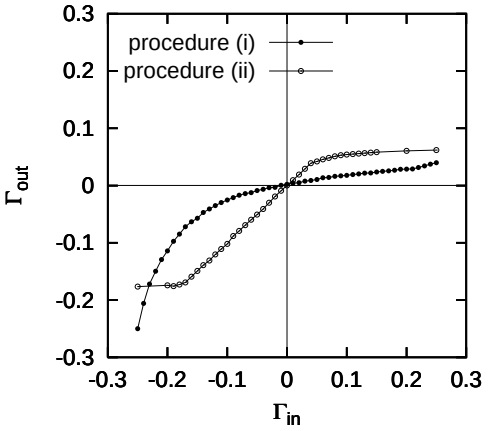

Figure 2.6: Same as Fig. 2.5 for a FCC structure.

configurations with extreme Γ_{out} are produced is an expected result if we note that the cluster "grows at random." By such a "random growing" of a cluster it comes always to the impossibility to order all the atoms in the cluster at any distance. It is worth to say that the FCC structure is frustrated "by definition". This is well seen in Fig. 2.6, where, in case of ordering ($\Gamma_1 > 0$), Γ_{out} stops to follow Γ_1 (becomes "saturated") at values that are obviously less than in all other cases. We can conclude that the results of procedure *ii* are those of a reliable method of generating configurations with certain degrees of short-range order.

The problem of using restricted configurations needs some discussion. A calculation of physical properties of disordered alloys should take into account all possible arrangements of the component atoms at the lattice sites. Configurational averages over all possible configurations are treated within the single site coherent potential approximation (presented in chapter 3) by means of Fourier transforms (see e.g. [11]). It is however impossible to include all configurations in a cluster calculation in real space, due to the very large number of possible configurations. In cluster calculations one has to confine oneself to a small number of configurations that are representative for the state of order to be treated. We think that for the averaging process only configurations by which the concentrations of components is within the limit of statistical fluctuations are acceptable. We imposed this limits in our procedure *ii*. The effect of further restrictions on concentrations (only those in which the ratio of the number of atoms of type A and B and the total number of atoms in the cluster equal exactly the concentrations c_A and c_B, respectively) and restrictions on SRO parameter (only values not far away from the desired Γ_1) was studied. We generated configurations by which the concentrations were allowed to vary within statistical limits and no restrictions on Γ_1 were imposed (denoted as non-restricted) and configurations by which only concentrations c_A and c_B were allowed and the

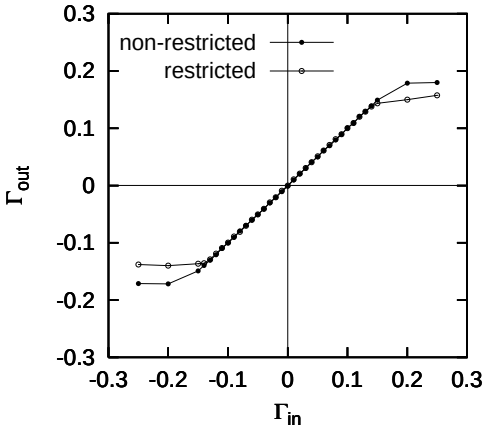

Figure 2.7: Relation between input and output SRO parameters for a BCC structure. Procedure *ii* was used. BCC clusters of 18 shells. $c_A = c_B = 0.5$. Restricted and non-restricted configurations are compared.

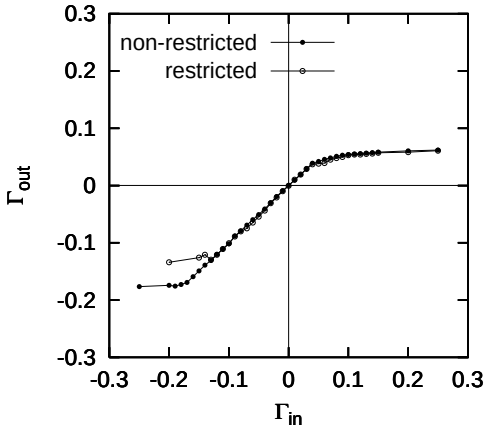

Figure 2.8: Same as Fig. 2.7 for a FCC structure. Clusters of 16 shells.

values of Γ_1 varied slightly around the desired value (denoted as restricted). The results are plotted in Figs. 2.7 and 2.8 for BCC and FCC lattices respectively.

For BCC structures the restrictions influence the results only in the regime of high (positive and/or negative) Γ_1's where the linear relation between Γ_{out} and Γ_1 does not hold for reasons explained above. The same is true for FCC structures in the regime of high negative Γ_1's. The regime of high positive Γ_1's is not affected by the restrictions imposed due to the fact that the FCC structure is frustrated. The generation of restricted configurations is significantly faster that the generation of non-restricted configurations. Thus, one can use either restricted or non-restricted configurations for configurational averages, depending on the lattice structure and the regime of interest for the SRO parameter.

Chapter 3

Theoretical Approach

First principles theories provide a tool for understanding the physical properties of metallic alloy systems in terms of the basic building blocks of matter, nuclei and electrons. Ideally the only input to such theories should be the atomic numbers of the constituent species. The calculation of physical observables relies on controlled approximations for the Schrödinger equation.

For ordered, translationally invariant systems like pure metals and ordered alloys the above scheme can be carried to a high degree of completion [55, 75]. The fundamental underpinning is provided by the *density functional theory* of Hohenberg and Kohn [38, 46]. In random alloy systems the translational invariance does not exist. This means that the band theory methods developed to solve the Schrödinger equation for periodic systems are no longer useful. However, the fact that a system does not possess translational invariance does not affect the applicability of the density functional methods.

The central problem in dealing with random alloys is that the effective one electron crystal potential function entering the Schrödinger equation is random. The study of the eigenvalue spectra of random Hamiltonians has resulted in the development of approximations which can be used to treat specific problems. The major development of concern here is that of the *coherent potential approximation* (CPA) [64, 23]. CPA is a single-site approximation and, as was shown by Velicky et al. [69], it is the best possible approximation within a hierarchy of single-site approximations.

In order to calculate observables one can attempt to solve the Schrödinger equation for the wave function. An alternative to this is the calculation of the Green function of the corresponding Hamiltonian. In experiments on random alloys the configurational averages of the observables are actually measured. Such configurational averages of observables need to be calculated theoretically, and they are related to the configurationally averaged Green function of the system in question. It is the task of alloy theory to find approximations for the configurationally averaged Green function. One way to proceed is the use of multiple scattering theory of particles.

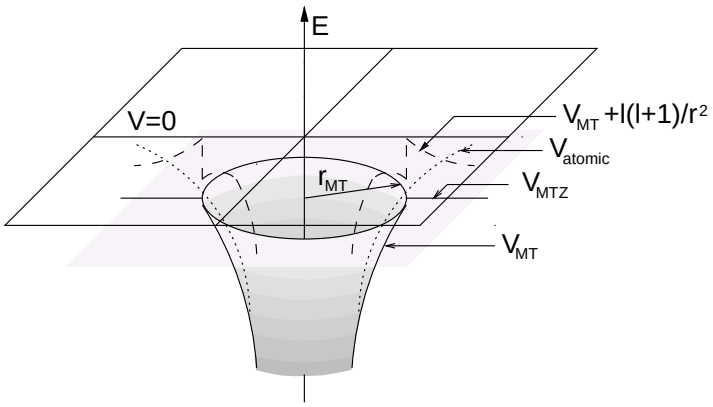

Figure 3.1: Muffin-tin potential V_{MT}, atomic potential V_{atomic} and the sum of V_{MT} and the centrifugal term $l(l+1)/r^2$. $V = 0$ is the zero of the atomic potential and V_{MTZ} is the muffin-tin zero.

3.1 Multiple Scattering Theory

Multiple scattering theory of particles by a distribution of scatterers has many applications. It was first applied to systems in which the wavelength is small compared to the separation between scatterers (without correlation between the positions of scatterers). L. L. Foldy [28] and M. Lax [50] applied the theory to correlated systems. The idea of describing atomic cores by means of phase shifts in the regular solid is due to Korringa [47] and Kohn and Rostoker [45] where it gives rise to the KKR method of calculating band structure.

The basic mathematical idea behind the scattering theory is the replacement of a region of space by a "black box" whose properties are completely defined by parameters which describe the matching conditions at the boundary of the region. We shall derive the relations of the multiple scattering theory considering first the scattering off of an electron from a single potential.

3.1.1 Single-Site Scattering of Electrons

Consider a single muffin-tin potential (Fig. 3.1) centered at the origin such that

$$v(\mathbf{r}) = \begin{cases} v(r), & r \leq r_{MT} \\ 0, & r \geq r_{MT} \end{cases} \tag{3.1}$$

Since the potential is spherically symmetric the solution to the Schrödinger equation (in atomic units $\hbar = 1$, $m = \frac{1}{2}$, $e^2 = 2$)

$$\left[-\nabla^2 + v(\mathbf{r}) - \epsilon\right] \psi(\mathbf{r}\,;\epsilon) = 0 \tag{3.2}$$

can be written in the form

$$\psi(\mathbf{r}\,;\epsilon) = 2 \sum_L a_L(\epsilon) R_l(r\,;\epsilon) Y_L(\hat{\mathbf{r}})\,, \tag{3.3}$$

where

$$\hat{\mathbf{r}} = \frac{\mathbf{r}}{|\mathbf{r}|} ,$$

$Y_L(\hat{\mathbf{r}})$ is a spherical harmonic with polar and azimuthal quantum numbers $(l, m) \equiv L$ and $R_l(r\,;\epsilon)$ is the solution of the radial Schrödinger equation

$$\left[-\frac{1}{r}\frac{d^2}{dr^2}\, r + \frac{l(l+1)}{r^2} + v(r) \right] R_l(r\,;\epsilon) = \epsilon\, R_l(r\,;\epsilon) \,. \tag{3.4}$$

For $r > r_{MT}$ Eq. (3.4) is the radial Schrödinger equation for free electrons, whose two linearly independent solutions are the spherical Bessel and Neumann functions $j_l(\sqrt{\epsilon}r)$ and $n_l(\sqrt{\epsilon}r)$, respectively. Thus for $r > r_{MT}$, $R_l(r\,;\epsilon)$ is a linear combination of j_l and n_l. Therefore, without loss of generality we may define $R_l(r\,;\epsilon)$ as

$$R_l(r\,;\epsilon) = \cos\delta_l(\epsilon)\; j_l(\sqrt{\epsilon}\, r) - \sin\delta_l(\epsilon)\; n_l(\sqrt{\epsilon}\, r) \tag{3.5}$$

Inside the muffin-tin sphere, that is for $r < r_{MT}$, $R_l(r\,;\epsilon)$ is that solution of Eq. (3.4) which is regular at the origin. At $r = r_{MT}$ its logarithmic derivative

$$\gamma_l(\epsilon) = \frac{1}{R_l(r\,;\epsilon)}\, \frac{d}{dr} R_l(r\,;\epsilon)\bigg|_{r=r_{MT}} \tag{3.6}$$

must be equal to the logarithmic derivative of $R_l(r\,;\epsilon)$ on the outside given in Eq. (3.5). From this condition it follows that

$$\delta_l(\epsilon) = \cot^{-1}\left[\frac{\sqrt{\epsilon}\; n_l'(\sqrt{\epsilon}r_{MT}) - \gamma_l(\epsilon) n_l(\sqrt{\epsilon}r_{MT})}{\sqrt{\epsilon}\; j_l'(\sqrt{\epsilon}r_{MT}) - \gamma_l(\epsilon) j_l(\sqrt{\epsilon}r_{MT})} \right] \tag{3.7}$$

Note that asymptotically

$$\lim_{r\to\infty} R_l(r\,;\epsilon) = \frac{1}{\sqrt{\epsilon}r} \sin\left[\sqrt{\epsilon}r - \frac{l\pi}{2} + \delta_l(\epsilon) \right] \tag{3.8}$$

differs from the free electron solution only by a shift of phase $\delta_l(\epsilon)$. Hence, $\delta_l(\epsilon)$ is usually referred to as the *phase shift* which, as indicated, is a function of the energy.

The connection between the phase shifts and the scattering theory can be seen if we recall that in scattering theory one seeks the solution of Eq. (3.2) such that $\psi_{\mathbf{k}}(\mathbf{r})$ is an eigenfunction with energy $\epsilon = k^2$ and asymptotically it can be written as the superposition of an incident plane wave and an outgoing spherical wave [52],

$$\psi_{\mathbf{k}}(\mathbf{r}) = e^{i\mathbf{k}\cdot\mathbf{r}} + f(\epsilon,\theta)\frac{e^{ikr}}{kr} \,, \tag{3.9}$$

where θ is the angle between the vectors $\mathbf{k}$ and $\mathbf{r}$. Requiring that $\psi(\mathbf{r}\,;\epsilon)$ in Eq. (3.3) has the asymptotic form given in Eq. (3.9) we find

$$a_L(\epsilon) = 4\pi i^l e^{i\delta_l} Y_L^*(\hat{\mathbf{k}}) \tag{3.10}$$

Furthermore

$$\psi_{\mathbf{k}}(\mathbf{r}) = 4\pi \sum_{L} i^l e^{i\delta_l} R_l(r\,;\epsilon) Y_L(\hat{\mathbf{r}}) Y_L^*(\hat{\mathbf{k}}) \tag{3.11}$$

and the scattering amplitude $f(\epsilon, \theta)$ is given by

$$f(\epsilon, \theta) = \sum_{L} (2l+1) f_l(\epsilon) P_l(\cos\ \theta) \tag{3.12}$$

where

$$f_l(\epsilon) = \sin \delta_l(\epsilon)\, e^{i\delta_l(\epsilon)} \tag{3.13}$$

Using the definition of the total scattering cross section

$$\sigma = \frac{2\pi}{\epsilon} \int_{-l}^{l} d(\cos\ \theta) |f(\theta)|^2 \tag{3.14}$$

one can show that

$$\sigma = \frac{4\pi}{\epsilon} \sum_{l} (2l+1) \sin^2 \delta_l(\epsilon) \tag{3.15}$$

Thus, a phase shift near $\pi/2$ means very strong scattering while δ_l near 0 or π means weak scattering.

A phase shift rising from 0 to π within a small energy interval Γ about ϵ_r where it is equal to $\pi/2$ is called a scattering resonance. It is customary to refer to ϵ_r and Γ as the position and the width of the resonance and parameterize the corresponding scattering amplitude by the Breit-Wigner form

$$f(\epsilon) = \frac{\Gamma}{(\epsilon - \epsilon_r) + i\Gamma} \tag{3.16}$$

Alternatively, one can write

$$\tan \delta(\epsilon) = \frac{\Gamma}{\epsilon - \epsilon_r} \tag{3.17}$$

The contribution of the resonance to the scattering cross section is a Lorentzian peak

$$\sigma \sim \frac{\Gamma}{(\epsilon - \epsilon_r)^2 + \Gamma^2} \tag{3.18}$$

which describe the rise and fall of the scattering strength of the potential as ϵ passes through ϵ_r.

An interesting result in the scattering theory is the relation between the time spent by an electron at the scattering center, the Wigner delay time, τ_w, and the phase shift [24]

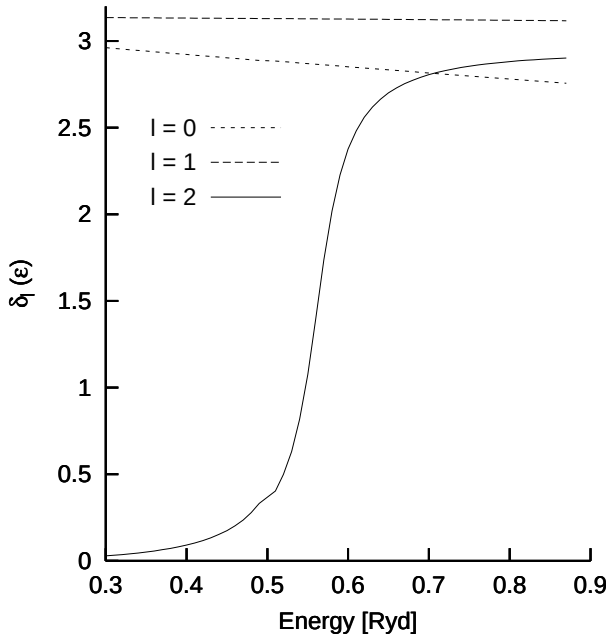

Figure 3.2: The phase shifts $\delta_l(\epsilon)$ for a muffin-tin potential well of Pd appropriate to a $Ag_{0.5}Pd_{0.5}$ random alloy.

$$\tau_w = 2\hbar \frac{\partial}{\partial \epsilon} \delta_l(\epsilon). \tag{3.19}$$

This shows that an electron with an energy near the resonance will spend a long time at the scattering center. As can be seen in Fig. 3.2, the Pd d-band straddles the resonant energy where

$$\delta_2^{Pd}(\epsilon_r) = \frac{\pi}{2} \tag{3.20}$$

Thus, an electron with energy in the d-band will spend a long time at each site as it travels through the lattice. Moreover, while at a site, its wavefunction will have predominantly d-character about that site. This is the same physical picture as provided by the tight-binding theory where one assumes that a d-electron in a narrow band is localized in an atomic d-state most of the time and hops to another site only occasionally. The different language is due to the fact that in the tight-binding picture one deals with bound states at negative energies which decay exponentially in space, while in scattering theory the zero of the potential energy is shifted bellow to the muffin-tin zero and with respect to this zero we work at positive energies where the scattered wave travels off to infinity with only its phase shifted by the interaction at a site.

To make this connection even more explicit we note that the $l = 2$ resonance in the Pd potential arises because the potential $v(r)+l(l+1)/r^2$ in Eq. (3.4) can almost form a bound state behind the centrifugal barrier shown in Fig. 3.1. Because we are

(in the sens mentioned above) at positive energies this state is metastable since an electron can always turn out. The long Wigner delay time is merely a reflection of the fact that the electron can be trapped into this metastable bound state. As one considers atomic potentials instead of single scatterers in an alloy, at the same absolute energy where previously we had a resonance, we will now have a real bound state whose wavefunction decays exponentially in space. This is the atomic bound state that enters into the tight-binding theory.

As is evident from Eqs. (3.9), (3.12) and (3.13) the phase shifts completely determine the scattering properties of the potential function. Thus the phase shifts are a very efficient description of the potential function for the problems where we are interested in the wavefunctions only outside the scattering region. This is particularly so in the case of muffin-tin potentials one encounters in most metals. It turns out that except for the f-band metals, $\delta_l(\epsilon)$ is practically zero for $l > 2$ in the energy range of the conduction band.

Let us return to Eq. (3.2) and construct its Green function. By definition this is

$$G(\mathbf{r}, \mathbf{r}'; \epsilon) = \sum_n \frac{\psi_n^*(\mathbf{r})\psi_n(\mathbf{r}')}{\epsilon - \epsilon_n + i\eta} \tag{3.21}$$

where the $\psi_n(\mathbf{r})$'s form an orthonormal complete set and are eigenfunctions of the Hamiltonian

$$H = -\nabla^2 + v(\mathbf{r}) \tag{3.22}$$

It can be shown that the functions $\psi_{\mathbf{k}}(\mathbf{r})$ in Eq. (3.11) for all $\mathbf{k}$ form a complete set provided the potential $v(\mathbf{r})$ has no bound states. Thus they can be used to evaluate Eq. (3.21) for positive energies. This gives

$$G(\mathbf{r}, \mathbf{r}\,'; \epsilon) = \int \frac{d^3k}{(2\pi)^3} \frac{\psi_{\mathbf{k}}^*(\mathbf{r})\psi_{\mathbf{k}}(\mathbf{r}\,')}{\epsilon - k^2 + i\eta} \tag{3.23}$$

As an alternative to constructing the Green function from the eigenfunctions of Eq. (3.2) as in Eq. (3.21), we could start with the integral equation

$$G(\mathbf{r}, \mathbf{r}\,'; \epsilon) = G_0(\mathbf{r}, \mathbf{r}\,'; \epsilon) + \int d^3r_i G_0(\mathbf{r}, \mathbf{r}_i; \epsilon) v(\mathbf{r}_i) G(\mathbf{r}_i, \mathbf{r}\,'; \epsilon) \tag{3.24}$$

which follows from Eq. (3.2) and Eq. (3.21) if one notes that the free particle Green function $G_0(\mathbf{r}, \mathbf{r}\,'; \epsilon)$ is defined by the equation

$$\left[\nabla^2 + \epsilon\right] G_0(\mathbf{r}, \mathbf{r}\,'; \epsilon) = \delta(\mathbf{r} - \mathbf{r}\,') \tag{3.25}$$

A way of solving Eq. (3.24) is to define the *single scatterer t-matrix* by the relation

$$G(\mathbf{r}, \mathbf{r}\,'; \epsilon) = G_0(\mathbf{r}, \mathbf{r}\,'; \epsilon) + \int d^3r_i \int d^3r_j G_0(\mathbf{r}, \mathbf{r}_i; \epsilon) t(\mathbf{r}_i, \mathbf{r}_j; \epsilon) G_0(\mathbf{r}_j, \mathbf{r}\,'; \epsilon) \tag{3.26}$$

and attempt to solve the integral equation

$$t(\mathbf{r},\mathbf{r}';\epsilon) = v(\mathbf{r})\delta(\mathbf{r}-\mathbf{r}') + \int d^3r_i v(\mathbf{r}_i) G_0(\mathbf{r},\mathbf{r}_i;\epsilon) t(\mathbf{r}_i,\mathbf{r}';\epsilon) \tag{3.27}$$

which follows from Eqs. (3.24) and (3.26).

In its full generality Eq. (3.27) is quite difficult to solve, however, the "on the energy shell" angular momentum components of $t(\mathbf{r},\mathbf{r}';\epsilon)$ turn out to be simple quantities. To define these consider the matrix elements of the t-matrix in the plane wave representation

$$t\left(\mathbf{k},\mathbf{k}';\epsilon\right) = \int d^3r_i \int d^3r_j \; e^{-i\mathbf{k}\cdot\mathbf{r}_i} \; t\left(\mathbf{r}_i,\mathbf{r}_j;\epsilon\right) \; e^{i\mathbf{k}'\cdot\mathbf{r}_j} \tag{3.28}$$

In general the above matrix elements are defined for all $\mathbf{k}$ and $\mathbf{k}'$, that is for arbitrary incoming and outgoing plane wave energies k^2 and k'^2 respectively. $t(\mathbf{k},\mathbf{k}';\epsilon)$ is the probability amplitude that a plane wave $|\mathbf{k}\rangle$ scatters into the state $|\mathbf{k}'\rangle$. If $k^2 = k'^2 = \epsilon$ we are describing elastic scattering. This situation is referred to as being "on the energy shell". Using the expansion of plane waves in terms of spherical functions

$$e^{i\mathbf{k}\cdot\mathbf{r}} = 4\pi \sum_L \; i^l j_l(kr) Y_L^*(\hat{\mathbf{k}}) Y_L(\hat{\mathbf{r}}) \tag{3.29}$$

one can show that

$$t(\mathbf{k},\mathbf{k}';\epsilon) = \sum_{L,L'} \; i^{-l+l'} (4\pi)^2 Y_L(\hat{\mathbf{r}}) t_{LL'}(\epsilon) Y_L^*(\hat{\mathbf{r}}) \tag{3.30}$$

where the angular momentum components of the "on the energy shell" t-matrix $t_{LL'}$ are defined as

$$t_{LL'}(\epsilon) = \int d^3r_i \int d^3r_j j_l(\sqrt{\epsilon}r_i) Y_L^*(\hat{\mathbf{r}}_i) t(\mathbf{r}_i,\mathbf{r}_j;\epsilon) Y_{L'}(\hat{\mathbf{r}}_j) j_{l'}(\sqrt{\epsilon}r_j) \tag{3.31}$$

We note that for a general potential we should be talking about a matrix $t_{LL'}(\epsilon)$. However, for a spherically symmetric potential $v(r)$ the t-matrix is diagonal and it is sufficient to define $t_{LL'}(\epsilon) = t_L(\epsilon)\delta_{LL'}$, with

$$t_L(\epsilon) = -\frac{1}{k} \; \sin\delta_l(\epsilon) \; e^{i\delta_l} = -\frac{1}{k} f_L(\epsilon) \tag{3.32}$$

called scattering amplitude [52].

Making use of Eqs. (3.5), (3.26), (3.31) and (3.32), the Green function can be written as

$$G(\mathbf{r},\mathbf{r}';\epsilon) = -ik \sum_{LL'} Z_L(\mathbf{r};\epsilon) t_{LL'}(\epsilon) h_{l'}^+(kr') Y_{L'}(\hat{\mathbf{r}}') \,, \tag{3.33}$$

where

$$Z_L(\mathbf{r};\epsilon) = -\sqrt{\epsilon} \; \frac{R_l(r;\epsilon)}{\sin\delta_l(\epsilon)} Y_L(\hat{\mathbf{r}}) \tag{3.34}$$

A detailed derivation of Eq. (3.33) is given in appendix A.

The phase shifts are a very convenient way of describing the scattering properties of a single muffin-tin well. The wave function and Green function outside the range of the potential are entirely specified in terms of them. They do not however contain sufficient information to specify the Green function within the range of the potential. As shall be seen later (section 3.4.1), $t_L(\epsilon)$ as given in Eq. (3.32) is sufficient to evaluate the change in the density of states due to a single scatterer.

3.1.2 Multiple Scattering of Electrons

Let us now consider the Schrödinger equation for the full crystal lattice with the appropriate muffin-tin potential on every site

$$V(\mathbf{r}) = \sum_i v_i(\mathbf{r} - \mathbf{R}_i). \tag{3.35}$$

We aim to calculate the Green function from the t-matrix for the full crystal potential defined as

$$G(\mathbf{r}, \mathbf{r}'; \epsilon) = G_0(\mathbf{r}, \mathbf{r}'; \epsilon) + \int d^3 r_i \int d^3 r_j \, G_0(\mathbf{r}, \mathbf{r}_i; \epsilon) T(\mathbf{r}_i, \mathbf{r}_j; \epsilon) G_0(\mathbf{r}_j, \mathbf{r}'; \epsilon) \tag{3.36}$$

or, using the operator notation,

$$G = G_0 + G_0 T G_0 \,. \tag{3.37}$$

The real space representation is obtained in the obvious manner $G(\mathbf{r}, \mathbf{r}'; \epsilon) = \langle \mathbf{r}|G|\mathbf{r}' \rangle$ etc.

As in the case of a single scatterer, we aim to find $T(\mathbf{r}, \mathbf{r}'; \epsilon)$ by solving

$$T(\mathbf{r}, \mathbf{r}'; \epsilon) = V(\mathbf{r}) \delta(\mathbf{r} - \mathbf{r}') + \int d^3 r_i \, V(\mathbf{r}) G_0(\mathbf{r}, \mathbf{r}_i; \epsilon) T(\mathbf{r}_i, \mathbf{r}'; \epsilon) \,. \tag{3.38}$$

which can be written in operator notation as

$$T = V + V G_0 T \,. \tag{3.39}$$

The t-matrix for the full crystal potential can be decomposed according to

$$T = \sum_{ij} \tau^{ij} \tag{3.40}$$

The quantities τ^{ij} were first introduced by Györffy and Stott [36] who called them *scattering-path operators*. The scattering-path operators are defined by

$$\tau^{ij} = t^i \delta_{ij} + \sum_{k \neq i} t^i G_0 \tau^{kj} \tag{3.41}$$

with

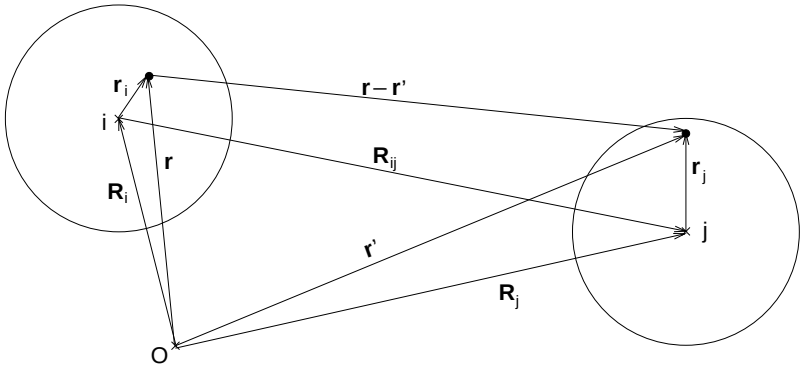

Figure 3.3: Graphical representation of the vectors involved in Eq. (3.43).

$$t^i = (1 - v_i G_0)^{-1} v_i \tag{3.42}$$

the single-site t-matrix for the potential at site i, v_i. The role of the single-site t-matrix, t^i, is to generate the scattered wave from the incident wave for the potential v_i, while the role of the full crystal t-matrix, T, is to do the same for the assembly of potential wells $\sum_i v_i$. Then the physical content of Eqs. (3.41) and (3.42) is clear. τ^{ij} generates the scattered wave at site i which results from the incident wave at site j.

The importance of this formulation of the problem to the crystal potential which consists of non-overlapping muffin-tin wells is that for non-overlapping potentials the "on the energy shell" part of Eq. (3.41) decouples from the rest and this gives rise to a particularly powerful tool for calculating the energy bands.

Let us define, in analogy with Eq. (3.31), the "on the energy shell" components of the matrix elements $\langle \mathbf{r}|\tau^{ij}(\epsilon)|\mathbf{r}\,'\rangle \equiv \tau^{ij}(\mathbf{r}, \mathbf{r}\,'; \epsilon)$ of the scattering path operator as

$$\tau^{ij}_{LL'}(\epsilon) = \int d^3 r_i \int d^3 r_j \, Y^*_L(\hat{\mathbf{r}}_i) j_l(kr_i) \tau^{ij}(\mathbf{r}_i, \mathbf{r}_j; \epsilon) j_{l'}(kr_j) Y_{L'}(\hat{\mathbf{r}}_j) \tag{3.43}$$

where L is the angular momentum about the site $\mathbf{R}_i$ and L' is that about the site $\mathbf{R}_j$, $\mathbf{r}_i = \mathbf{r} - \mathbf{R}_i$ and $\mathbf{r}_j = \mathbf{r}' - \mathbf{R}_j$ (see Fig. 3.1.2). The use of these spatial variables is legitimate since it follows from the integral equation version of Eq. (3.41) that $\tau^{ij}(\mathbf{r}, \mathbf{r}\,'; \epsilon)$ depends on $\mathbf{r}$ and $\mathbf{r}\,'$ only through $\mathbf{r} - \mathbf{R}_i$ and $\mathbf{r}\,' - \mathbf{R}_j$.

We now want to find an expression for $\tau^{ij}_{LL'}(\epsilon)$ in terms of $t^i_L(\epsilon)$ from Eq. (3.41). To do this, take the matrix elements of this equation between the states $|\mathbf{r}\rangle$ and $|\mathbf{r}'\rangle$ inserting the identity operator $I = \int d^3 r \, |\mathbf{r}\rangle\langle\mathbf{r}|$ between operator products and then take the "on the energy shell" components of both sides of the equation by the operation defined in Eq. (3.43).

For $\mathbf{r}$ in the muffin-tin sphere surrounding $\mathbf{R}_i$ and $\mathbf{r}\,'$ in the muffin-tin sphere surrounding $\mathbf{R}_j$ with $i \neq j$ we can write

$$G_0(\mathbf{r},\mathbf{r}';\epsilon) = \sum_{LL'} Y_L(\hat{\mathbf{r}}_i) j_l(kr_i) G_{LL'}(\mathbf{R}_{ij};\epsilon) j_{l'}(kr_j) Y^*_{L'}(\hat{\mathbf{r}}_j) \tag{3.44}$$

where $G_{LL'}(\mathbf{R}_{ij};\epsilon)$ are the real space KKR structure constants. These are important quantities for one of the methods we used in our calculations (section 3.3.2). As different authors give different expressions for the structure constants, we present the derivation of them in Appendix B.

Returning to the problem of finding the scattering path operator, by using Eq. (3.44) it can be shown that

$$\tau^{ij}_{LL'}(\epsilon) = t^i_L(\epsilon)\delta_{ij}\delta_{LL'} + \sum_{k\neq i}\sum_{L''} t^i_L(\epsilon) G_{LL''}(\mathbf{R}_{ik};\epsilon)\tau^{kj}_{L''L'}(\epsilon) \tag{3.45}$$

Eq. (3.45) is the fundamental multiple scattering equation "on the energy shell". It gives $\tau^{ij}_{LL'}(\epsilon)$ in terms of $t^i_L(\epsilon)$, that is to say in terms of the phase shifts, and the structure constants, $G_{LL'}(\mathbf{R}_{ij};\epsilon)$, which do not depend on the potential function and are determined completely by the spatial arrangement of the scattering sites. Eq. (3.45) is valid for any arrangement of potentials even if we have a different scatterer at each site. Thus, it is a good starting point to discuss pure metals, liquids as well as random alloys. The only limitation on its validity is the requirement that the potential wells at the different sites may not overlap. If they are allowed to overlap we need an expression for $G_0(\mathbf{r},\mathbf{r}';\epsilon)$ which is valid for $\mathbf{r}=\mathbf{r}'$ where Eq. (3.44) cannot be used. The unfortunate consequence of overlapping potentials is that the "on the energy shell" part of the problem becomes coupled to the "off the energy shell" part and, except for some simplified models, the problem becomes intractable. The physical reason for the "off the energy shell" component coming in for overlapping potentials is easy to see. For non-overlapping potentials one elastic scattering process is completely over before the next one begins. So, you stay on the energy shell, and the only information about the potential which matters are the phase shifts. For overlapping scatterers, before a scattering process is over (i.e. one is still within the scattering region) the next one begins, because the tail of the next potential hangs into the scattering region of the first. Under these circumstances the inelastic virtual processes begin to play a role.

Before going on, in the next subsection, to write down an approach to the muffin-tin model of a random alloy, we will give a general expression for the Green function $G(\mathbf{r},\mathbf{r}';\epsilon)$ for the assembly of scatterers which will be of use in later sections when we wish to obtain expressions for observables (Section 3.4). To this end it is helpful to consider two cases separately. Firstly, the case when both $\mathbf{r}$ and $\mathbf{r}'$ are near some lattice site i, secondly, the case where $\mathbf{r}$ is near some site i and $\mathbf{r}'$ is near some other site j.

For the case where both $\mathbf{r}$ and $\mathbf{r}'$ are near the site i we use Eq. (3.40) to rewrite Eq. (3.37) as

$$G = G^i + G^i T_{ii} G^i\,, \tag{3.46}$$

where

$$G^i = G_0 + G_0 t^i G_0 \tag{3.47}$$

is the Green function for the an electron moving in the field of the potential at site i and

$$T_{ii} = \sum_{n \neq i} \sum_{m \neq i} \tau^{nm} \,. \tag{3.48}$$

$G^i(\mathbf{r}, \mathbf{r}\,'; \epsilon)$ can also be written in the form

$$G^i(\mathbf{r}, \mathbf{r}'; \epsilon) = -ik \sum_{LL'} Z^i_L(\mathbf{r}; \epsilon) t^i_{LL'}(\epsilon) h^+_{l'}(kr') Y_{L'}(\hat{\mathbf{r}}') \,, \tag{3.49}$$

where $Z^i_L(\mathbf{r}\,; \epsilon)$ is given by Eq. (3.34) and $r' > r$ and $r' > r_{MT}$. One obtains for the Green function [26]

$$G(\mathbf{r}, \mathbf{r}'; \epsilon) = \sum_{LL'} \left\{ Z^i_L(\mathbf{r}; \epsilon) \tau^{ii}_{LL'} Z^i_{L'}(\mathbf{r}'; \epsilon) - Z^i_L(\mathbf{r}; \epsilon) J^i_L(\mathbf{r}'; \epsilon) \delta_{LL'} \right\} \,, \tag{3.50}$$

where τ^{ii} is given by the solution of Eq. (3.45) for the case $j = i$. This expression is valid for any value of $\mathbf{r}$ and $\mathbf{r}\,'$ as long as they do not lie in any of the bounding spheres except the i^{th}.

To obtain an expression for the Green function when $\mathbf{r}$ is near the site i and $\mathbf{r}\,'$ is near the site j it is best to decompose G in the form

$$G = G^{ij} + G^i T_{ij} G^j \,, \tag{3.51}$$

where

$$G^{ij} = (G_0 t^i + 1)(1 + t^j G_0) \tag{3.52}$$

and

$$T_{ij} = \sum_{n \neq i} \sum_{m \neq j} \tau^{nm} \,, \tag{3.53}$$

from which it can be shown that

$$G(\mathbf{r}, \mathbf{r}'; \epsilon) = \sum_{LL'} Z^i_L(\mathbf{r}; \epsilon) \tau^{ij}_{LL'} Z^j_{L'}(\mathbf{r}'; \epsilon) \,. \tag{3.54}$$

Eq. (3.54) is valid as long as $\mathbf{r}$ is within no bounding sphere other than the i^{th} and $\mathbf{r}'$ is within no bounding sphere other than the j^{th}. Eqs. (3.50) and (3.54) can be combined into the general expression

$$G(\mathbf{r}, \mathbf{r}\,'; \epsilon) = \sum_{LL'} \left\{ Z^i_L(\mathbf{r}; \epsilon) \tau^{ij}_{LL'} Z^j_{L'}(\mathbf{r}\,'; \epsilon) - Z^i_L(\mathbf{r}; \epsilon) J^i_L(\mathbf{r}\,'; \epsilon) \delta_{LL'} \delta_{ij} \right\} \tag{3.55}$$

which is valid for all i and j including $i = j$.

This particular form of the Green function has a number of nice features. Firstly, it is valid for any array of non-overlapping potentials and, as such, it is an excellent starting point for the calculation of the average densities of states in a random alloy. Secondly, the wavefunction dependent information contained in the Z^i is completely separated from the multiple scattering information contained in the τ^{ij}. As we shall see, this also greatly facilitates the calculation of averaged values of observables. A final point worth to note is that formulae for observables derived from this form of the Green function usually turn out to be extremely easy to evaluate numerically, usually involving simple integrals over the unit cell of quantities which are simple functions of the Z^i.

3.2 The KKR-CPA Method

Let us assume a binary alloy of two components $\alpha = A$ and B, distributed randomly over the lattice sites with probabilities c_A and c_B such that the condition $c_A + c_B = 1$ is fulfilled. This condition of full randomness implies complete neglect of statistical correlations and is essential for the further theoretical development. In addition to that also the positional disorder is neglected, which would imply displacements of atoms from their positions in an underlying ideal lattice. By introducing the single-site approximation, a particular one-electron potential $v_i(\mathbf{r})$ depends only on the occupation of a given site i by an atom of the type α. In other words, at each site i we have two potentials v_i^α with probabilities c_α. The single-site approximation thus consists in neglecting all local environment effects.

We seek the best possible effective medium in the form of an ordered lattice of scatterers each described by the same effective scattering amplitude $t_L^C(\epsilon)$. The problem is, then, to find a suitable condition which would determine $t_L^C(\epsilon)$ in such a way that an electron would most nearly mistake the medium for the random lattice.

Notice that in this approach we bypass the problem of finding a "coherent potential" to describe the effective medium by implicitly assuming that it is of the non-overlapping muffin-tin form and therefore all we want to know about it are the scattering amplitudes $t_L^C(\epsilon)$.

The condition that determines the effective medium, called the CPA condition, is [32]

$$c_A t^{A,i} + c_B t^{B,i} = 0 \tag{3.56}$$

which means that the extra scattering produced by a real atom (A or B) embedded in the CPA medium vanishes on the average.

One can rewrite the CPA condition in terms of the "on the energy shell" matrix elements of τ^{ij}, determined in section 3.1.2

$$c_A \tau^{A,ij} + c_B \tau^{B,ij} = \tau^{C,ij} \tag{3.57}$$

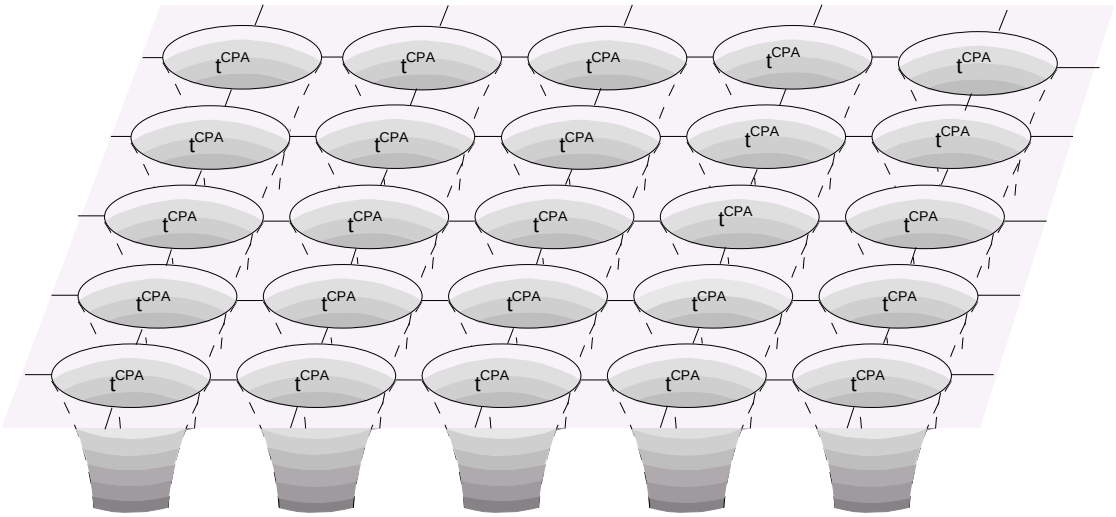

Figure 3.4: Muffin-tin CPA potentials.

where the matrices τ^{ij} are now to be regarded as matrices in the angular momentum index L. The $\tau^{C,ij}$ then is to be calculated for an ordered array of t^C's situated at the lattice sites R_i and $\tau^{ij}_{A(B)}$ is to be calculated for the same array except that at the site i there is an "impurity", $t^{A(B)}$ the t-matrix corresponding to a single $v_{A(B)}$ muffin-tin well. In practice it is only necessary to satisfy the self-consistency condition for the special case $j = i = 0$ say

$$c_A\tau^{A,00} + c_B\tau^{B,00} = \tau^{C,00} \tag{3.58}$$

which is the CPA condition, since it can be shown that the solution of this case implicitly contains the solution of Eq. (3.57).

The way to proceed is now fairly straightforward [65, 34]. Consider an A impurity at $\mathbf{R}_0$ in the coherent potential lattice. The scattering from that site is described by $\tau^{A,00}_{LL'}(\epsilon)$ which is the solution of Eq. (3.45) with

$$t^i_L = t^C_L + (t^A_L - t^C_L)\delta_{ij} \tag{3.59}$$

Similarly the scattering from a B impurity at $\mathbf{R}_0$ is described by $\tau^{B,00}_{LL'}(\epsilon)$. After some matrix algebra it can be shown that

$$\begin{aligned} \tau^{A,00}_{LL'}(\epsilon) &= \left[\left[1 + \tau^{C,00}[(t^A)^{-1} - (t^C)^{-1}]\right]^{-1}\tau^{C,00}\right]_{LL'} \\ \tau^{B,00}_{LL'}(\epsilon) &= \left[\left[1 + \tau^{C,00}[(t^B)^{-1} - (t^C)^{-1}]\right]^{-1}\tau^{C,00}\right]_{LL'} \end{aligned} \tag{3.60}$$

where

$$\tau^{C,00}_{LL'}(\epsilon) = \frac{1}{\Omega_{BZ}} \int d^3q \, \left[(t^C)^{-1} - G(\mathbf{q};\epsilon) \right]^{-1}_{LL'} \tag{3.61}$$

The CPA condition (3.58) that the averaged scattering from the site at $\mathbf{R}_0$ should be the same as in the pure coherent potential lattice now reads as

$$c_A \tau^{A,00}_{LL'}(\epsilon) + c_B \tau^{A,00}_{LL'}(\epsilon) = \tau^{C,00}_{LL'}(\epsilon) \tag{3.62}$$

Using Eq. (3.60) this condition can be rearranged into the following more useful form [35]

$$t^C_L = c_A (t^A_L)^{-1} + c_B (t^B_L)^{-1} + \left[(t^A_L)^{-1} - (t^C_L)^{-1} \right] \tau^{C,00}_{LL} \left[(t^B_L)^{-1} - (t^C_L)^{-1} \right] \tag{3.63}$$

This is then the fundamental equation for the effective scattering amplitude in the KKR-CPA. It determines $t^C_L(\epsilon)$ in terms of the A site and B site scattering amplitudes $t^A_L(\epsilon)$, $t^B_L(\epsilon)$ and the crystal structure which fixes the structure constants $G_{LL'}(\mathbf{q};\epsilon)$.

It is worth remembering that t^A_L and t^B_L need not be the same scattering amplitudes which determine the band structure of the pure metals A and B respectively. Thus, the KKR-CPA together with a prescription for the alloy potential is a first principles theory of the electronic states in random alloys in the same sense as one talks about first principles band theory for pure systems.

Obviously, there is no limitation to the applicability of the theory arising from the size and energy dependence of the scattering amplitudes. They can correspond to pure metals band structure with unequal band widths. Moreover, there can be any number of such bands overlapping and hybridizing in an arbitrary fashion.

As does the KKR, this method makes full use of the fact that for most metals only the first few phase shifts matter. Since $t^C_L(\epsilon)$ will have the cubic symmetry of the crystal lattice for $l \leq 2$, we will have at most four coupled equations to solve. These features play an important role in making the KKR-CPA tractable.

Model calculations and general theorems suggest that Eq. (3.63) can always be solved by iteration. One assumes some value for t^C_L and calculates $\tau^{C,00}_{LL'}$ numerically using Eq. (3.61). A new value of t^C_L is obtained by evaluating the right-hand side of Eq. (3.63) for the assumed value of t^C_L. This process is continued until the new value is the same as the assumed value at the beginning of the last step. The difficult part of the calculation is the evaluation of the Brillouin zone integral in Eq. (3.61) at each iteration.

In spite of its many desirable properties the CPA does not provide a fully satisfactory theory for calculating the properties of substitutionally disordered alloys. All drawbacks of the CPA stem from its single-site nature. As a single-site theory the CPA yields k-independent momentum-state lifetimes and in general is incapable of treating rigorously the transport properties and the localization of states in disordered systems (although it can give very accurate results in some cases). The effects

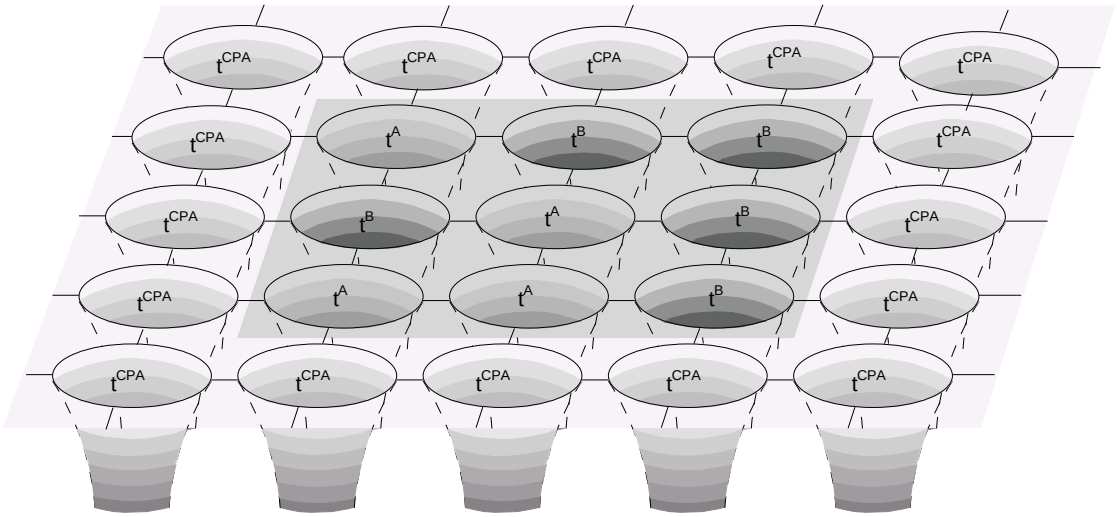

Figure 3.5: Muffin-tin potentials of a cluster embedded in a CPA medium

of short range order and of charge transfer cannot be taken properly into account within any single-site theory. In principal, all of these limitations of the CPA could be overcome to a large extent within the framework of a many-site or cluster theory.

3.3 Cluster Methods

There have been many attempts to develop a cluster generalization of the CPA. It appears that there are two well-separated problems associated with the development of such theories. The first and by far the most difficult problem is that of determining an optimal choice of effective medium. Preferably such a medium should take account of local environment fluctuations in a self-consistent way. No method is known which yields satisfactory results to this problem. The second problem associated with the formulation of a cluster theory of disordered systems is that of finding a computationally practical technique for evaluating the Green function for a cluster of real atoms embedded in a given effective medium. This problem has in principle been solved and the associated technique is the embedded cluster method (ECM). This is one of the methods we used in our calculations. We used another method which has not been used until now where we evaluated the Green function for an isolated cluster of real atoms not embedded in any medium. We call it isolated cluster method (ICM).

3.3.1 The Embedded Cluster Method (ECM)

Consider a cluster of impurity atoms embedded in a translationally invariant effective medium such as determined by the single-site CPA (Fig. 3.5). In order to treat an

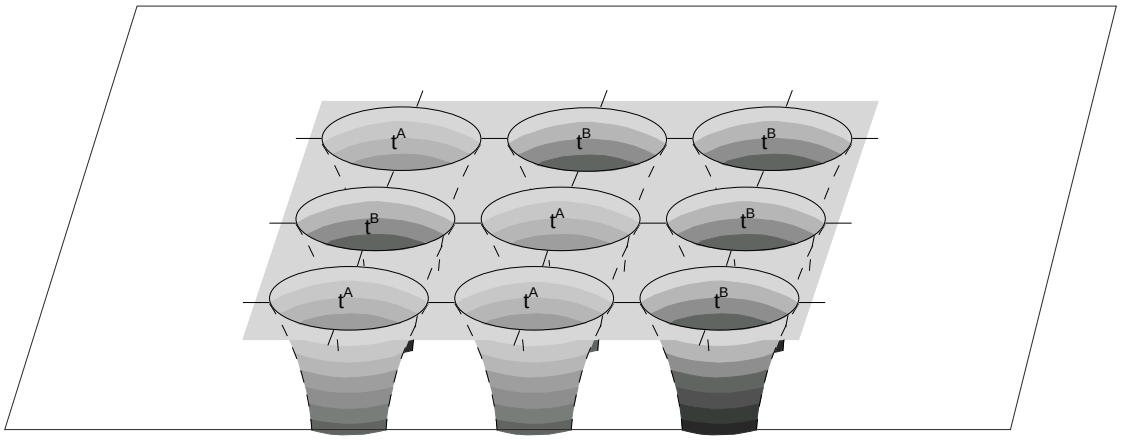

Figure 3.6: Muffin-tin potentials of an isolated cluster

embedded cluster exactly non-site-diagonal scattering-path operators have to be calculated. This can be done using an equation similar to Eq. (3.61)

$$\tau^{C,ij}_{LL'}(\epsilon) = \frac{1}{\Omega_{BZ}} \int d^3q \, \left[\left[(t^{C,i})^{-1} - G^{ij}(\mathbf{q};\epsilon) \right]^{-1} e^{i\mathbf{k}\cdot(\mathbf{R}_i - \mathbf{R}_j)} \right]_{LL'} \tag{3.64}$$

These $\tau^{C,ij}$ have to fulfill the condition

$$c_A \tau^{A,ij} + c_B \tau^{B,ij} = \tau^{C,ij} \tag{3.65}$$

where

$$\begin{aligned} \tau^{A,ij}_{LL'}(\epsilon) &= \left[\left[1 + \tau^{C,ij} [(t^{A,i})^{-1} - (t^{C,i})^{-1}] \right]^{-1} \tau^{C,ij} \right]_{LL'} \\ \tau^{B,ij}_{LL'}(\epsilon) &= \left[\left[1 + \tau^{C,ij} [(t^{B,i})^{-1} - (t^{C,i})^{-1}] \right]^{-1} \tau^{C,ij} \right]_{LL'} \end{aligned} \tag{3.66}$$

3.3.2 The Isolated Cluster Method (ICM)

An alternative to solving Eq. (3.58) by the lattice Fourier transform method and the evaluation of $\tau^{C,ij}$ from Eq. (3.64) is to regard τ^C as a matrix in both site and angular momentum indices and to solve Eq. (3.45) directly by matrix inversion.

$$\tau^{C,ij}_{LL'} = \left[(t^i)^{-1} \delta_{ij} \delta_{LL'} - G^{ij}_{LL'} \right]^{-1}_{LL'} \tag{3.67}$$

where the structure constants $G^{ij}_{LL'}$ of Eq. (B.14) are involved.

Of course the difficulty with Eq. (3.67) is that we have to invert a matrix whose dimension is infinite since it involves the site index. Eq. (3.67) does however offer the possibility that, for the purpose of calculating the matrix elements of the scattering

path operator for the central site, it may be sufficient to consider approximating the infinite array of t^C's by a small cluster of t^C's surrounding the central site.

The calculation of observables for clusters of real atoms is related in a simple manner to the scattering path operators calculated within the two cluster methods presented above.

3.4 Calculation of Observables

3.4.1 DOS Calculation

The density of states is related to the imaginary part of the Green function through the well known formula

$$n(\epsilon) = -\frac{1}{\pi} \,\mathrm{Im} \int d^3r G(\mathbf{r}, \mathbf{r}; \epsilon) \tag{3.68}$$

Some interesting aspects can be found from considering the density of states due to a single muffin-tin potential. From Eq. (3.23) it follows that

$$\mathrm{Im}\, G(\mathbf{r}, \mathbf{r}\,'; \epsilon) = -\sqrt{\epsilon} \sum_L R_l(r\,;\epsilon) R_l(r'\,;\epsilon) Y_L^*(\hat{\mathbf{r}}) Y_L(\hat{\mathbf{r}}') \tag{3.69}$$

where we have made use of Eq. (3.11). For free electrons, Eq. (3.69) reads

$$\mathrm{Im}\, G_0(\mathbf{r}, \mathbf{r}\,'; \epsilon) = -\sqrt{\epsilon} \sum_L j_l(\sqrt{\epsilon}\, r) j_l(\sqrt{\epsilon}, r') Y_L^*(\hat{\mathbf{r}}) Y_L(\hat{\mathbf{r}}') \tag{3.70}$$

Using Eq. (3.69) and (3.31) we can write

$$\mathrm{Im}\, G(\mathbf{r}, \mathbf{r}\,'; \epsilon) = \sum_L Z_L^*(r\,;\epsilon) Z_L(r'\,;\epsilon) \mathrm{Im}\, t_L(\epsilon) \tag{3.71}$$

with $t_L(\epsilon)$ defined in Eq. (3.32) and $Z_L(r\,;\epsilon)$ defined in Eq. (3.34)

The change in the density of states due to the introduction of the potential is [37]

$$\begin{aligned} \Delta\, n(\epsilon) &= n(\epsilon) - n_0(\epsilon) \\ &= \frac{\sqrt{\epsilon}}{\pi} \sum_l (2l+1) \int_0^\infty dr\, r^2 \left[R_l^2(r\,;\epsilon) - j_l^2(\sqrt{\epsilon}\, r) \right] \\ &= \frac{1}{\pi} \sum_l (2l+1) \frac{\partial}{\partial \epsilon} \delta_l(\epsilon) \end{aligned} \tag{3.72}$$

This is the Friedel sum and it shows how a phase shift varying rapidly with energy can give rise to a large density of states near the resonance energy. The density of states curve (Fig. 3.7) is not to be confused with the d-band density of states. Here Δn is due to a single muffin-tin potential in a flat potential background. Its width is the width of the d-resonance Γ (Eq. 3.16) and not the width of the d-band. However,

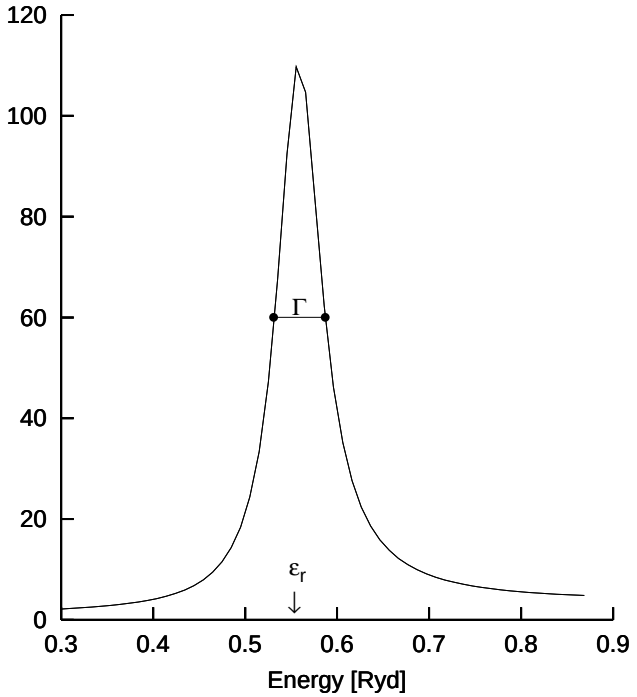

Figure 3.7: The Friedel sum contribution to the density of states for the Pd muffin-tin potential discussed in text.

when scattering from more potentials is included, this resonance peak will broaden out into the d-band. It remains true that a sharp resonance will give rise to a narrow d-band and a broad resonance to a broad band.

In order to calculate the average densities of states we must first obtain an expression for the average Green function $\langle G(\mathbf{r},\mathbf{r}';\epsilon)\rangle$ when $\mathbf{r}=\mathbf{r}'$. This is easily achieved with the help of the site diagonal form of the Green function for an arbitrary array of scatterers Eq. (3.50). The averaging process proceeds then in two stages. First the average is taken over the possible occupancies ($A(B)$ for the case of an $A_{c_A}B_{c_B}$ random alloy) of this site. The result of this process is

$$\begin{aligned}\langle G(\mathbf{r},\mathbf{r}';\epsilon)\rangle \;=\; \sum_{LL'}\Big\{ & c_A Z_L^A(\mathbf{r}_n;\epsilon)\,\langle\tau_{LL'}^{nn}\rangle_A\, Z_{L'}^A(\mathbf{r}_n;\epsilon) + c_B Z_L^B(\mathbf{r}_n;\epsilon)\,\langle\tau_{LL'}^{nn}\rangle_B\, Z_{L'}^B(\mathbf{r}_n;\epsilon) \\ & - \Big[c_A Z_L^A(\mathbf{r}_n;\epsilon) J_L^A(r_n;\epsilon) \;+c_B Z_L^B(\mathbf{r}_n;\epsilon) J_L^B(r_n;\epsilon)\Big]\,\delta_{LL'}\Big\} \qquad (3.73)\end{aligned}$$

The quantities $\langle\tau_{LL'}^{nn}\rangle_A$ and $\langle\tau_{LL'}^{nn}\rangle_B$ are the conditional averages of Eq. (3.45) for the case that there is definitely an A or B on the site n but the occupancy of all other sites has been averaged over. Eq. (3.73) is an exact expression for the average site diagonal Green function, since as defined above the $\langle\tau_{LL'}^{nn}\rangle_{A(B)}$ are the exact restricted averages.

In order to obtain a formula for the site diagonal Green function with the CPA we must find an approximation to the exact restricted averages $\langle\tau_{LL'}^{nn}\rangle_{A(B)}$. Bearing

in mind the single site nature of the CPA, these exact averages are approximated by

$$\begin{aligned} \tau^{A,nn} &\approx \langle \tau^{nn} \rangle_A \\ \tau^{B,nn} &\approx \langle \tau^{nn} \rangle_B \end{aligned} \tag{3.74}$$

A formal derivation of the correctness of these replacements within the CPA is given in the paper of Faulkner and Stocks [26]. Thus the CPA approximation $G_c(\mathbf{r}, \mathbf{r}'; \epsilon)$ to the average Green function $\langle G(\mathbf{r}, \mathbf{r}'; \epsilon) \rangle$ is obtained by substituting the approximations Eq. (3.74) into Eq. (3.73). The CPA approximation $\overline{n}(\epsilon)$ to the exact average density of states is then given by

$$\overline{n}(\epsilon) = -\frac{1}{\pi} \text{ Im } F^C \tau^{C,nn} \tag{3.75}$$

where

$$F^C = \int_\Omega d^3r \; F^C(\mathbf{r}, \mathbf{r}) = c_A F^A D^A + c_B F^B D^B \tag{3.76}$$

Here the matrix elements of F^A and F^B are given by

$$F^\alpha_{LL'}(\epsilon) = \int_\Omega d^3r Z^\alpha_L(\mathbf{r}; \epsilon) Z^\alpha_{L'}(\mathbf{r}; \epsilon) \tag{3.77}$$

and D^A and D^B correspond to the operators

$$D^\alpha = \left[1 + \tau^{C,nn} \left((t^\alpha)^{-1} - (t^C)^{-1} \right) \right]^{-1} \tag{3.78}$$

In Eqs. (3.77) and (3.78) α stays for A and B. The integrals in Eqs. (3.76) and (3.77) are over a single unit cell. From these equations it is clear that we can resolve the total density of states $\overline{n}(\epsilon)$ into components $\overline{n}_A(\epsilon)$ and $\overline{n}_B(\epsilon)$, which can be thought of as average densities of states on an A-type site and B-type site in the alloy, according to

$$\overline{n}(\epsilon) = c_A \overline{n}_A(\epsilon) + c_B \overline{n}_B(\epsilon) \tag{3.79}$$

where $\overline{n}_\alpha(\epsilon)$, $\alpha = A, B$ are given by

$$\overline{n}_\alpha(\epsilon) = -\frac{1}{\pi} \text{Im Tr} F^\alpha D^\alpha \tau^{\alpha,nn} \tag{3.80}$$

The above formulae for the total densities of states are those derived by Faulkner and Stocks [26]. These equations are simple to evaluate once the cluster CPA equations have been solved. They involve the t^C and $\tau^{C,nn}$ which are obtained during a cluster CPA calculation and the wavefunctions $Z^A_L(r; \epsilon)$ and $Z^B_L(r; \epsilon)$ and the phase shifts for a single A and B type muffin-tin well.

Making use of Eqs. (3.77) and (3.78), Eq. (3.80) can be put into the more useful form

$$\begin{aligned}\overline{n}_\alpha(\epsilon) &= -\frac{1}{\pi}\int_{\text{cell }n} d^3r \text{Im}G(\mathbf{r}_n,\mathbf{r}_n;\epsilon) \\ &= -\frac{1}{\pi}\sum_{LL'}\int_{\text{cell }n} d^3r Z_L^{\alpha,n}(\mathbf{r};\epsilon)Z_{L'}^{\alpha,n}(\mathbf{r};\epsilon)^* \\ &\quad \times \begin{cases} \text{Im}\tau_{LL'}^{\alpha,nn,CPA}(\epsilon) & \text{CPA} \\ \text{Im}\tau_{LL'}^{\alpha,nn,C}(\epsilon) & \text{cluster (isolated or embedded)} \end{cases}\end{aligned} \tag{3.81}$$

that allow the calculation of densities of states once the CPA and/or cluster scattering path operators are known.

3.4.2 Conductivity Calculation

Linear-response theory provides very general expressions for transport coefficients which are exact in the limit of weak external fields. The frequency-dependent electrical conductivity tensor $\sigma(\omega)$ can be written as [48], [22], [33]

$$\sigma_{\mu\nu}(\omega) = \frac{1}{V}\int_0^\infty dt\ e^{-i\omega t}\int_0^{1/kT} d\lambda \left\langle J^\nu(-i\hbar\lambda)J^\mu(t)\right\rangle \tag{3.82}$$

where V is the volume of the system, and J is the current operator in the unperturbed Heisenberg picture. $\langle ...\rangle$ denotes a thermodynamic average. This expression, although very general and exact, is not suitable for practical calculations. However, by making some additional assumptions one can derive an equation which is more useful. In particular, one assumes a one-electron picture of the electronic system, considers merely elastic scattering by static impurities and neglects the motion of the ions. The diagonal components of the electrical conductivity tensor of a disordered metallic conductor at zero temperature, that is with disorder originating from the atomic arrangement only, can then be written as

$$\sigma_{\mu\mu} = \frac{\pi\hbar}{V}\left\langle \text{Tr}\ \left[\delta(\epsilon - H)J^\mu\delta(\epsilon - H)J^\mu\right]\right\rangle \tag{3.83}$$

This is one of the forms of the Kubo-Greenwood equation. By using the Green function of the system one obtains an alternative form

$$\sigma_{\mu\mu} = \frac{\hbar}{\pi V}\left\langle \text{Tr}\ \left[J^\mu \text{Im}\, G(\epsilon)J^\mu \text{Im}\, G(\epsilon)\right]\right\rangle_{conf} \tag{3.84}$$

where J^μ denotes the current operator in the μ^{th} spatial direction. The average has to be taken over all possible configurations of the disordered system in both cases.

In terms of the scattering path operator (Eqs. (3.64) and (3.67)), the Kubo-Greenwood equation can be rewritten as

$$\sigma_{\mu\mu}(\epsilon) = -\frac{m_e^2}{\pi\hbar^3 V}\sum_{z_1,z_2} s_{z_1,z_2}$$

$$\times \sum_{mn} \sum_{L_1,L_2,L_3,L_4} \left\langle J^{m\mu}_{L_4L_1}(z_2,z_1)\tau^{mn}_{L_1L_2}(z_1)J^{n\mu}_{L_2L_3}(z_1,z_2)\tau^{nm}_{L_3L_4}(z_2)\right\rangle_{conf} \quad (3.85)$$

where $s_{z_1,z_2} = 2\delta_{z_1,z_2} - 1$, and z_1 and z_2 are the two side limits of the complex energies defined by $z_{1,2} = \epsilon \pm i\eta$, with $\eta \longrightarrow 0$.

The configurational average in Eq. (3.87) within the CPA was derived by Butler [11]. In our calculations we used the form given in [5],

$$\begin{aligned}\sigma_{\mu\mu}(\epsilon) = &-\frac{m_e^2}{\pi\hbar^3 V}\sum_{z_1,z_2} s_{z_1,z_2} \\ &\times \sum_{\alpha\beta}\Big[\frac{1}{V_{BZ}}\int_{BZ} d^3\,k\left(c_\alpha c_\beta J^{\alpha\mu}(z_2,z_1)\tau(\mathbf{k},z_1)J^{\beta\mu}(z_1,z_2)\tau(\mathbf{k},z_2)\right) \\ &+ c_\alpha c_\beta J^{\alpha\mu}(z_2,z_1)\tau^{CPA}(z_1)\left[J^{\alpha\mu}(z_1,z_2) - J^{\beta\mu}(z_1,z_2)\right]\tau^{CPA}(z_2)\Big] \quad (3.86)\end{aligned}$$

We calculated and discussed the behavior of the inverse of the function

$$\sigma(\epsilon) = \sum_{\mu}\sigma_{\mu\mu}(\epsilon) \quad (3.87)$$

denoted

$$\rho(\epsilon) = \frac{1}{\sigma(\epsilon)} \quad (3.88)$$

We emphasize that $\sigma(\epsilon)|_{\epsilon=E_F}$ is the electrical conductivity and $\rho(\epsilon)|_{\epsilon=E_F}$ represents the electrical resistivity of the system.

For the cluster methods we calculated $\rho(\epsilon)$ at each energy and for each configuration using the Eqs. (3.85), (3.87) and (3.88). Its configurational average was taken to be the algebraic average over the number of configurations used in calculations.

With the use of Eqs. (3.82) and (3.88) densities of states and resistivities can be calculated within the framework of CPA and cluster methods.

Chapter 4

Results

The aim of this work was the development, implementation and use of some approach to the theory of alloys able to take into account the effects of the local environment on the electronic properties of alloys. As was shown in chapter 3, cluster methods based on the coherent potential approximation could, in principle, solve the problem. In this chapter we will try to show that indeed the isolated cluster and embedded cluster methods described in section 3.3 are good alternatives to the single-site CPA method when multi-site effects are involved. The first part of the chapter is dedicated to an extensive discussion of the results of the two cluster methods when applied to disordered systems. The regime of the applicability of the cluster methods and their advantages over the CPA will be discussed (see also [21]). The second part of the chapter will deal with the application of the cluster methods to alloys with short-range order.

4.1 General Parameters and Definitions

The potentials used for all electronic structure calculations were self-consistent alloy potentials generated in a first step by iterating the KKR–CPA equations until charge self-consistency was achieved.

The Fermi energies determined in the KKR–CPA calculations were used for all the cluster calculations. A *scalar relativistic* approach including all relativistic effects except spin-orbit interaction was chosen. Angular momentum expansions were carried out up to a maximum value of $l = 2$ in almost all cases. Spherical clusters were generated (for their construction see section 2).

The functions $n(\epsilon)$ (density of states) given in Eq. (3.82) and $\rho(\epsilon)$, Eq. (3.88), and their behavior in various situations were calculated and plotted. Note that the function $\rho(\epsilon)$ has no special physical meaning except at the Fermi energy, where it gives the resistivity of the alloy considered.

4.2 Symmetry Tests

Prior to the actual calculations some tests were performed to check the correct implementation of the formalism. All possible configurations of a 1-shell cluster (one

central atom plus 12 neighboring atoms) in an FCC lattice, i.e. $2^{13} = 8192$ configurations, were divided into equivalence classes characterized by their equivalence under one of the 48 symmetry operations of the cubic symmetry group. There are 288 such equivalence classes.

The following tests were successfully carried out: (i) the density of states and the trace of the conductivity tensor are identical for all members of one particular equivalence class; (ii) although various configurations belonging to the same equivalence class in general yield different diagonal elements of the conductivity tensor, the difference is always merely a permutation of the three spatial components; (iii) while for general occupations of the clusters with A- or B-atoms the three diagonal components of the conductivity tensor are different, degeneracies occur whenever the occupation shows certain symmetries. If, e.g., in a 1-shell cluster the first shell contains only one A-atom, the remaining atoms being of type B, two diagonal components of the conductivity tensor are identical.

4.3 Calculations for Disordered Alloys

Three different binary alloy systems were treated: the FCC alloy systems Ag–Pd and Cu–Pt and the FCC alloy $Mo_{0.2}Ni_{0.8}$. Ag–Pd is a "classical" alloy for discussing the electronic structure of disordered alloys. Already Mott used this alloy to demonstrate the influence of d-bands on the transport properties of alloys [57] and many other authors did the same later. Cu–Pt is known to have a high residual resistivity which makes it attractive for cluster calculations as will be explained later. $Mo_{0.2}Ni_{0.8}$ has an even higher resistivity and was used for cluster calculations by Nicholson et al. [58]. It also displays a very strong dependence of the resistivity on the short-range order, thus being well suited for studying this dependence.

Three situations were considered: (i) the infinite system described by the CPA, (ii) isolated clusters of a certain size where each lattice site was occupied by one of the alloy potentials, or (iii) clusters of a given size occupied by said potentials but embedded in an infinite CPA medium. Clearly, only the single-site scattering case (CPA) is treated fully self-consistently in this way, whereas the treatment of the clusters was only approximately self-consistent. However, as in most calculations only clusters were permitted which had compositions corresponding to the macroscopic concentration, deviations from self-consistency should be small.

By the use of the cluster methods, various sets of calculations were carried out: the number of configurations used for the average, the size of the involved clusters and the embedding medium (none or CPA) were varied.

The occupations of each lattice site of a given cluster of an alloy in a disordered state were determined with a random number generator. The occupation probability of each atom type was assumed to be proportional to the macroscopic concentration of the respective component. For most calculations an additional boundary condition was imposed on the construction of configurations: only configurations in which the

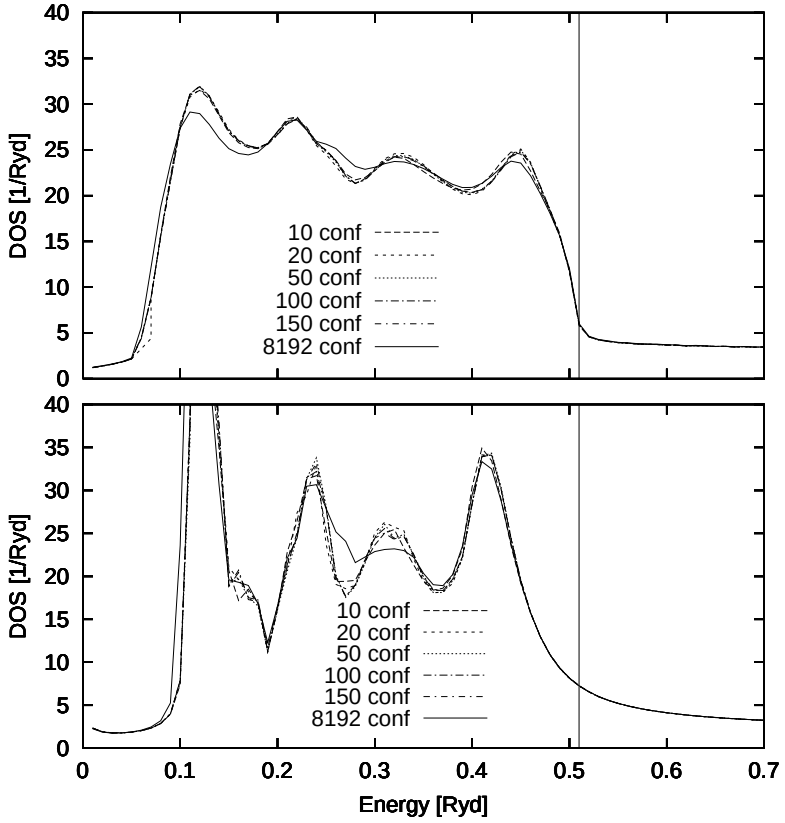

Figure 4.1: Configurationally averaged density of states of spherical 1-shell (13 atoms) $Ag_{0.5}Pd_{0.5}$ clusters (embedded in a CPA medium: upper plot, isolated: lower plot) as a function of energy. Varying number of random configurations (restricted except for the case of 8192 configurations), cluster occupation in first shell: 3×Ag, 3×Pd. Vertical line: Fermi energy.

number of A- and B-atoms corresponded to their macroscopic concentrations, c_A and c_B, respectively, were considered. For a $A_{0.2}B_{0.8}$ alloy, e.g., only configurations containing 20% A- and 80% B-atoms in the cluster were allowed. If necessary the occupation numbers were rounded to the next integer. Such configurations will be called "restricted" configurations.

Furthermore, in the configurational averages it was ensured that $c_A \times N$ of a total of N configurations had an A-atom at the central site, the remaining $c_B \times N$ configurations having a B-atom in the center. This condition is important only for the DOS calculation which is sensitive to the occupation of the central site.

4.3.1 Calculations for Entire Bands

In a first set of calculations the density of states and the $\rho(\epsilon)$ function were determined for energies covering the entire d-band and some of the region above and below, i.e. between -0.1 and 0.7 Ryd above the muffin-tin zero for $Ag_{0.5}Pd_{0.5}$, be-

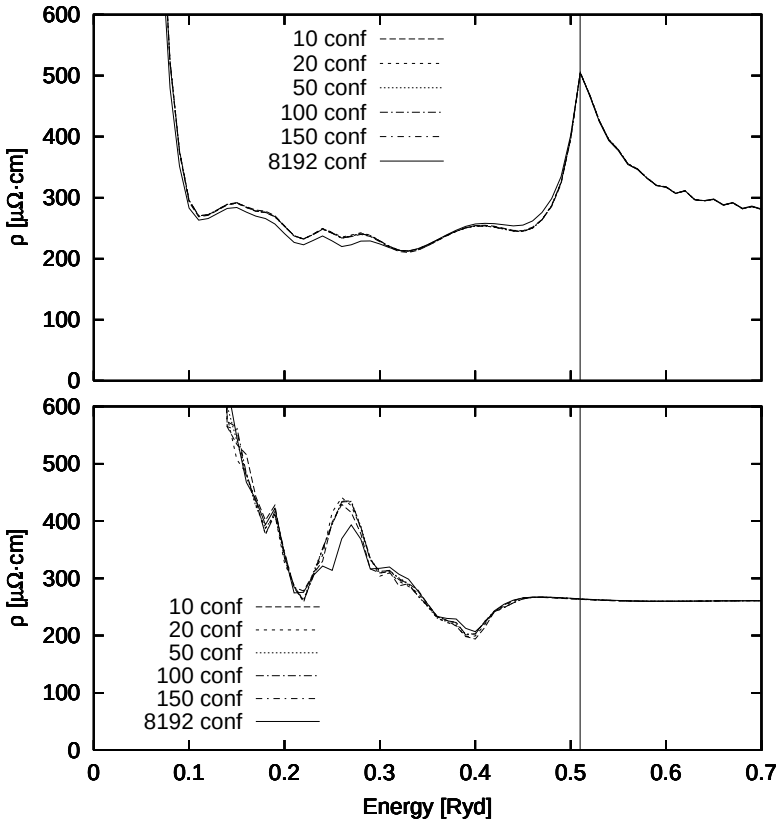

Figure 4.2: Same as Fig. 4.1 for resistivity.

tween 0.0 and 0.7 Ryd above the muffin-tin zero for $Cu_{0.5}Pt_{0.5}$ and between 0.0 and 1.0 Ryd above the muffin-tin zero for $Mo_{0.2}Ni_{0.8}$. Calculations were carried out for each of a given set of restricted cluster configurations and for various cluster sizes. The single results were then averaged yielding configurationally averaged densities of states and $\rho(\epsilon)$ functions.

Configurational Averaging

In order to be able to assess the importance of the number of configurations necessary for a correct representation of disorder, configurational averages including from 10 to 8192 (i.e. all, but of which only the 288 inequivalent configurations were treated explicitly) configurations for 1-shell clusters (13 atoms) of silver and palladium atoms were carried out. Fig. 4.1 shows the density of states at the central site of a 1-shell spherical cluster calculated by the embedded and isolated cluster method. Fig. 4.2 shows the corresponding $\rho(\epsilon)$ functions.

One can see from Fig. 4.1 that: (i) the density of states shows a certain sensitivity to the number of configurations but only for energies close to the band edges; (ii) for most other energies quite precise results are already obtained for 10 configurations; (iii) the full average is a bit different from the averages which merely

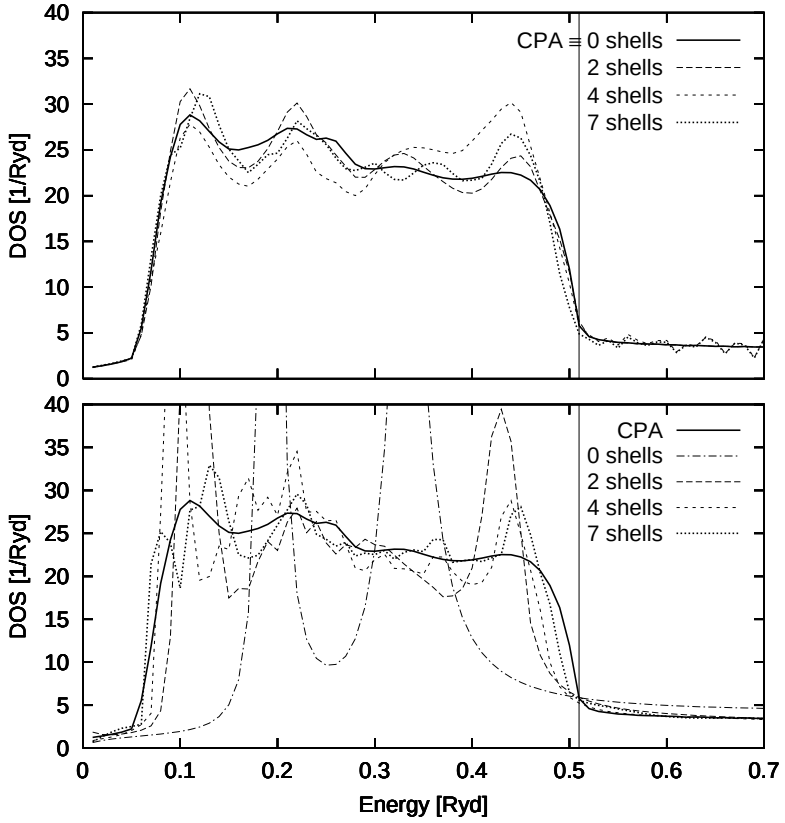

Figure 4.3: Configurationally averaged density of states of spherical $Ag_{0.5}Pd_{0.5}$ clusters of various sizes (embedded in a CPA medium: upper plot, isolated: lower plot) as a function of energy (averaged with 10 restricted configurations). Vertical line marks Fermi energy.

contain restricted configurations. This is due to the presence of the full range of configurations that include also configurations corresponding to certain degrees of order; (iv) the same is true for the $\rho(\epsilon)$ function shown in Fig. 4.2.

These findings are important because they allow to confine the calculations to a fairly low number of configurations thus saving much computation time.

Shell Size Dependence of Density of States

Another objective of the calculations was to investigate the behaviour of the density of states and the $\rho(\epsilon)$ function as the dimension (i.e. number of shells) of the cluster is increased. Ten randomly chosen restricted configurations were used for the configurational average and spherical clusters containing up to 7 shells (135 atoms) were constructed. Fig. 4.3 shows the density of states at the central site of spherical Ag-Pd clusters for various cluster sizes calculated by the isolated and embedded cluster method. The clusters consist of equal numbers of Ag and Pd atoms. The results of CPA calculations are also shown for matters of comparison.

The densities of states for the CPA and for embedded clusters do not deviate

from each other very much (see Fig. 4.3 upper plot). This is easy to understand: for the 0-shell "cluster" this is exactly true owing to the definition of the CPA as single-site average. For larger shells the cluster results deviate from the CPA values for two reasons: firstly, as only 10 configurations are taken into account in the configurational average the sampling of disorder is not perfect thus leading to some deviations (see Fig. 4.1). As will be shown later, the density of states is quite sensitive to the environment of a cluster. The restricted configurational average therefore might influence the density of states. Secondly, even if all configurations were included in an average (what is impractical for large cluster sizes) the DOS would deviate from the CPA. One reason is that the embedded cluster formalism is a non-self-consistent method. Another reason is that, within the CPA all the sites have the same environment that consists of scatterers with a scattering matrix $t = t^{CPA}$ at each site. Within the cluster methods the environment of each site is different and contains scattering matrices $t = t^A$ and $t = t^B$ depending on the arrangement of the two types of atoms arround one site. Thus, the cluster method includes local environment effects which lead to a more complex electronic structure.

The density of states of isolated clusters (Fig. 4.3 lower plot) is quite different from that of embedded clusters. This is because especially for small clusters the neighborhood of the central site is quite different in an isolated cluster as compared to an embedded cluster. Fig. 4.3 nicely shows how the bands are formed as the cluster size is increased (see also the discussion in Section 3.1.1). For the 0-shell "cluster" (only central atom) two pronounced peaks are present. They are the sum of the density of states of a single silver and a single palladium atom. Both densities of states are broadened in energy because one is dealing with energies belonging to the continuous spectrum of the single atom potentials. The two peaks are centered at the energies where the two components have their d-like scattering resonances. As the cluster size is increased the d-bands build up and the cluster density of states moves closer and closer towards the corresponding rectangular shaped density of states of the CPA. However, one can still see some oscillations of the DOS especially near the band edges even for 7 shells (135 atoms). This is typical for finite systems (see Refs. [66, 76] for similar calculations). Only in the limit of very large (infinite) clusters the density of states is expected to get rounded off near the band edges and get close to the CPA result. However, even in this case local environment effects would lead to some differences.

Comparison between ECM and ICM Densities of States

In Fig. 4.4 the ECM and ICM densities of states are plotted together for $Ag_{0.5}Pd_{0.5}$ clusters of 7 shells. As one can see, the differences between the two are minor and come mainly from the fact that within the ICM one deals with a finite system while within the ECM the system is infinite. The ECM density of states should be accurate. It contains the effects of the local environment. Its shape influenced mainly by the local environment while the arrangement of the atoms in shells far

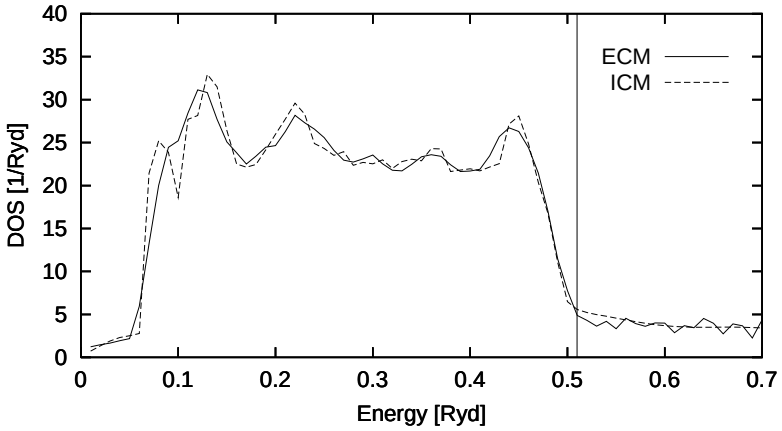

Figure 4.4: Configurationally averaged density of states of spherical $Ag_{0.5}Pd_{0.5}$ clusters of 7 shells embedded in a CPA medium (solid line) and isolated (dashed line) as a function of energy (averaged with 10 restricted configurations). Vertical line marks Fermi energy.

away from the site considered is less important. Thus, the CPA embedding medium ensures that the system is infinite and its contribution to the shape of the density of states is, for sufficiently large clusters, not important. It can be concluded that both methods give reliable results for the DOS with the observation that the ICM results suffer due to the finiteness of the system considered.

Shell Size Dependence of $\rho(\epsilon)$ Function

Fig. 4.5 compares the $\rho(\epsilon)$ functions calculated by means of ICM and ECM for spherical $Ag_{0.5}Pd_{0.5}$ clusters of various sizes. Figs. 4.6 and 4.7 give $\rho(\epsilon)$ for the alloys $Cu_{0.5}Pt_{0.5}$ and $Mo_{0.2}Ni_{0.8}$ (ICM calculations only). Figs. 4.5 to 4.7 show that the tendency observed for the density of states can also be found for the $\rho(\epsilon)$ function: the cluster values get closer to the corresponding CPA values as the shell number is increased. This is true for both types of clusters. Three energy regimes can be distinguished: (i) in the low energy regime the cluster values of the $\rho(\epsilon)$ function, especially that of isolated clusters, exceed the CPA values by a factor of 50 and more. This applies to all three alloys investigated; (ii) in an intermediate regime which is about the regime of the d-bands the cluster values get quite close to the CPA ones as the cluster size is increased. Embedded clusters (results only shown for Ag–Pd) lead to results slightly closer to the CPA than isolated clusters in this regime; (iii) finally, for the energy regime above the d-band complex, i.e. above the Fermi energy, the cluster values deviate more from the CPA ones again. Especially Ag–Pd where the CPA values drops to very low values above the Fermi energy, shows this strong discrepancy. Moreover, for high energies embedded and isolated cluster values of the $\rho(\epsilon)$ function

The explanation for the different regimes is straightforward: a cluster approach can yield a correct value for the $\rho(\epsilon)$ function only if the mean free path of the

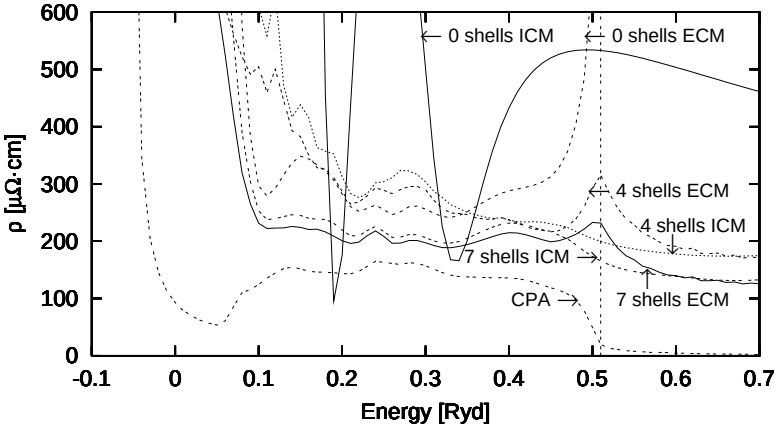

Figure 4.5: Configurationally averaged resistivity of spherical $Ag_{0.5}Pd_{0.5}$ clusters of various sizes (embedded in a CPA medium: marked "ECM," isolated clusters: marked "ICM") as a function of energy (averaged with 10 restricted configurations). Vertical line marks Fermi energy.

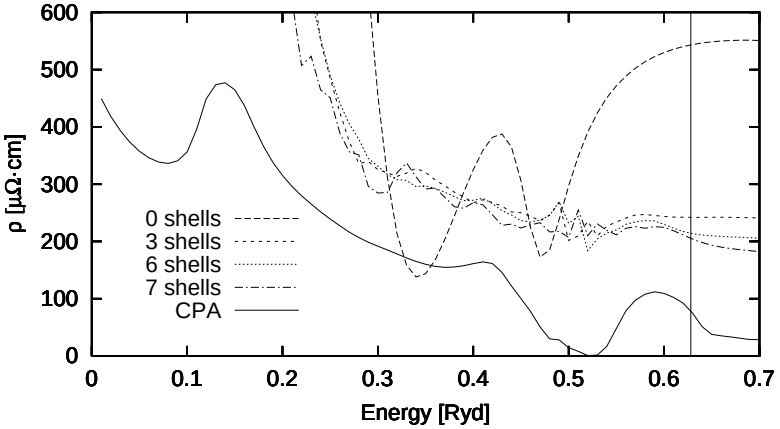

Figure 4.6: Same as Fig. 4.5 for $Cu_{0.5}Pt_{0.5}$ (only isolated clusters).

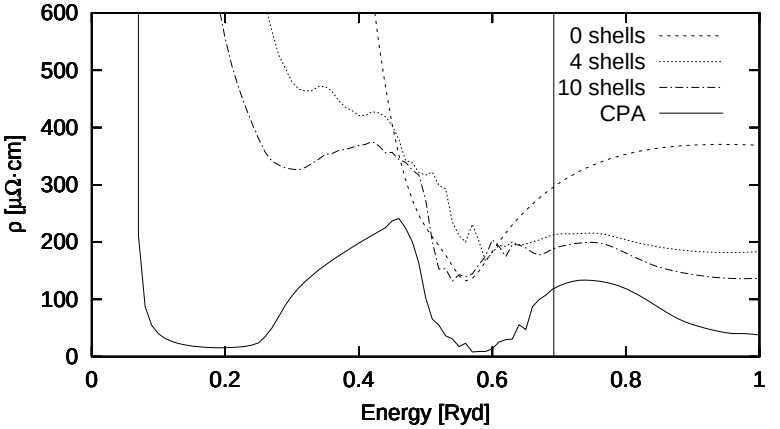

Figure 4.7: Same as Fig. 4.5 for $Mo_{0.2}Ni_{0.8}$ (only isolated clusters).

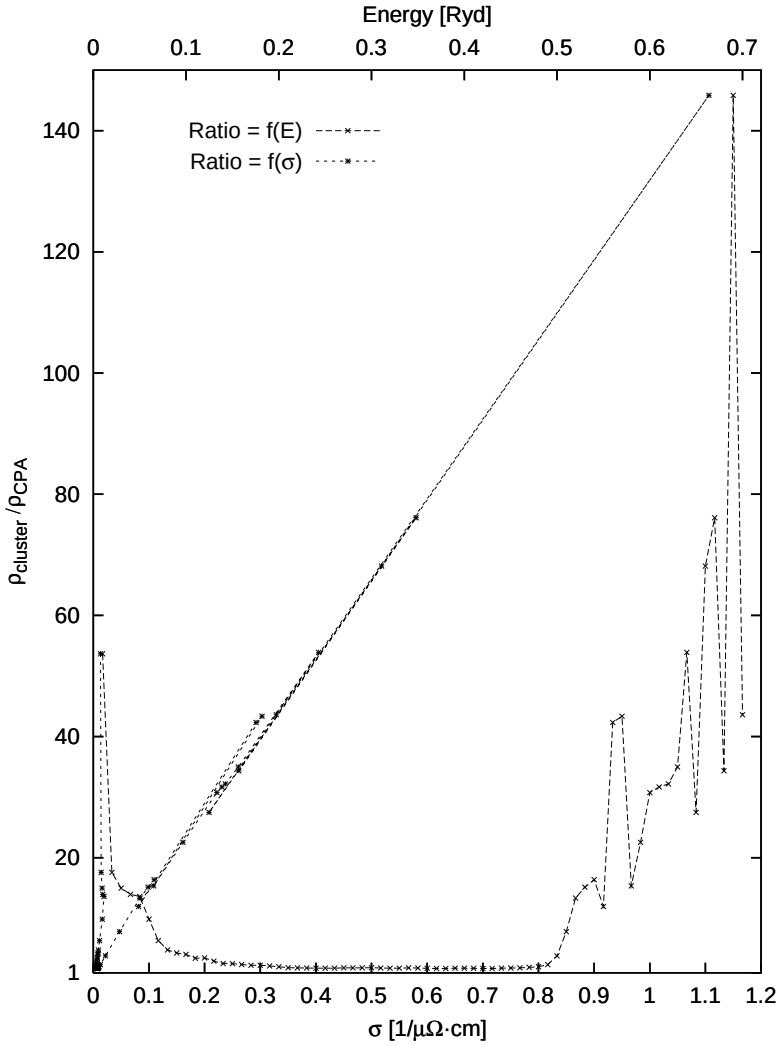

Figure 4.8: Ratio of cluster and CPA $\rho(\epsilon)$ ($\rho_{cluster}(\epsilon)/\rho_{CPA}(\epsilon)$) for $Ag_{0.5}Pd_{0.5}$ shown as a function of energy, $f(E)$, and as a function of $\sigma_{CPA}(\epsilon)$, f(σ). Calculations based on isolated 7-shell clusters and 10 restricted configurations.

conduction electrons is in the range of the cluster size or smaller. If the mean free path is much longer the scattering processes which are responsible for the finite values of $\rho(\epsilon)$ cannot be expected to be included in the cluster representation any more. As $\rho(\epsilon)$ takes its highest values for energies in the d-bands of a transition metal (corresponding to short mean free paths) the cluster methods yield their best results in this energy regime. Using the CPA one clearly does not have this problem because the CPA treats an infinite averaged medium and is therefore capable of treating any mean free path. In contrast, approximations with small clusters only work well for systems with strong scattering (high $\rho(\epsilon)$). It is important to emphasize that the fact that cluster $\rho(\epsilon)$ get closer to the corresponding CPA values with increasing cluster sizes does not mean that there is an actual convergence. Convergence cannot be

expected. Even a very large (infinite) cluster would give results deviating from the CPA because cluster calculations include multi-site effects that cannot be treated within a single-site formalism such as the CPA.

That the interpretation given is indeed plausible can be seen by looking at the deviation of cluster and CPA resistivities expressed by the ratio $\rho_{cluster}(\epsilon)/\rho_{CPA}(\epsilon)$ as a function of both energy and CPA conductivity as it is displayed in Fig. 4.8. The ratio as a function of energy shows high values for low energies, i.e. below about 0.1 Ryd, and energies above about 0.5 Ryd as one can of course already see from Fig. 4.5. Looking at the ratio as a function of conductivity one finds an almost linear relationship except for the lowest energies. Therefore, the smaller the CPA conductivity is (indicating a short mean-free path) the smaller the ratio between cluster and CPA resistivities. Extrapolating the conductivity to zero one sees that the ratio tends towards one. This means that the cluster resistivities get very close to the CPA if the mean free path is negligible compared to the cluster diameter. However, as already pointed out, one cannot expect an exact agreement because of the principal differences between single-site CPA and cluster expansions which contain multi-site effects.

It is interesting to note a major difference between the density of states and $\rho(\epsilon)$ calculated by ECM. In the discussion of the results for the density of states (section 4.3.1) we said that a 0-shell "cluster" embedded in a CPA medium is, when averaged over the 2 possible configurations, the CPA. This can be proved using Eq. (3.82). The situation is somewhat different for the $\rho(\epsilon)$ function. One can show, using Eq. (3.85) that the ECM $\sigma(\epsilon)$ for the 0-shell "cluster," averaged over the 2 possible configurations is

$$\sigma(\epsilon) = -\frac{4m_e^2}{\pi\hbar^3 V}\sum_{\alpha} c_\alpha J^{\alpha\mu}(z_2, z_1)\tau^{CPA}(z_1)J^{\alpha\mu}(z_1, z_2)\tau^{CPA}(z_2) \tag{4.1}$$

which is different from the result for the CPA given in Eq. (3.86). This difference leads to the difference between ECM and CPA values of $\rho(\epsilon)$ and to a correct behavior of the values of $\rho(\epsilon)$ with respect to the dimension of the cluster.

4.3.2 Calculations at the Fermi Energy

A second set of calculations was carried out at the Fermi energy only. Spherical clusters containing up to 11 shells (201 atoms) were considered. The average was again performed over 10 restricted configurations (except for the 0-shell cluster which only contains the central atom where only the two possible configurations were used). The three alloys $Ag_{0.5}Pd_{0.5}$, $Cu_{0.5}Pt_{0.5}$ and $Mo_{0.2}Ni_{0.8}$ were considered. Figures 4.9 and 4.10 show the density of states and the resistivity of clusters plotted as a function of cluster size (total number of shells and atoms given). The plots show the results for the single configurations as well as for the average. The corresponding CPA results are given by horizontal lines in Fig. 4.9, whereas the CPA-resistivity has been subtracted from the cluster results in Fig. 4.10 to allow for displaying all

results in one plot. In Fig. 4.9 the individual results for the density of states are marked differently according to the type of atom in the center of the cluster.

Density of States at the Fermi Energy

The densities of states of various isolated and embedded clusters at the Fermi energy are shown in Fig. 4.9. It is evident that the values for individual configurations scatter very much even if the atom in the center (at which the DOS is calculated) is the same. The spread of the results is smaller for isolated clusters than for embedded clusters. Looking at the results more closely, one finds that, (i) for the two alloys of an s-band metal (Ag, Cu) with a d-band metal (Pd, Pt) the DOS is low for the s-band atom at the center, high for the d-band metal at the center, (ii) the configurations with the s-band metal at the center are less sensitive to the occupation in the surrounding cluster than the ones with a d-band metal in the center, (iii) for the configurations with a d-band metal in the center very high DOS (e.g. about 30 states/ryd for Ag–Pd) are found for configurations with many other d-band metal atoms in the cluster. These findings are not surprising if we note that for a pure d-band metal the Fermi energy lies in a region where the density of states is high and has a rich structure as a function of energy. Changes in the environment of a d-band atom therefore cause a strong change of the DOS, whereas the DOS of an s-band metal – in which the Fermi energy lies in the flat s-band with a low DOS – is relatively insensitive to the composition of its neighborhood. $Mo_{0.2}Ni_{0.8}$ with two d-band constituents consequently shows about the same behavior of the DOS no matter which of the atoms is in the center.

The averages of 10 restricted configurations (only two for 0-shell "clusters") can be compared with the CPA density of states. One finds that, (i) for a 0-shell embedded "cluster" the two quantities are the same by definition of the CPA; (ii) the averaged embedded cluster-DOS is quite close to the CPA-DOS for all cluster sizes (see discussion in Sec. 4.3.1); (iii) the averaged isolated cluster densities of states deviate more from the CPA-DOS especially for small clusters. The isolated 0-shell "cluster"-DOS is far away from the CPA result in $Mo_{0.2}Ni_{0.8}$, in which the Fermi energy is close to the band edge where such deviations tend to be more pronounced (see Sec. 4.3.2 and Fig. 4.3) and quite close to the CPA-DOS for $Ag_{0.5}Pd_{0.5}$, in which the Fermi energy is far above the band edge. For large isolated clusters all densities of states move towards the CPA as expected.

Resistivity

Turning to the resistivity which is shown in Fig. 4.10 for ten restricted configurations and as configurational average for both isolated and embedded clusters of varying sizes one notes that, i) in contrast to the density of states the resistivity is strongly cluster size dependent; ii) the scatter between individual configurations is much smaller than for the DOS; iii) an increase of cluster size leads to averaged resistivities which slowly approach the CPA resistivity (which is represented by the value "0"

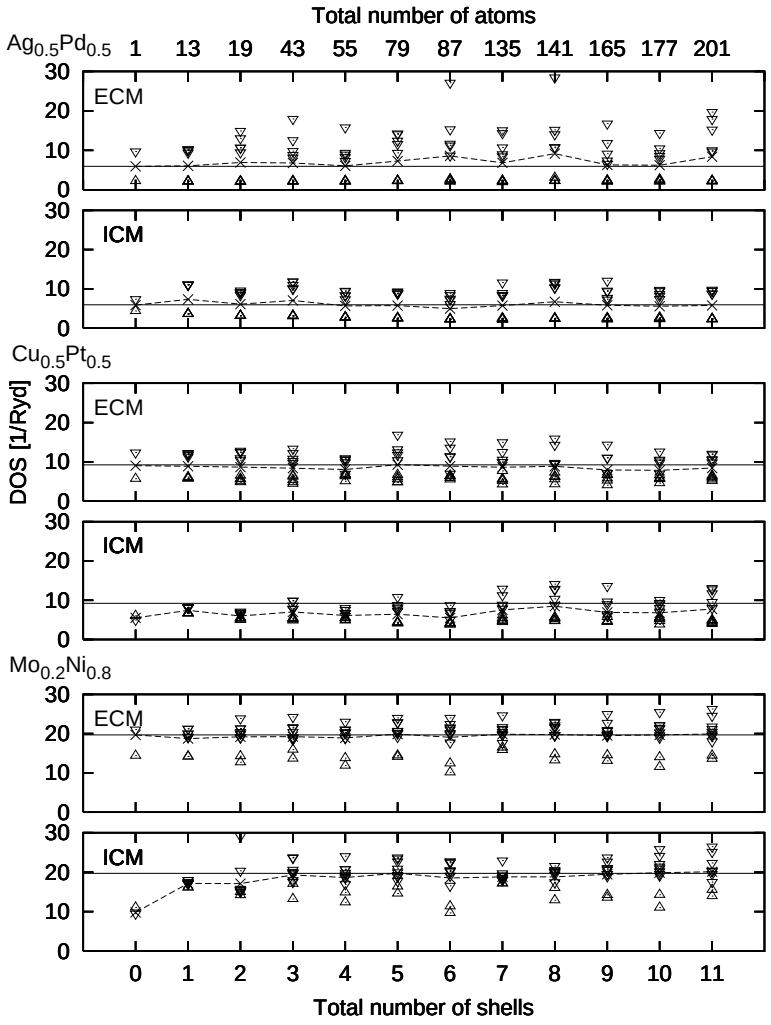

Figure 4.9: Density of states of isolated (ICM) and embedded (ECM) $Ag_{0.5}Pd_{0.5}$, $Cu_{0.5}Pt_{0.5}$ and $Mo_{0.2}Ni_{0.8}$ clusters at the Fermi energy. Component projected DOS for single configurations (A-atom in the center: up triangles, B-atom in the center: down triangles, both DOS not concentration weighted) and the corresponding configurational averages of total DOS (crosses) are shown. CPA results are given by horizontal lines.

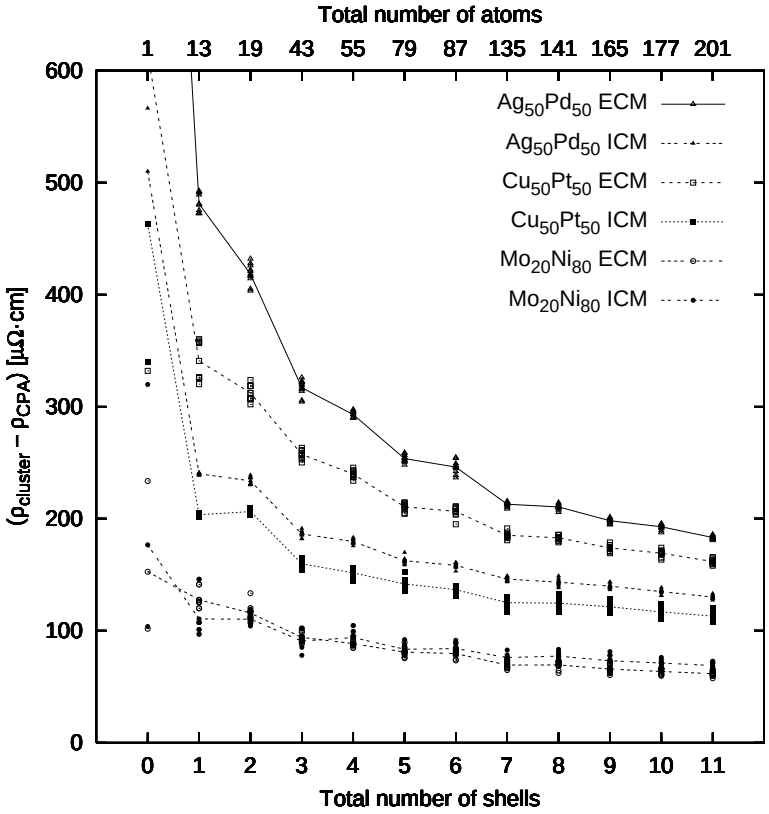

Figure 4.10: Resistivities of isolated (ICM) and embedded (ECM) clusters at the Fermi energy for $Ag_{0.5}Pd_{0.5}$, $Cu_{0.5}Pt_{0.5}$ and $Mo_{0.2}Ni_{0.8}$. Results for the ten restricted configurations and the corresponding configurational averages are shown. Resistivities are given relative to the CPA resistivity ($Ag_{0.5}Pd_{0.5}$: 23.1$\mu\Omega$·cm, $Cu_{0.5}Pt_{0.5}$: 80.2$\mu\Omega$·cm, $Mo_{0.2}Ni_{0.8}$: 120$\mu\Omega$·cm)

in Fig. 4.10); iv) the resistivities lie closest to the CPA for $Mo_{0.2}Ni_{0.8}$, followed by $Cu_{0.5}Pt_{0.5}$ and $Ag_{0.5}Pd_{0.5}$; v) isolated and embedded clusters show a similar tendency. For $Ag_{0.5}Pd_{0.5}$ and $Cu_{0.5}Pt_{0.5}$ isolated clusters lead to lower resistivities while for $Mo_{0.2}Ni_{0.8}$ the opposite is true; vi) the changes in resistivity when one increases the cluster size are more pronounced for small clusters and when the shell added has many atoms.

The behavior of the density of states differs from that of the resistivity because the DOS is a local quantity describing the electronic structure at one particular location in the cluster (the center), whereas for the resistivity all sites of a cluster are treated in the same way. Moreover, from what was said in Sec. 4.3.1 one knows that the resistivity is strongly shell-size dependent especially when the mean free path is in the range or larger than the shell diameter because then the scattering process cannot be represented properly and each increase in shell size adds significant contributions to the resistivity. Only when the mean free path is much shorter than the diameter of the cluster one would expect that the resistivity saturated out as a

function of shell size. Such an effect does clearly not exist for the density of states which is not influenced very much by distant atoms. For $Cu_{0.5}Pt_{0.5}$ a mean-free path of 1.7 nm was determined from the Boltzmann equation as described in Ref. [2] which corresponds to about 4.5 lattice spacings or slightly less than the diameter of a 5-shell cluster. For $Ag_{0.5}Pd_{0.5}$ the mean free path is about three times as long, for $Mo_{0.2}Ni_{0.8}$ it is about half the mean free path for $Cu_{0.5}Pt_{0.5}$. This perfectly explains the magnitude of deviation between cluster resistivities and CPA as seen in Fig. 4.10 which increases from $Mo_{0.2}Ni_{0.8}$ to $Cu_{0.5}Pt_{0.5}$ and $Ag_{0.5}Pd_{0.5}$. From Fig. 4.10 it is also obvious that a convergence of the resistivity (to some 'infinite cluster"-value, not to the CPA resistivity) has not been achieved for 11-shell clusters (201 atoms) and that still larger clusters are necessary to obtain convergence.

4.3.3 Calculations for Varying Alloy Compositions

A third set of calculations was devoted to the comparison of different alloys. For this the whole range of Ag–Pd and Cu–Pt alloys was considered. Figures 4.11 and 4.12 show resistivities at the Fermi energy averaged over 10 restricted random configurations of isolated clusters for each alloy as a function of concentration. Spherical clusters of various sizes up to 11 shells (201 atoms) were considered. CPA resistivities are given for matters of comparison.

Resistivity for Different Alloys

From what was discussed in the previous sections the results for the cluster resistivities for alloys of different compositions shown in Figures 4.11 and 4.12 are not surprising. While the CPA calculation for the alloys Ag–Pd and Cu–Pt reveals the typical distorted Nordheim-like curve with a maximum near 60 and 50 at.% Pd or Pt, respectively, and the drop to zero resistivity for the pure components, the cluster resistivities do not show this behaviour. The cluster results are closest to the CPA resistivity for binary alloys in about the middle of the composition range, while the deviations are largest for dilute alloys. Extrapolation of cluster results to pure components lead to finite resistivities while the (infinite) pure metal should have zero resistivity. This comparison can be visualized best by looking at the ratio between cluster resistivity and the corresponding CPA resistivity and plotting it as a function of composition (Fig. 4.13).

The reason for the better agreement of cluster resistivities with the corresponding CPA results for concentrated alloys clearly again lies in the shorter mean free path in these alloys as was already discussed before. To make this clear the mean free path is shown in Fig. 4.13 and compared to the deviation ratio. The former was determined by using the semiclassical Boltzmann equation[2]. The mean free path given is an average over all electrons in the innermost sheet of the Fermi surface. These electrons carry at least 80% of the electric current. The remaining sheets of the Fermi surface contain slow electrons with a much shorter mean free path.

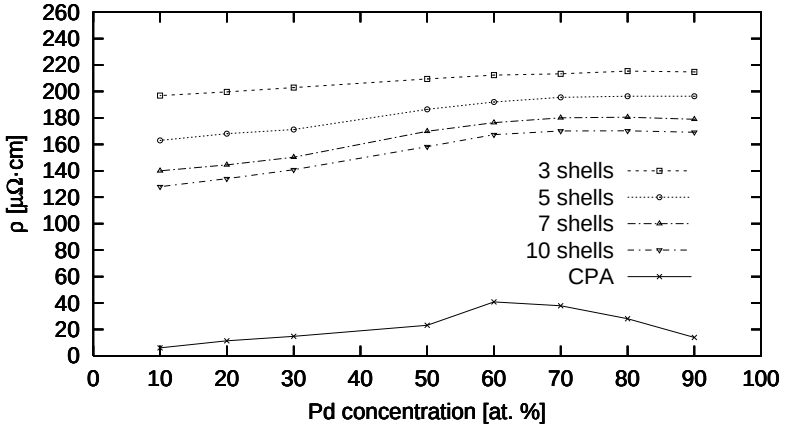

Figure 4.11: Configurationally averaged resistivity of Ag–Pd alloys calculated at the Fermi energy with finite isolated clusters (average over 10 restricted configurations, occupation with number of Ag and Pd atoms corresponding to macroscopic concentration. CPA results are given for matters of comparison.

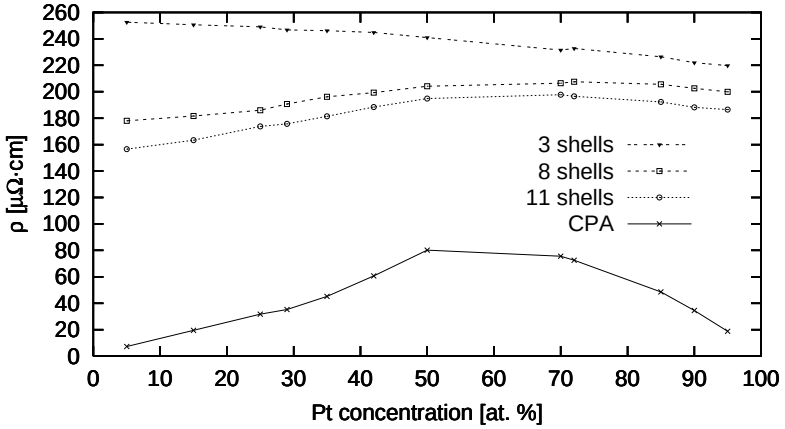

Figure 4.12: Same as Fig. 4.11 for Cu–Pt.

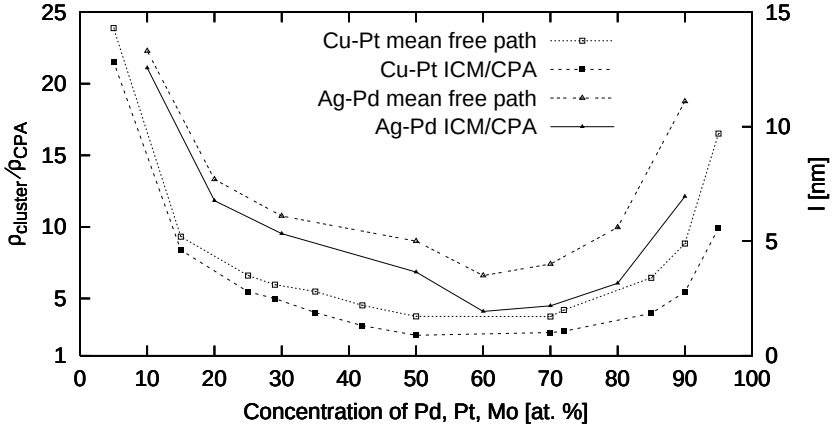

Figure 4.13: Deviation of cluster from CPA resistivities expressed as the ratio $\frac{\rho_{cluster}}{\rho_{CPA}}$ as a function composition (E=E$_F$). Isolated 11-shell clusters and an average with 10 restricted configurations were used. Moreover, the mean free path of the electrons of the innermost sheet of the Fermi surface is given for each alloy.

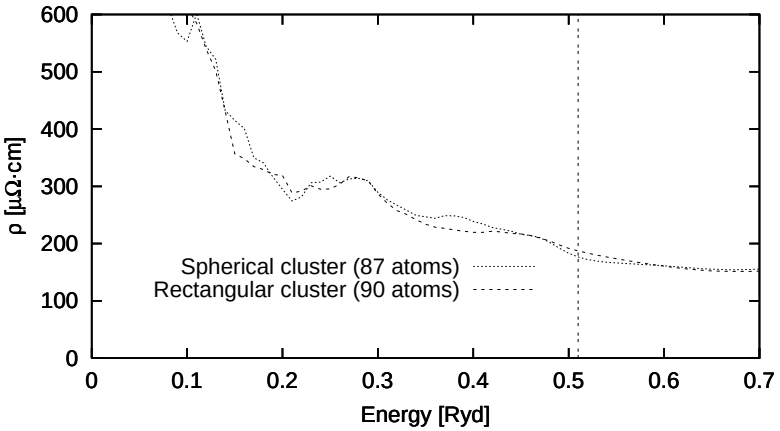

Figure 4.14: Resistivity of isolated spherical clusters with 6 shells (87 atoms) compared to the resistivity of isolated rectangular clusters with 90 atoms. Cluster composition $Ag_{0.5}Pd_{0.5}$. 10 restricted configurations used for averaging.

Fig. 4.13 shows that mean free path and deviation ratio $\rho_{\text{cluster}}/\rho_{\text{CPA}}$ are nearly proportional. Therefore, the larger the mean free path is the more one needs a large cluster in order to get a realistic value for the cluster resistivity. For $Mo_{0.2}Ni_{0.8}$, e.g., the diameter of the 11-shell cluster used is equal to four times the mean free path (0.87 nm). This situation allows for a quite reasonable description of the resistivity by a cluster approximation, although the CPA resistivity is still lower by a factor of 1.7. For alloys such as $Ag_{0.9}Pd_{0.1}$, however, the mean free path is three times the diameter of the largest cluster used and the resistivity based on such clusters is completely wrong.

4.3.4 Influence of Cluster Type

The influence of the cluster type on the $\rho(\epsilon)$ function was studied, in that, besides spherical clusters (for their construction see Section 2), rectangular clusters were

Table 4.1: Rectangular clusters in a FCC lattice.

no. of x-translations	no. of y-translations	no. of z-translations	no. of sites
0	0	0	4
1	0	0	6
1	1	1	14
3	2	1	30
4	4	3	90
6	6	4	192

also generated. Rectangular clusters were constructed as follows: we started from the 4 atoms in the FCC unit cell. In the first step we translated the atoms from the ($y = 0$, $z = 0$)-plane in the x direction by the lattice constant d. In the next step the atoms from the ($y = d/2$, $z = d/2$)-plane were translated in x direction too. The same procedure was then applied in the y and z directions. The number of translations need not be the same in each direction. Table 4.1 shows the dimensions of some rectangular clusters obtained with this construction.

In order to see how important the particular cluster shape is, two calculations were carried out with spherical and rectangular isolated clusters of a similar size, namely a spherical cluster of six shells (87 atoms) and a rectangular cluster of 90 atoms. The alloy $Ag_{0.5}Pd_{0.5}$ was chosen and 10 restricted configurations were used for the average in both cases. The results in Fig. 4.14 show that there is little difference between the two cluster types. The difference comes from the fact that the configurations generated for the two cluster types were different, although random configurations were assumed in both cases.

4.4 Calculations for Short-Range Ordered Alloys

From the results presented above it seems realistic that for highly resistive alloys short-range order effects can be modeled by means of cluster calculations. The alloy to be used in such calculations has to have high residual resistivity and to show a strong dependence of the resistivity on the state of order. Experimental and theoretical studies on $Mo_{20}Ni_{80}$ ([12, 58]) show that this alloy has a resistivity of about 120 $\mu\Omega$·cm and an increase of the resistivity with ordering of about 14%. The increase of the resistivity with ordering is considered a rather unusual effect. Thomas [68], who first drew attention to the fact that the resistivity of some alloys decreases when deformed (i.e. order is broken down), attributed the high ρ of the undeformed (ordered) alloy to a distinct structural state which he called "komplex" state being in fact a state with short-range order. This phenomenon has been known as the "K-state" effect.

In order to study this effect on $Mo_{0.2}Ni_{0.8}$ we generated configurations with various short-range order parameters using the procedure denoted (ii) in section 2.4. Only correlations between the first nearest neighbors were included in the construction of the ordered configurations. We denoted the first order short-range order parameter with Γ_1. Disordered configurations were simulated by using a short-range order parameter $\Gamma_1 = 0$. Configurations with different states of order were generated by increasing Γ_1 in small steps. The highest order parameter used in our calculations was $\Gamma_1 = 0.0361$ which is close to the order parameter measured experimentally in the work of Chakravarti et al. [12] ($\Gamma_1 = 0.03264$ for an as quenched sample and $\Gamma_1 = 0.03888$ for a 5 minutes at 650°C ordered sample). The electrical resistivity was calculated for each Γ_1 and the dependence of ρ on Γ_1 was plotted. The calculations were performed using both isolated clusters and clusters embedded in a CPA

medium. Spherical clusters of 11 shells (201 atoms) were considered. Calculations were carried out at the Fermi energy, $E_F \approx 0.692$ Ryd above muffin-tin zero, as determined from CPA calculations.

In Fig. 4.15 the results of an ECM calculation are shown. The upper plot shows the change of the absolute value of the resistivity as the order parameter Γ_1 is increased. The crosses stand for the resistivities of each of the 10 configurations used for the configurational average at each Γ_1. The solid line joins the configurational averaged resistivities. There is an obvious increase of the resistivity with order. As was seen and explained in the previous section, the absolute values of the resistivity calculated by means of cluster methods are higher than the values obtained by using CPA calculations. The cluster values are also higher than the experimental values. We will return to the comparison of the calculated values with experimental values in the next section. In order to be able to compare our calculations with experiment and with other calculations, we plotted in Fig. 4.15 (lower plot) the change with order of the configurationally averaged resistivities relative to the resistivity of the disordered state. The crosses are the results of our calculation.

The filled circles are from the theoretical calculations of Nicholson et al. [58]. They were obtained by means of a KKR-CPA based cluster method, the big cell linearized KKR described in [25, 10]. In their calculations, Nicholson et al. used clusters containing 154 Ni and 38 Mo atoms (80% and 20% from a total of 192 atoms, respectively). The lattice sites of six of these clusters were populated by atoms in such a manner that the SRO parameters equal those determined by diffuse X-ray scattering by Chakravarti et al. [12] on quenched samples. In the remaining six cells the atoms were placed at random. They used one-electron single-site potentials taken from self-consistent KKR-CPA calculations at a Mo atom fraction of 0.2. Nicholson obtained for the resistivity 147 $\mu\Omega$·cm for the SRO samples and 129 $\mu\Omega$·cm for the random ones.

The open circles are experimental results from Lei et al. [51]. The short-range ordered $Mo_{0.2}Ni_{0.8}$ alloy in [51] was obtained by quenching from 950°C. In this state the resistivity measured at room temperature was 144 $\mu\Omega$·cm. The alloy was then cold worked until a 68% reduction of area was achieved, where it was supposed that the order was completely destroyed. For the disordered alloy a resistivity of 124 $\mu\Omega$·cm was measured. The direct comparison of our results to those of [51] is not possible as no values for the SRO parameter are given there. Thus, we assumed that the SRO parameter for the alloy in the ordered state is that measured on the as-quenched sample in the work of Chakravarti et al. [12], namely $\Gamma_1 = 0.03264$. We further assumed that the relation between the SRO parameter and the reduction of area is linear and determined the correspondence given in Table 4.2 from the experimental points given by Lei et al.

The same increase of the resistivity with short-range order encountered by ECM calculations can be seen also in the case of isolated clusters (Fig. 4.16). The absolute values of the resistivity are higher than in the case of clusters embedded in a CPA medium. The increase of the resistivity with order relative to the resistivity for the

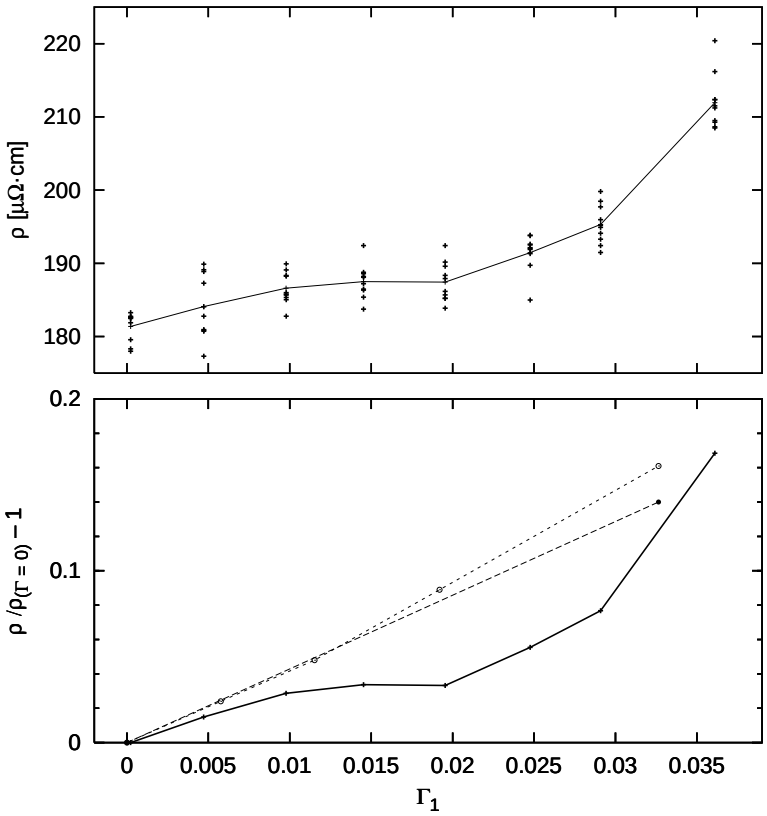

Figure 4.15: Variation of the resistivity with the first order SRO parameter for a 11-shells (201 atoms) $Mo_{0.2}Ni_{0.8}$ cluster embedded in a CPA medium (ECM). Upper plot: absolute resistivity values. Lower plot: resistivities relative to the resistivity of the disordered state ($\Gamma_1 = 0$).

Table 4.2: Interpolated SRO parameters corresponding to the measured area reduction of cold-worked $Mo_{0.2}Ni_{0.8}$ in Lei et al. [51]

Red. of area	Γ_1
0	0.03264
0.28	0.01920
0.44	0.01152
0.56	0.00576
0.68	0.0

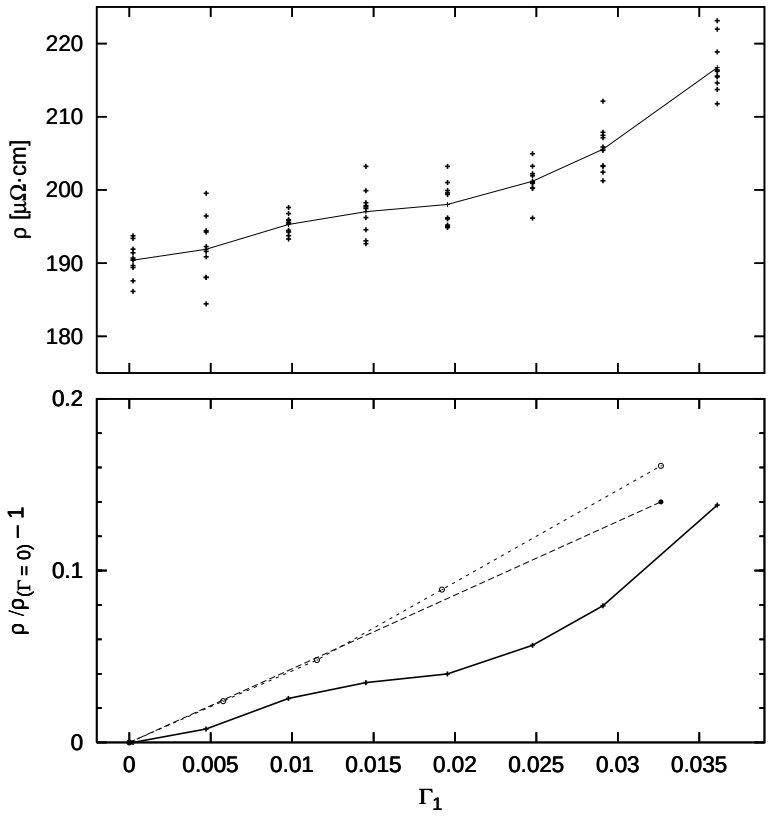

Figure 4.16: Same as Fig. 4.15, ICM calculation.

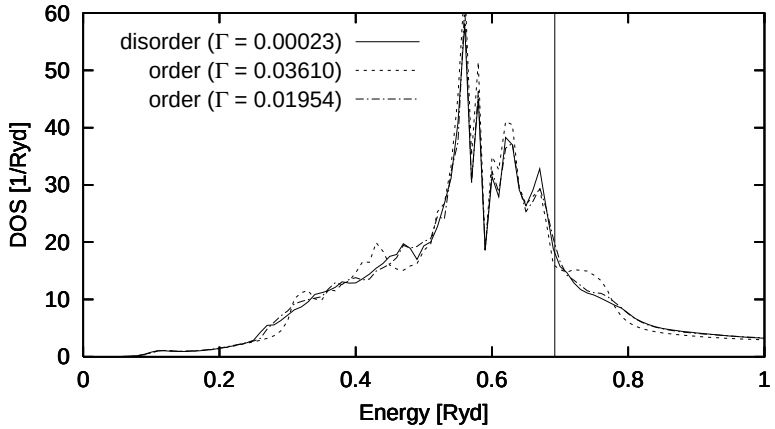

Figure 4.17: Comparison between densities of states of disordered and ordered 11-shells (201 atoms) $Mo_{0.2}Ni_{0.8}$ isolated clusters.

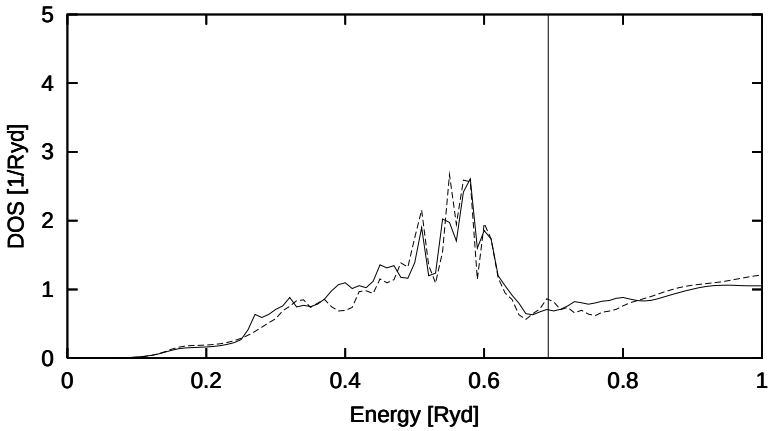

Figure 4.18: Comparison between the contribution of the p-states of Mo to the total density of states of a disordered and an ordered 11-shells (201 atoms) $Mo_{0.2}Ni_{0.8}$ isolated cluster.

disordered alloy is very similar to that in Fig. 4.15.

One can conclude that our cluster calculations provide results in good agreement with the experiment.

Nicholson observed a relation between the resistivity and the density of states for the alloy studied. The p-d conductivity is proportional to the product of the p and d component DOS's at the Fermi level. We plotted the densities of states for a $Mo_{0.2}Ni_{0.8}$ isolated cluster of 201 atoms in Fig. 4.17. As one can see in the plot, the density of states of the disordered system is higher than that of the ordered one at the Fermi energy. The reason for the decrease of the density of states with order can be found in Figs. 4.18 – 4.21. While the p-like densities of states for both Ni and Mo increase slightly with the order (Figs. 4.18 4.19), the d-like DOS of Mo is almost unchanged (Fig. 4.20) and the d-like DOS of Ni drops drastically (Fig. 4.21) at the Fermi level. As the increase of the SRO parameter means more Mo-Ni pairs one can conclude that Mo-Ni pairs are less favorable in the electron conduction.

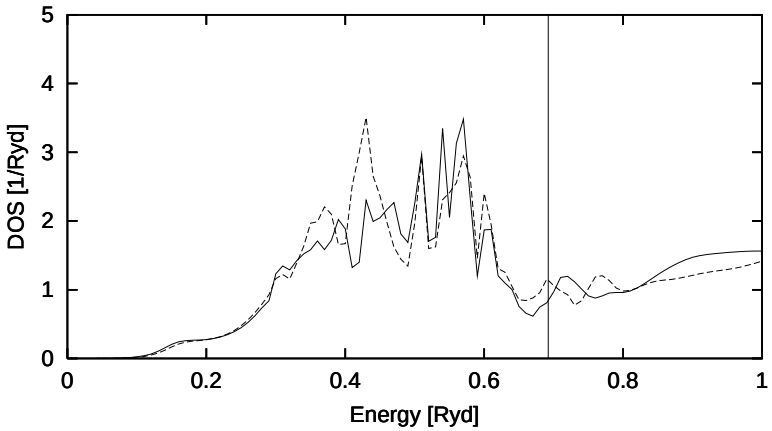

Figure 4.19: Same as Fig. 4.18 for Ni.

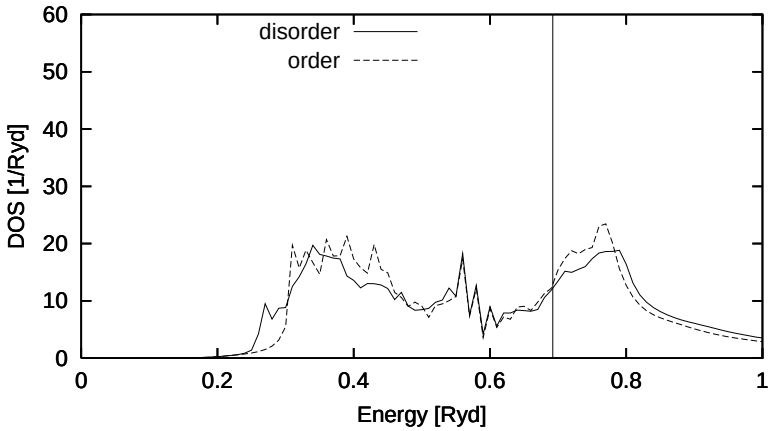

Figure 4.20: Comparison between the contribution of the d-states of Mo to the total density of states of a disordered and an ordered 11-shells (201 atoms) $Mo_{0.2}Ni_{0.8}$ isolated cluster.

We have to note that our attempt to determine the contribution to the total resistivity (conductivity) from different kind of pairs (Mo-Mo, Mo-Ni, Ni-Ni) led to non-physical results. Thus, at this stage, the only explanation of the increase of the resistivity with order is the decrease of the density of states at the Fermi level.

In order to see the influence of the correlation between the second nearest neighbors on the resistivity, one calculation was performed on configurations being disordered with respect to the first nearest neighbors. We assumed three values of Γ_2 (correlations between the second nearest neighbors): (i) one negative value indicating that most of the second nearest neighbors of an atom are of the same kind as the atom itself; (ii) one positive value indicating that most of the second nearest neighbors of an atom are of different kind than the atom itself; (iii) a $\Gamma = 0$ value indicating that there is no preference for one or other type of atoms as second nearest neighbors of an atom. The calculation represented in Fig. 4.22 show that the influence of the correlation between second nearest neighbors is very small. How-

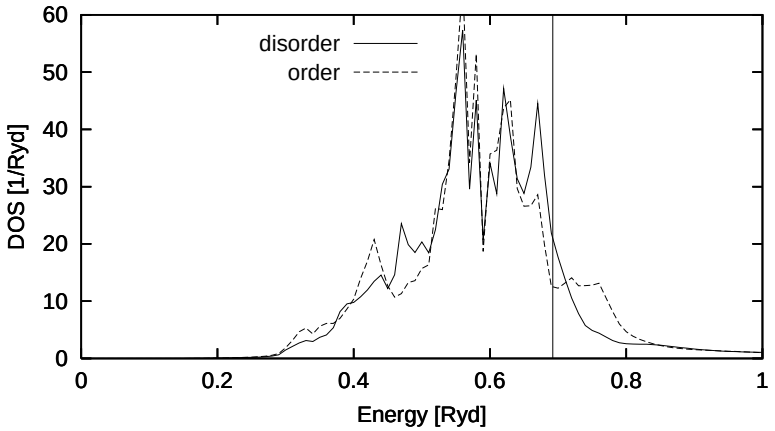

Figure 4.21: Same as Fig. 4.20 for Ni.

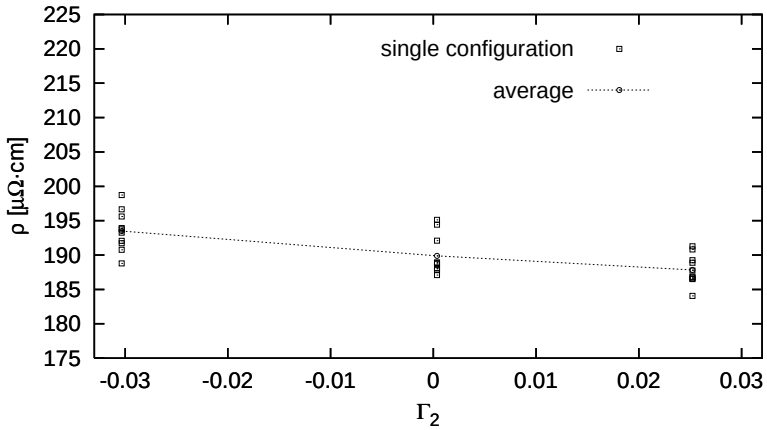

Figure 4.22: Dependence of the resistivity on the second order SRO parameter for $\Gamma_1 = 0$. 11-shells $Mo_{0.2}Ni_{0.8}$ isolated clusters were used.

ever, the measurements of the second order SRO from Chakravarti et al. [12] give values of Γ_2 very close to 0, which means that the second nearest neighbors of an atom at one site are randomly distributed.

Fig. 4.23 shows calculations on $Cu_{0.5}Pt_{0.5}$. This alloy has also a quite high resistivity and it is therefore interesting for cluster calculations. However, a long-range ordered state rather than a short-range ordered one is specific to it and this is out of the scope of our calculations. The few experimental measurements of resistivity on short-range ordered probes are made at high temperatures and include effects due to the finite temperature which were not included in our calculations. Thus, a direct comparison of our calculations with measured data cannot be done. The experimental measurements could not establish an obvious change of the resistivity with the variation of the short-range order. Our calculations for Γ_1's up the about 0.035 show no significant change of the resistivity. One has to note that the slight variations of the averaged resistivity are within the range of the scattering of the

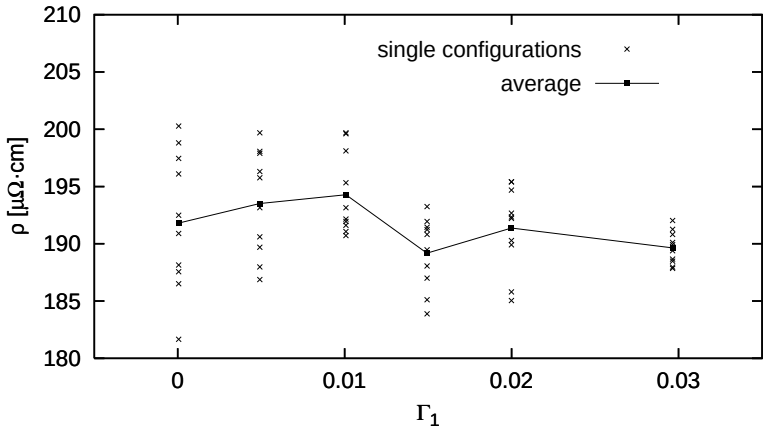

Figure 4.23: Variation of the resistivity with the first order SRO parameter for a 11-shells (201 atoms) $Cu_{0.5}Pt_{0.5}$ isolated cluster.

results, this means that no obvious change of the resistivity can be predicted.

4.5 Comparison to Experimental Resistivities

The comparison of theoretical calculations with experiment is a very delicate problem. Due to the very complex nature of the real systems one is always constrained to make several approximations. While in some cases several different experimental methods can predict the importance of one or other of the many possible contribution to a certain property, in other cases there are no possibilities to make such predictions. A resistivity measurement gives one value which cannot be resolved in different contributions. Thus, it is impossible to evaluate the importance of different contributions to the resistivity from experiment. The most of the theoretical calculations of resistivity of binary alloys containing transition metals use expansions of the wavefunctions up to $l = 2$ (d-states). The argument is that the density of f-states are very low and thus non-important in the most of the electronic properties. Calculations using expansions of the wavefunctions up to $l = 3$ (f-states) show that the density of f-states, although low, are very important for resistivity calculations, because they allow to take into account additional terms that come from p-f scattering. Brown et al. [10] suggest that accurate comparison with experiment require an inclusion of $l = 4$. Table 4.3 compares some values of resistivities calculated using CPA and the isolated cluster method. Experimental values are also given. For the three alloys $Ag_{0.5}Pd_{0.5}$, $Cu_{0.5}Pt_{0.5}$ and $Mo_{0.2}Ni_{0.8}$ the experimental resistivity extrapolated to T=0 is 29 [16], 82 [41] and 117 [51] (all in $\mu\Omega$·cm), respectively. We calculated resistivities using the CPA method and $l = 2$ for $Ag_{0.5}Pd_{0.5}$, $Cu_{0.5}Pt_{0.5}$ and $Mo_{0.2}Ni_{0.8}$. For $Mo_{0.2}Ni_{0.8}$ we performed a CPA calculation using $l = 3$. ICM calculations using disordered clusters of 7 shells (135 atoms) were done only for $Mo_{0.2}Ni_{0.8}$. As one can see, CPA calculations with $l = 2$ provide results very close to those measured experimentally. The hope that the CPA despite its single-site nature, provide very good results for the resistivity dies as soon as one take $l = 3$

Table 4.3: Comparison between computed and experimental resistivities. Various methods (CPA and ICM) and results for different maximum angular momentum used in the expansion of wavefunctions are also compared (see text)

ρ	$Ag_{0.5}Pd_{0.5}$	$Cu_{0.5}Pt_{0.5}$	$Mo_{0.2}Ni_{0.8}$
exp	29	82	117
CPA: $l = 2$	23.1	80.2	120 (116 [58])
CPA: $l = 3$	–	–	71
7 shells cluster: $l = 2$	–	–	198
7 shells cluster: $l = 3$	–	–	148

into account. Comparing the values obtained by us using a 7-shells isolated cluster of $Mo_{0.2}Ni_{0.8}$ one can see that the results are about 25% less than for $l = 2$. One has to note, however, that the calculations with $l = 3$ need much more computational system resources and computation time. This is why we could not treat clusters greater than 7-shells (135 atoms).

Chapter 5

Conclusions and Outlook

The main aim of this work was to find some approach to the calculation of electrical transport properties for concentrated binary alloys from first principles in order to study the influence of short-range order on the electrical resistivity. One existing approach, which gives good results by the calculation of electronic properties for disordered alloys is the coherent potential approximation (CPA). The CPA is, however, a single-site approximation and, as such, cannot, in principle, give right answers to the problem of calculating properties which depend on multi-site effects. In addition, as a mean field theory, the CPA cannot be applied to ordered systems. There were many attempts to study the influence of order on electronic properties of alloys by means of cluster methods. Due to the complexity of the problem, however, the influence of order on electrical resistivity was not systematically studied until now.

Order plays an important role in the theory of alloys as the "natural" states of many of the alloys are states of order. We outlined in chapter 2 the most important definitions and notions of the theory of order in alloys which form a solid basis of most of the studies of ordered structures. The detection of order in alloys by means of diffuse X-ray scattering and residual resistivity measurements was also described. The diffuse X-ray scattering experiments and the corresponding theory are reliable in most of the studies of short-range order in alloys. They cannot give, however, a direct relation between resistivity and short-range order. Within residual resistivity measurements a direct relation between short-range order and resistivity is measured, but the theory of this relation is not entirely applicable, due to its complexity. In order to study the relation between resistivity and short-range order, we developed two procedures for generation of short-range ordered alloy structures by which we aimed to arrange the atoms in a cluster so that states with certain short-range order parameters to be formed, without caring about the stability of a particular arrangement. We showed that the appropriate way to generate structures with short-range order is by taking into account the correlations of an atom with all its neighbors. We also emphasized the importance of frustration by obtaining states with short-range order.

The theoretical treatment adopted here relies on a one-electron picture, within

the framework of density functional theory, using the multiple scattering theory to solve the electronic structure problem. For transport calculations the Kubo-Greenwood formula of linear response theory was used. The theoretical framework was the subject of chapter 3. The multiple scattering theory shows that the scattering path operators, that result from the decomposition of the Green function, are the most important quantities involved in the calculation of observables. The calculation of the scattering path operators within the CPA for disordered systems was presented. It was also shown how these operators could be calculated by means of cluster methods in order to allow the take into account of information about the local arrangement of atoms in a cluster. One of the cluster methods, the embedded cluster method (ECM), was already used in many calculations of electronic properties and was shown to give reliable results. Its applications to resistivity calculations was, however, only sporadic. Beside ECM we proposed another cluster method, namely the isolated cluster method (ICM), which was for the first time applied to calculations of properties.

Chapter 4 was entirely devoted to applications of CPA, ECM and ICM to calculation of densities of states and resistivities of concentrated binary alloys. The possibility for alloys, the possibility for approximately representing an infinite lattice by finite clusters could be evaluated.

It was found that especially for the resistivity a small number of configurations is sufficient for the average because the resistivity is quite insensitive to the arrangement of the atoms in a cluster. Resistivities of clusters were calculated and compared with corresponding results given by the CPA for various situations: energy dependent resistivities were calculated, quantities only at the Fermi level were given a closer look and, finally, various alloys were treated for matters of comparison. The general result obtained was that, i) the larger the clusters are the closer the results lie to the CPA and, ii) that cluster and CPA resistivities are quite close together whenever the resistivity of the system is high, or, the mean free path of conduction electrons is small compared to the cluster diameter. In the alloys considered this is true for energies which lie in the d-band complex. Therefore, the cluster methods yield good results for the resistivity only if the Fermi level lies in the d-band. Not very much difference was seen between the resistivity of isolated and embedded clusters so that most calculations were performed within the simpler isolated cluster scheme.

It was shown that for highly resistive alloys short-range order effects can be modeled. Thus, the resistivity change associated with a rearrangement of atoms after short-range ordering could be calculated this way.

The results showed that both ECM and ICM are well suited for modeling short-range order in alloys with high resistivity giving the right tendency of the change in the resistivity due to ordering processes. The ECM is superior in case one needs to calculate properties such as DOS and in case one is interested in absolute values of the resistivity. The reason for the bad results in some other calculations is the fact that the embedding CPA medium is not self-consistent with the medium described

by the cluster. ICM does not have the drawback of using an artificially determined embedding medium. It was shown that, despite the use of finite clusters, the resistivities calculated by means of ICM are, when using sufficiently big clusters, good enough to give reliable results.

It was argued that the widespread procedure of including only up to d-states ($l = 2$) in calculations of electronic properties is not appropriate when one aims to calculate electrical resistivities. For comparison of such calculations with experiment the inclusion of at least f-states ($l = 3$) is absolutely necessary. It is, however, possible to study qualitatively resistivity changes even for $l = 2$.

We think that with this work an important step toward a systematical study of the electrical resistivity in real alloy systems was done. We see, however, many important improvement possibilities of which some are enumerated below. A better choice of the potentials, tallow for the account of changes due to local environment effects, could, in principle, lead to better results for the calculation of the properties. Another possible improvement of the methods consists in the choice of the configurations to be used in configurational averages. There are many possibilities for the arrangement of the atoms even for one and the same nearest neighbors correlation parameter. A study of the stability of a certain configuration based on the counting of more than two short-range order parameters could help on the better choice of the configurations to be used in calculations. Information about different contributions to the electrical resistivity could complete the actual possibilities to analyze the results.

Appendix A

Derivation of Equation (3.33)

In order to get Eq. (3.33) one starts from Eq. (3.26)

$$G(\mathbf{r},\mathbf{r}\,';\epsilon) = G_0(\mathbf{r},\mathbf{r}\,';\epsilon) + \int d^3r_i \int d^3r_j G_0(\mathbf{r},\mathbf{r}_i;\epsilon) t(\mathbf{r}_i,\mathbf{r}_j;\epsilon) G_0(\mathbf{r}_j,\mathbf{r}\,';\epsilon) \tag{A.1}$$

The Green function of the free particle in terms of spherical functions is

$$G_0(\mathbf{r},\mathbf{r}';\epsilon) = -i\sqrt{\epsilon}\sum_L j_l(\sqrt{\epsilon}\,r) Y_L(\hat{\mathbf{r}}) h_l^+(\sqrt{\epsilon}\,r') Y_L^*(\hat{\mathbf{r}}') \tag{A.2}$$

We put Eq. (A.2) into (A.1) (for more clarity we make the substitution firts only in the second term on the right hand side of Eq. (A.1)). We then get

$$\begin{aligned} G(\mathbf{r},\mathbf{r}\,';\epsilon) &= G_0(\mathbf{r},\mathbf{r}\,';\epsilon) \\ &+ \int d^3r_i \int d^3r_j \Bigg[(-i\sqrt{\epsilon}) \sum_L h_l^+(\sqrt{\epsilon}\,r) Y_L(\hat{\mathbf{r}}) j_l(\sqrt{\epsilon}\,r_i) Y_L^*(\hat{\mathbf{r}}_i) \\ &\quad \times\ t(\mathbf{r}_i,\mathbf{r}_j;\epsilon) \\ &\quad \times\ (-i\sqrt{\epsilon}) \sum_{L'} j_{l'}(\sqrt{\epsilon}\,r_j) Y_{L'}(\hat{\mathbf{r}}_j) h_{l'}^+(\sqrt{\epsilon}\,r') Y_{L'}^*(\hat{\mathbf{r}}') \Bigg] \end{aligned} \tag{A.3}$$

Looking at Eq. (3.31)

$$t_{LL'}(\epsilon) = \int d^3r_i \int d^3r_j j_l(\sqrt{\epsilon}r_i) Y_L^*(\hat{\mathbf{r}}_i) t(\mathbf{r}_i,\mathbf{r}_j;\epsilon) Y_{L'}(\hat{\mathbf{r}}_j) j_{l'}(\sqrt{\epsilon}r_j) \tag{A.4}$$

we can rewrite (A.3) as

$$G(\mathbf{r},\mathbf{r}\,';\epsilon) = G_0(\mathbf{r},\mathbf{r}\,';\epsilon) + (-i\sqrt{\epsilon})^2 \sum_{LL'} h_l^+(\sqrt{\epsilon}\,r) Y_L(\hat{\mathbf{r}}) t_{LL'}(\epsilon) h_{l'}^+(\sqrt{\epsilon}\,r') Y_{L'}^*(\hat{\mathbf{r}}') \tag{A.5}$$

We substitute now $G_0(\mathbf{r},\mathbf{r}\,';\epsilon)$ in Eq. (A.5) with the expression in Eq. (A.2).

$$
\begin{aligned}
G(\mathbf{r},\mathbf{r}\,';\epsilon) &= (-i\sqrt{\epsilon})\sum_{L'} j_{l'}(\sqrt{\epsilon}\,r_j)Y_{L'}(\hat{\mathbf{r}}_\mathbf{j})h^+_{l'}(\sqrt{\epsilon}\,r')Y^*_{L'}(\hat{\mathbf{r}}') \\
&+ (-i\sqrt{\epsilon})^2\sum_{LL'} h^+_l(\sqrt{\epsilon}\,r)Y_L(\hat{\mathbf{r}})t_{LL'}(\epsilon)h^+_{l'}(\sqrt{\epsilon}\,r')Y^*_{L'}(\hat{\mathbf{r}}') \qquad \text{(A.6)}
\end{aligned}
$$

We can rearrange Eq. (A.6) and get

$$
\begin{aligned}
G(\mathbf{r},\mathbf{r}\,';\epsilon) &= -i\sqrt{\epsilon}\sum_{LL'}\left[j_{l'}(\sqrt{\epsilon}\,r)Y_{L'}(\hat{\mathbf{r}})t^{-1}_{LL'}(\epsilon) - i\sqrt{\epsilon}h^+_l(\sqrt{\epsilon}\,r)Y_L(\hat{\mathbf{r}})\right] \\
&\times t_{LL'}(\epsilon)h^+_{l'}(\sqrt{\epsilon}\,r')Y^*_{L'}(\hat{\mathbf{r}}') \qquad \text{(A.7)}
\end{aligned}
$$

In order to write Eq. (A.7) in a more compact form we take Eq. (3.5)

$$R_l(r\,;\epsilon) = j_l(\sqrt{\epsilon}\,r)\cos\delta_l(\epsilon) - n_l(\sqrt{\epsilon}\,r)\sin\delta_l(\epsilon) \qquad \text{(A.8)}$$

and rewrite it in terms of spherical bessel and hankel functions by substituting n_l with $(-ih^+_l + ij_l)$. We get

$$
\begin{aligned}
R_l(r\,;\epsilon) &= j_l(\sqrt{\epsilon}\,r)\cos\delta_l(\epsilon) - ij_l(\sqrt{\epsilon}\,r)\sin\delta_l(\epsilon) + ih^+_l(\sqrt{\epsilon}\,r)\sin\delta_l(\epsilon) \\
&= j_l(\sqrt{\epsilon}\,r)e^{-i\delta_l(\epsilon)} + ih^+_l(\sqrt{\epsilon}\,r)\sin\delta_l(\epsilon) \qquad \text{(A.9)}
\end{aligned}
$$

We multiply Eq. (A.9) with $(-\sqrt{\epsilon})$ and with $Y_L(\hat{\mathbf{r}})$ and divide it by $(\sin\delta_l(\epsilon))$.

$$-\sqrt{\epsilon}\,\frac{R_l(r\,;\epsilon)}{\sin\delta_l(\epsilon)}Y_L(\hat{\mathbf{r}}) = j_l(\sqrt{\epsilon}\,r)\left(-\sqrt{\epsilon}\,\frac{e^{-i\delta_l(\epsilon)}}{\sin\delta_l(\epsilon)}\right)Y_L(\hat{\mathbf{r}}) - i\sqrt{\epsilon}\,h^+_l(\sqrt{\epsilon}\,r)Y_L(\hat{\mathbf{r}}) \qquad \text{(A.10)}$$

Looking to Eq. (3.32)

$$t_L(\epsilon) = -\frac{1}{k}\,\sin\delta_l(\epsilon)\,e^{i\delta_l} \qquad \text{(A.11)}$$

Eq. (A.10) can be written as

$$Z_L(\mathbf{r};\epsilon) = j_l(\sqrt{\epsilon}\,r)t^{-1}_L(\epsilon)Y_L(\hat{\mathbf{r}}) - i\sqrt{\epsilon}\,h^+_l(\sqrt{\epsilon}\,r)Y_L(\hat{\mathbf{r}}) \qquad \text{(A.12)}$$

where we introduced the notation

$$Z_L(\mathbf{r};\epsilon) = -\sqrt{\epsilon}\,\frac{R_l(r;\epsilon)}{\sin\delta_l(\epsilon)}Y_L(\hat{\mathbf{r}}) \qquad \text{(A.13)}$$

Noting that $t_L(\epsilon) = t_{LL'}(\epsilon)\delta_{LL'}$ and comparing the right hand side of Eq. (A.13) with the square bracket in Eq. (A.7) we finally obtain Eq. (3.33).

$$G(\mathbf{r},\mathbf{r}';\epsilon) = -ik\sum_{LL'} Z_L(\mathbf{r};\epsilon)t_{LL'}(\epsilon)h^+_{l'}(kr')Y_{L'}(\hat{\mathbf{r}}')\,, \qquad \text{(A.14)}$$

Appendix B

Structure constants

The analytical form for the KKR structure constants are given in many text books [32, 73] and review articles [11, 24, 37, 66]. Between formulae given by different authors there are sometimes great differences. We derived a formula for the KKR structure constants which is consistent within the notations and definitions we adopted throughout this work.

We start from the integral form of the Green function, Eq. (3.23)

$$G(\mathbf{r},\mathbf{r}';\epsilon) = \int \frac{d^3k}{(2\pi)^3} \frac{\psi^*_{\mathbf{k}}(\mathbf{r})\psi_{\mathbf{k}}(\mathbf{r}')}{\epsilon - k^2 + i\eta} \tag{B.1}$$

and integrate it for the case of free particles (the wavefunctions of which are plane waves). Then, the following formula for the free particle Green function $G_0(\mathbf{r},\mathbf{r}';\epsilon)$ is obtained [22, 32]

$$G_0(\mathbf{r},\mathbf{r}';\epsilon) = -\frac{1}{4\pi} \frac{e^{ik|\mathbf{r}-\mathbf{r}'|}}{\mid \mathbf{r}-\mathbf{r}' \mid} \tag{B.2}$$

or, in angular momentum representation,

$$G_0(\mathbf{r},\mathbf{r}';\epsilon) = -ik \sum_L j_l(kr_<) Y_L(\hat{\mathbf{r}}) h^+_l(kr_>) Y^*_L(\hat{\mathbf{r}}') \tag{B.3}$$

where $r_>$ ($r_<$) denotes the larger (smaller) of the lengths r and r'. Letting $\mathbf{r} = \mathbf{R}_i + \mathbf{r}_i$ and $\mathbf{r}' = \mathbf{R}_j + \mathbf{r}_j$, where $\mathbf{R}_i$ and $\mathbf{R}_j$ are lattice site vectors, we can rewrite Eqs. (B.2) and (B.3) as

$$\frac{e^{ik|\mathbf{r}_i - (\mathbf{R}_{ij}+\mathbf{r}_j)|}}{\mid \mathbf{r}_i - (\mathbf{R}_{ij}+\mathbf{r}_j) \mid} = 4\pi ik \sum_{L_2} j_{l_2}(kr_i) Y_{L_2}(\hat{\mathbf{r}}_i) h^+_{l_2}(k \mid \mathbf{R}_{ij} + \mathbf{r}_j \mid) Y^*_{L_2}(\widehat{\mathbf{R}_{ij} + \mathbf{r}_j}) \tag{B.4}$$

or as

$$\frac{e^{ik|(\mathbf{r}_i - \mathbf{r}_j) - \mathbf{R}_{ij}|}}{\mid (\mathbf{r}_i - \mathbf{r}_j) - \mathbf{R}_{ij} \mid} = 4\pi ik \sum_{L_1} j_{l_1}(k \mid \mathbf{r}_i - \mathbf{r}_j \mid) Y_{L_1}(\widehat{\mathbf{r}_i - \mathbf{r}_j}) h^+_{l_1}(kR_{ij}) Y^*_{L_1}(\hat{\mathbf{R}}_{ij}) \tag{B.5}$$

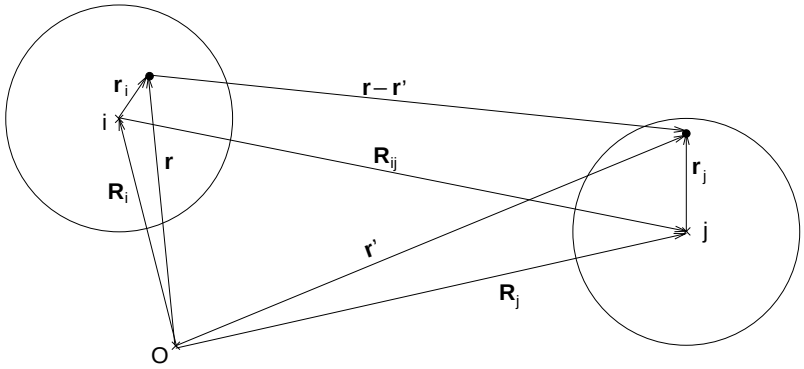

Figure B.1: Graphical representation of the vectors involved in the decomposition of the free particle Green function around sites i and j

Using Bauer's identity

$$e^{i\mathbf{k}\cdot\mathbf{r}} = 4\pi \sum_{L} i^l j_l(kr) Y_L(\hat{\mathbf{r}}) Y_L^*(\hat{\mathbf{k}}) \tag{B.6}$$

the following expressions can be written

$$\begin{aligned} e^{i\mathbf{k}\cdot(\mathbf{r}_i-\mathbf{r}_j)} &= 4\pi \sum_{L_1} i^{l_1} j_{l_1}(k \mid \mathbf{r}_i - \mathbf{r}_j \mid) Y_{L_1}(\widehat{\mathbf{r}_i - \mathbf{r}_j}) Y_{L_1}^*(\hat{\mathbf{k}}) \\ &= (4\pi)^2 \sum_{L_2} \sum_{L_3} i^{l_2-l_3} j_{l_2}(kr_i) Y_{L_2}(\hat{\mathbf{r}}_i) Y_{L_2}^*(\hat{\mathbf{k}}) j_{l_3}(kr_j) Y_{L_3}^*(\hat{\mathbf{r}}_j) Y_{L_3}(\hat{\mathbf{k}}) \end{aligned} \tag{B.7}$$

Multiplying the second part of Eq. (B.7) with $Y_{L_1}(\hat{\mathbf{k}})$, integrating over the whole k-space, and denoting

$$C(L_1 L_2 L_3) = \int d^3k \; Y_{L_1}^*(\hat{\mathbf{k}}) Y_{L_2}(\hat{\mathbf{k}}) Y_{L_3}(\hat{\mathbf{k}}) \tag{B.8}$$

we get

$$\begin{aligned} j_{l_1}(k \mid \mathbf{r}_i - \mathbf{r}_j \mid) Y_{L_1}(\widehat{\mathbf{r}_i - \mathbf{r}_j}) &= 4\pi \sum_{L_2} \sum_{L_3} i^{l_2-l_3-l_1} C(L_1 L_2 L_3) \\ &\quad \times j_{l_2}(kr_i) Y_{L_2}(\hat{\mathbf{r}}_i) j_{l_3}(kr_j) Y_{L_3}^*(\hat{\mathbf{r}}_j) \end{aligned} \tag{B.9}$$

The quantities $C(L_1 L_2 L_3)$ are called Gaunt coefficients and their calculation is given in [15].

From the equality of Eqs. (B.4) and (B.5) it follows

$$\sum_{L_2} j_{l_2}(kr_i) Y_{L_2}(\hat{\mathbf{r}}_i) h_{l_2}^+(k \mid \mathbf{R}_{ij} + \mathbf{r}_j \mid) Y_{L_2}^*(\widehat{\mathbf{R}_{ij} + \mathbf{r}_j})$$

$$= \sum_{L_1} 4\pi \sum_{L_2} \sum_{L_3} i^{l_2-l_3-l_1} C(L_1 L_2 L_3) j_{l_2}(kr_i) Y_{L_2}(\hat{\mathbf{r}}_i) j_{l_3}(kr_2) Y^*_{L_3}(\hat{\mathbf{r}}_j) h^+_{l_1}(kR_{ij}) Y^*_{L_1}(\hat{\mathbf{r}}_i)$$
$$= \sum_{L_2} j_{l_2}(kr_i) Y_{L_2}(\hat{\mathbf{r}}_i) \sum_{L_2} \sum_{L_3} 4\pi i^{l_2-l_3-l_1} C(L_1 L_2 L_3) j_{l_3}(kr_j) Y^*_{L_3}(\hat{\mathbf{r}}_j) h^+_{l_1}(kR_{ij}) Y^*_{L_1}(\hat{\mathbf{r}}_i) \tag{B.10}$$

from which we can express

$$h^+_{l_2}(k \mid \mathbf{R}_{ij} + \mathbf{r}_j \mid) Y^*_{L_2}(\mathbf{r}_i \widehat{+} \mathbf{r}_j)$$
$$= \sum_{L_2} \sum_{L_3} 4\pi i^{l_2-l_3-l_1} C(L_1 L_2 L_3) j_{l_3}(kr_2) Y^*_{L_3}(\hat{\mathbf{r}}_j) h^+_{l_1}(kR_{ij}) Y^*_{L_1}(\hat{\mathbf{r}}_i) \tag{B.11}$$

Introducing Eq. (B.11) in Eq. (B.4), we find for the free particle Green function

$$G_0(\mathbf{r}, \mathbf{r}'; \epsilon) = -4\pi i k \sum_{L_2} j_{l_2}(kr_i) Y_{L_2}(\hat{\mathbf{r}}_i) \sum_{L_1} \sum_{L_3} i^{l_2-l_3-l_1} C(L_1 L_2 L_3)$$
$$\times j_{l_3}(kr_j) Y^*_{L_3}(\hat{\mathbf{r}}_j) h^+_{l_1}(kR_{ij}) Y^*_{L_1}(\hat{\mathbf{R}}_{ij}) \tag{B.12}$$

Comparing Eq. (B.12) with Eq. (3.44)

$$G_0(\mathbf{r}, \mathbf{r}\,'; \epsilon) = \sum_{LL'} Y_L(\hat{\mathbf{r}}_i) j_l(kr_i) G_{LL'}(\mathbf{R}_{ij}; \epsilon) j_{l'}(kr_j) Y^*_{L'}(\hat{\mathbf{r}}_j) \tag{B.13}$$

we find for the structure constants the following expression

$$G_{L_2 L_3} = -4\pi i k \sum_{L_1} i^{l_2-l_3-l_1} C(L_1 L_2 L_3) h^+_{l_1}(kR_{ij}) Y^*_{L_1}(\hat{\mathbf{R}}_{ij}) \tag{B.14}$$

Finaly, we want to give some formulae that are given in literature.
[24] gives

$$G_{LL'}(\mathbf{R}_{\alpha\beta}) = -4\pi i \sqrt{\epsilon} \sum_{L''} i^{l-l'-l''} C^{L''}_{LL'} h^+_{l''}(\sqrt{\epsilon} R_{\alpha\beta}) Y^*_{L''}(\hat{\mathbf{R}}_{\alpha\beta}) \tag{B.15}$$

with

$$C^{L''}_{LL'} = \int d\Omega \; Y^*_L Y_{L'} Y_{L''} \tag{B.16}$$

which is the same as our formula in Eq. (B.14)
[11] gives

$$g^{mn}_{LL'}(z) = -4\pi i^{l-l'} k \sum_{L''} i^{-l''} C(LL'L'') h^+_{l''}(kR_{mn}) Y_{L''}(\hat{\mathbf{R}}_{mn}) \tag{B.17}$$

with

$$C(LL'L'') = \int d\hat{\mathbf{r}} \; Y_L(\hat{\mathbf{r}}) Y_{L'}(\hat{\mathbf{r}}) Y_{L''}(\hat{\mathbf{r}}) \tag{B.18}$$

which is different from our formula in Eq. (B.14) in that the spherical harmonics are considered real (no complex conjugate involved).

[37] gives

$$G_{LL'}(\mathbf{R}_i - \mathbf{R}_j; \epsilon) = 4\pi\sqrt{\epsilon}\sum_{L''} C_{LL'}^{L''} i^{l''} h_{l''}^{+}(\sqrt{\epsilon}|\mathbf{R}_i - \mathbf{R}_j|) Y_{L''}(\widehat{\mathbf{R}_i - \mathbf{R}_j}) \tag{B.19}$$

with

$$C_{LL'}^{L''} = \int d\Omega\, Y_L(\Omega) Y_{L''}(\Omega) Y_{L'}^{*}(\Omega) \tag{B.20}$$

which obviously differes from our formula.

A last example is that given in [66]

$$g_{LL''}^{ij}(\epsilon) = 4\pi k i^{l-l'+1} \sum_{L''} C_{LL'}^{L''} i^{l''} h_{l''}^{+}(k|\mathbf{R}_i - \mathbf{R}_j|) Y_{L''}(\widehat{\mathbf{R}_i - \mathbf{R}_j}) \tag{B.21}$$

with

$$C_{LL'}^{L''} = \int d\Omega\, Y_L(\Omega) Y_{L''}(\Omega) Y_{L'}(\Omega) \tag{B.22}$$

which seems to be very similar to the formula given in [37].

Comparing all these different formulae we want to conclude that by using one or other of these care is to be taken. Our suggestion is to prove the correctness and consistence of each formula with the other notations and conventions used by different authors.

Bibliography

[1] J. Banhart, P. Weinberger and J. Voitländer, Phys. Rev. B **40**, 12079 (1989)

[2] J. Banhart, P. Weinberger and J. Voitländer, J. Phys. Condens. Matter **1**, 7013 (1989)

[3] J. Banhart, *Thesis*, Universität München (1989)

[4] J. Banhart and H. Ebert, Europhys. Lett., **32**, 517 (1995)

[5] J. Banhart, Phil. Mag. **77**, 106 (1998)

[6] J. Banhart, Phys. Rev. Lett. **82**, 2139 (1999)

[7] H. A. Bethe, Proc. Roy. Soc. A **150**, 552 (1935)

[8] M. Browers, J. Giner, J. Van der Rest and F. Brouers, Solid State Commun. **17**, 229 (1975)

[9] W. L. Bragg and E. J. Williams, Proc. Roy. Soc. A **145**, 699 (1934)

[10] R. H. Brown, P. B. Allen, D. M. Nicholson and W. H. Butler, Phys. Rev. Lett. **62**, 661 (1989)

[11] W. H. Butler, Phys. Rev. B **31**, 3260 (1985)

[12] B. Chakravarti, E. A. Starke, Jr., C. J. Sparks and R. O. Williams, J. Phys. Chem. Solids **35**, 1317 (1974)

[13] D. R. Chipman, J. Appl. Phys. **27**, 739 (1956)

[14] J. B. Cohen and M. E. Fine, J. de Physique Radium **23**, 749 (1962)

[15] C. Cohen-Tannoudji, B. Diu and F. Laloë, *Quantum mechanics*, (Hermann, Paris, 1977)

[16] B. R. Coles and J. C. Taylor, Proc. Roy. Soc. **267**, 139 (1962)

[17] J. M. Cowley, J. Appl. Phys. **21**, 24 (1950)

[18] J. M. Cowley, Phys. Rev. **77**, 669 (1950)

[19] J. M. Cowley, Phys. Rev. **120**, 1648 (1960)

[20] A. C. Damask, J. Phys. Chem. Solids **1**, 23 (1956)

[21] L. Dulca, J. Banhart and G. Czycholl, Phys. Rev. B **61**, 16502 (2000)

[22] E. N. Ecomomou, *Green's Functions in Quantum Physics* (Springer, Berlin, 1983)

[23] H. Ehrenreich and L. Schwartz, in *Solid State Physics*, edited by H. Ehrenreich, F. Seitz and D. Turnbull (Academic Press, New York, 1976), Vol. 31, p. 149

[24] J. S. Faulkner, J. Phys. C **10**, 4661 (1977)

[25] J. S. Faulkner, Phys. Rev. B **19**, 6186 (1979)

[26] J. S. Faulkner and G. M. Stocks, Phys. Rev. B **21**, 3222 (1980)

[27] J. S. Faulkner, in *Progress in Material Science*, edited by J. W. Christian, P. Haasen and T. B. Massalski (Pergamon Press, New York, 1982), Vol. 27, p. 1

[28] L. L. Foldy, Phys. Rev. **67**, 107 (1945)

[29] D. de Fontaine, J. Phys. Chem. Solids **34**, 1285 (1973)

[30] D. de Fontaine, in *Solid State Physics* **34**, 73 (1979)

[31] J. B. Gibson, J. Phys. Chem. Solids **1**, 27 (1956)

[32] A. Gonis, *Green Functions for Ordered and Disordered Systems*, (Elsevier, North-Holland, 1992)

[33] D. A. Greenwood, Proc. Phys. Soc. **71**, 585 (1958)

[34] B. L. Györffy, Phys. Rev. B **5**, 2382 (1972)

[35] B. L. Györffy and G. M. Stocks, J. de Phys. **35**, C4-45 (1974)

[36] B. L. Györffy and M. J. Stott, in *Band Structure Spectroscopy of Metals and Alloys*, edited by D. J. Fabian, L. M. Watson, 385 (Academic Press, London, 1973)

[37] B. L. Györffy and G. M. Stocks, in *Electrons in Disordered Metals and at Metallic Surface*, edited by P. Phariseau, B. L. Györffy and L. Scheire, 89 (Plenum Press, New York, 1979)

[38] P. Hohenberg and W. Kohn, Phys. Rev. **136**, B864 (1964)

[39] W. Hume-Rothery, *Electrons, Atoms, Metals and Alloys* (Dover, New York, 1963)

[40] W. Hume-Rothery, R. E. Smallman and C. W. Haworth, *The Structure of Metals and Alloys* (Institut of Metals and the Institution of Metallurgists, London, 1969)

[41] C. H. Johansson and J. O. Linde, Ann. Phys. **82**, 449 (1927)

[42] C. H. Johansson and J. O. Linde, Ann. Phys. (5) **25**, 1 (1936)

[43] Ch. Kittel, *Einführung in die Festkörperphysik*, (R. Oldenbourg Verlag, München, 1991),

[44] W. Kleber, *Einführung in die Kristallographie*, (Verlag Technik, Berlin, 1990),

[45] W. Kohn and N. Rostoker, Phys. Rev. **94**, 1111 (1954)

[46] W. Kohn andL. J. Sham, Phys. Rev. **140**, A1133 (1965)

[47] J. Korringa, Physica **13**, 392 (1947)

[48] R. Kubo, H. Hasegawa, N. Hashitsume, *Statistical Physics II, Nonequilibrium Statistical Mechanics* (Springer, Berlin, 1959)

[49] Max von Laue, *Roentgenstrahl-Interferenzen* (Akadem. Verl., Frankfurt a.M., 1960)

[50] M. Lax, Rev. Mod. Phys. **23**, 287 (1951)

[51] T. S. Lei, K. Vasudevan and E. E. Standbury, Mater. Res. Soc. Symp. Proc. **39**, 163 (1985)

[52] P. Lloyd and P. V. Smith, Adv. Phys. **21**, 69 (1972)

[53] M. Migschitz, A. Korner, W. Garlipp and W. Pfeiler, Acta Mater. **44**, 2821, (1996)

[54] M. Migschitz, W. Garlipp and W. Pfeiler, Acta Mater. **44**, 2831 (1996)

[55] V. L. Moruzzi, J. F. Janak and A. R. Williams, *Calculated Electronic Properties of Metals*, (Pergamon, New York, 1978)

[56] S. C. Moss, J. Appl. Phys. **35**, 3547 (1964)

[57] N. F. Mott and H. Jones, *The Theory of the Properties of Metals and Alloys* (Dover Publications, New York, 1958)

[58] D. M. C. Nicholson and R. H. Brown, Phys. Rev. Lett. **21**, 3311 (1993)

[59] W. Pfeiler, Acta Met. **36**, 2417 (1988)

[60] W. Pfeiler, in *Properties of Complex Inorganic Solids*, Ed. A. Gonis, A. Meike, P. E. A. Turchi (Kluwer Academic Publishers, Dordrecht, 1997)

[61] P. L. Rossiter, *The Electrical Resistivity of Metals and Alloys* (Cambridge University Press, 1987)

[62] R. Reihsner, W. Pfeiler, J. Phys. Chem. Solids **46**, 1431 (1985)

[63] K. Schröder, *CRC Handbook of Electrical Resistivities*, (CRC Press, Boca Raton, 1983)

[64] P. Soven, Phys. Rev. **156**, 809 (1967)

[65] P. Soven, Phys. Rev. B **2**, 4715 (1970)

[66] G. M. Stocks and H. Winter, in *The Electronic Structure of Complex Systems*, Ed. P. Phariseau, W. M. Temmerman, NATO-ASI Series B, Physics, **113**, 463 (Plenum Press, New York, 1984)

[67] J. C. Swihart, W. H. Butler, G. M. Stocks, D. M. Nicholson and R. C. Ward, Phys. Rev. Lett. **57**, 1181 (1986)

[68] H. Thomas, Z. Phys. **129**, 219 (1951)

[69] B. Velicky, S. Kirkpatrick and H. Ehrenreich, Phys. Rev. **175**, 747 (1968)

[70] C. B. Walker and D. T. Keating, Acta. Cryst. **14**, 1170 (1960)

[71] C. B. Walker and D. T. Keating, J. Appl. Phys. **34**, 2309 (1963)

[72] B. E. Warren, B. L. Averbach and B. W. Roberts, J. Appl. Phys. **22**, 1493 (1951)

[73] P. Weinberger, *Electron Scattering Theory for Ordered and Disordered Matter* (Clarendon Press, Oxford, 1990)

[74] Z. W. Wilchinsky, J. Appl. Phys. **15**, 806 (1944)

[75] A. R. Williams, J. Kübler, C. D. Gelatt, Jr., Phys. Rev. B **19**, 6094 (1979)

[76] H. Winter and G. M. Stocks, Phys. Rev. B **27**, 882 (1983)

[77] J. M. Ziman, *Principles of the Theory of Solids* (Cambridge Univeristy Press, Cambridge, 1972)

[78] J. M. Ziman, *Models of Disorder* (Cambridge Univerisity Press, London, 1979)

Acknowledgements

I would like to address my thanks to Prof. Dr. Gerd Czycholl for giving me the possibility to work independent in a pleasant atmosphere. His “dummy” questions were precious step-stones and the discussions with him were treasure.

For everything I learned from him, for his permanent support and encouragement during long and pleasant afternoons, a sincere “thank you” to Dr. Hab. John Banhart.

My best wishes and special thanks to my former teachers, colleagues and friends for all they did for me, for being friends: Prof. Dr. Vasile Crişan, Dr. András Vernes, Dr. Voicu Popescu.

For patience, understanding and being with me, heartfelt thanks to Mirella and Inge.

I am especially grateful to my sister Dorina and to my parents for their love and understanding, for everything they gave and taught me, for helping me to be what I am.

I have no words to express my gratitude and love to my mother. This thesis is dedicated to my dear Mami.